Universidad Zaragoza
1542

Trabajo Fin de Grado

Analysis of laser-material interaction in metallic materials

Análisis de los procesos de interacción laser-materia en materiales metálicos

Autor/es

Zunuraini Binti Haron

Director/es

Luis Alberto Angurel Lamban

Escuela de Ingeniería y Arquitectura Zaragoza

2018

ABSTRACT

After several years of research and development, laser technology has become one of the most common devices that is being used in almost any industry. Laser is well known for its high precision, environmentally friendly and profitable for production. For this reason, new applications of lasers keep emerging especially in manufacturing industry.

The goal of this project is to study the interaction of laser on the surface of metals, in particular when sub-nano lasers are used. In this project we have been focused in the interaction of these lasers with Aluminum 6061. Two different wavelengths are used throughout this study, which are Infrared laser (n-IR) and Ultraviolet laser. Laser parameters have been modified in order to observe the development of process and structures that are formed on the sample surface. After each experiment, the treated surfaces were analyzed by using Field Emission Scanning Electron Microscopy (FESEM) provided by the Servicio de Microscopia Electrónica de Materiales del Servicio General de Apoyo a la Investigación –SAI de la Universidad de Zaragoza.

This report explains about the fundamentals of laser, the influence of material properties on laser-material interaction and the generation of LIPSS on metal surface. Results have been analyzed in order to determine the influence of different processing parameters (laser wavelength, fluence values, incubation energy, polarization direction and atmosphere during the interaction) on the nanostructures generated on the Al 6061 surface.

RESUMEN (SPANISH)

Después de varios años de investigación y desarrollo, la tecnología láser se ha convertido en uno de las herramientas más comunes que se utilizan en casi cualquier industria. El láser es bien conocido por su alta precisión, ambientalmente amigable y rentable para la producción. Por esta razón, siguen surgiendo nuevas aplicaciones de láser, especialmente en la industria manufacturera.

El objetivo de este proyecto es estudiar la interacción del láser cuando incide sobre la superficie de los metales, en particular cuando se utilizan láseres emitiendo pulsos de centenares de ps. En este proyecto nos hemos centrado en la interacción de los láseres con el Aluminio 6061. Se ha trabajado con láseres emitiendo con dos longitudes de onda, un láser de Infrarrojo cercano (n-IR) y uno de Ultravioleta (UV). Se han modificado los parámetros láser de procesado con el fin de analizar qué procesos y estructuras se generan en la superficie del metal. Después de cada experimento, las superficies tratadas se han analizado con microscopía electrónica de barrido de emisión de campo (FESEM) disponible en el Servicio de Microscopia Electrónica de Materiales del Servicio General de Apoyo a la Investigación -SAI de la Universidad de Zaragoza.

En este trabajo se describen los fundamentos del láser, la influencia de las propiedades del material en el proceso de interacción láser-materia y la generación de LIPSS en la superficie del metal. Los resultados se han analizado con el fin de determinar la influencia de diversas variables de procesado (longitud de onda del láser, los valores de fluencia, la energía de incubación, la dirección de polarización y la atmósfera de procesado) en las nanoestructuras que se han generado en la superficie del metal.

Escuela de Ingeniería y Arquitectura Universidad Zaragoza

DAO

TRABAJOS DE FIN DE GRADO / FIN DE MÁSTER

Escuela de Ingeniería y Arquitectura Universidad Zaragoza

DECLARACIÓN DE AUTORÍA Y ORIGINALIDAD

(Este documento debe acompañar al Trabajo Fin de Grado (TFG)/Trabajo Fin de Máster (TFM) cuando sea depositado para su evaluación).

D./Dª. Zunuraini Binti Haron,

con nº de DNI Y3090780P en aplicación de lo dispuesto en el art. 14 (Derechos de autor) del Acuerdo de 11 de septiembre de 2014, del Consejo de Gobierno, por el que se aprueba el Reglamento de los TFG y TFM de la Universidad de Zaragoza,

Declaro que el presente Trabajo de Fin de (Grado/Máster) Grado, (Título del Trabajo) Análisis de los procesos de interacción laser- materia en materiales metálicos.

es de mi autoría y es original, no habiéndose utilizado fuente sin ser citada debidamente.

Zaragoza, 13 de Septiembre 2018

Fdo: Zunuraini Binti Haron

ACKNOWLEDGEMENTS

First and foremost, I would like to express my very great appreciation to my supervisor, Luis Alberto Angurel Lamban who was always gave valuable and constructive suggestions during the planning and development of this project and he is the one who helped me in handling the instruments. His willingness to give his time so generously has been very much appreciated.

Besides, I would like to acknowledge the persons of the Department of Science and Technology of Materials and Fluids, of the Aragón Materials Science Institute (ICMA) and the Servicio General de Apoyo a la Investigación (SAI) of the University of Zaragoza for the contribution of materials and equipment involved in this project.

Furthermore, I would like to offer my very special thanks to Cristina Gallego for the help in handling the FESEM machine to analyze the surface morphologies of the samples.

Lastly, I wish to thank my parents and my family in Malaysia for their support and encouragement during my studies.

Thank you,
Zunuraini Binti Haron.

Contents

AIM AND OBJECTIVES

The main purpose of this study is to advance in the understanding of the phenomena that control the interaction on lasers with the surface of metals, in particular, when short pulses lasers are used. The technology has evolved in the last years and the use of these lasers generates a new phenomenology, with new nanostructures on the metal surface that is not completely understood.

Most of the scientific works use fs lasers to analyze these phenomena. We have the possibility of using lasers with pulse widths in the order of 300-800 ps. The main objective of this project is to explore if with these sub-nano lasers it is also possible to modify the surface of the metal creating different nanostructures. In particular we are going to apply this laser technology to modify the surface of Al 6061 alloys that are being used in some applications for aeronautic industry.

In this context we have studied the following problems:

- Observe the effect of interaction laser-material with different wavelengths and pulse widths.
- Determine the most important laser parameters that determine the modification induced on the metal surface due to laser treatment.
- Analyze the effect of scanning angle on the metal surface.
- Determine the effect of laser polarization in the interaction between laser and material.
- Analyze the effect of atmosphere during the laser treatment on the generated surface nanostructures.

This memory is structured into five sections. The interaction of the laser with materials depends on the laser characteristics and materials properties. Both aspects are described in section 1. In addition, I analyze the nanostructures that short pulses lasers are generating on the surface of different materials.

Section 2 shows the characteristics of the lasers that have been used in this work, as well as the experimental techniques that have been used for the processing and the characterization.

The different experiments have been presented in section 3. The full set of laser parameters used in each of these experiments has been collected in Annex III. The work finishes with the conclusions (section 4) and the references (section 5).

1. INTRODUCTION

1.1 Introduction of the topic

The rapid technological developments of laser systems have contributed to some huge progress in both scientific investigations and industrial applications. One example is the aeronautic industry, where laser technologies have played a major role especially in the development of new manufacturing processes. As the number of new airplanes keep growing, nowadays, the improvement and optimization in aircraft security is the main concern and research in this field is necessary in order to avoid any incident that involves hundreds of lives. In this context, ice formation in some critical points of aircraft body is one of the problems that aircraft industry is studying. For instance, according to Aircraft Icing Handbook [1], in the past 50 years, ice has played a role in numerous accidents that have killed crews and passengers and destroyed aircrafts. This icing problem destroys the smooth flow of air and increases drag while decreasing the ability of the aircraft to create lift. Besides, ice can also cause some sensors to give an incorrect reading to pilots. And despite the development of new technology, training and procedures, this unpredictable incident has forced the aviation industry manufacturers to investigate and create a more detail designs in order to solve the problem. One of them is to modify the surface in order to improve the icephobicity of material used on some critical points of the aircraft. To carry out this idea, laser treatments is one of the most effective methods to tailor the surface of material in nano- and microscopic scales. Furthermore, laser technology is mainly used in engineering surface thanks to its high density of energy generates a high increase of surface temperature in a very short time with a minimum alteration of thermal properties and dimensions in the inner side of the material.

Besides, laser could be modulated in time, space and frequency. This versatility has broadened its applications especially in material processing and more attention has been paid to it. There has been a large amount of theoretical and experimental works aimed at understanding the interaction of laser on materials and using this understanding to control the interaction effect for a specific application. However, one of the main limitations of the application of laser technology is how to transfer the results obtained in small areas (as it is done in most academic studies) to the processing of large areas, as it is required in these aeronautic applications.

Aluminum alloys are frequently used in aeronautic applications for their low density and for this reason it is interesting to analyze the possibilities that laser technology can offer in the surface modification of these materials. In particular, it is important to explore the use of the new short pulse laser systems.

1.2 Fundamentals of laser

The term LASER is an acronym and stand for *Light Amplification by Stimulated Emission of Radiation*. Basically, the laser is an electro-optic device that transforms the energy that is generated by electronic transitions of an active medium into a beam of monodirectional light, where all waves have the same frequency (monochromatic) and they are in phase (coherent light). The high spatial coherence achieved with lasers permits extreme focusing and directional irradiation at high energy densities. The monochromaticity of laser light, opens up the possibility of highly selective narrow-band excitations. Moreover, it also allows for control of the depth of heat treatment or selective, non-thermal excitation, either within the surface of the material or within the molecules of the surrounding medium, simply by changing the laser wavelength.

The first laser was developed in 1960 by Theodore Maiman at the Hughes Research Laboratory in California [2], by shining a high-power flash lamp on a ruby rod with silver coated surfaces to produce a red laser light with 694 nanometers wavelength. By now, many types of lasers using various technologies have been created and many others are currently in development.

A laser can operate either in continuous or pulse mode. During the operation in continuous mode, the power is constant over time. This laser is known as continuous wave (CW) and frequently induces heating or melting processes. In the operation of pulsed mode, the energy is emitted in the form of pulses at a certain frequency. The energy of each pulse can reach extremely high energy density values and it is also possible to induce the ablation processes. In the last years, technology has evolved to produce lasers emitting with very short pulses, with pulse widths lower than ns. In this study, we are more interested in the pulse mode operation where the laser radiation interacts with the surface in a short duration with highly energetic pulses. Short pulses maximize the energy transfer in the upper surface layer, reducing the heat that is transferred to the substrate (Figure 1). Furthermore, rapid energy delivery and reduction of the heat-affected areas are the most pronounced advantages of the technique compared to effects induced by longer pulses, which reflect the merit of the method as a potential tool for fabrication of surface structures at micro and nanoscales.

In order to characterize the laser treatments, several parameters can be defined. The pulse repetition rate, also called frequency of the laser, describes the number of emitted pulses per second. The pulse energy can be calculated by dividing the average power by the number of pulses per second (frequency).

$$E_{pulse} = \frac{power\ (watt)}{laser\ frequency\ (Hz)}$$

In consequence, the energy of a pulse is a function of repetition rate. Therefore, a higher repetition rate decreases the energy of a pulse for the same power.

Other than that, it is also necessary to consider the duration of the pulse, also called pulse width, because the shorter the pulse duration, the higher the peak power intensity is applied and the stronger the shock wave is produced. Depending on the material treated, short pulses can have a peak power that can damage the substrate, though it can prevent heat

accumulation of the substrate. The duration of laser pulse can vary between milliseconds (ms) to femtoseconds (fs). For pulses duration between ms-ns, the amount of heat involved in the process is important and melting processes are relevant, even if some ablation is induced. By contrast, while operating with ps-fs pulses, there is no time for heating process to occur and the main effect is associated to ablation. Therefore, choosing the right optimal pulse duration is absolutely necessary to develop the desired surface process.

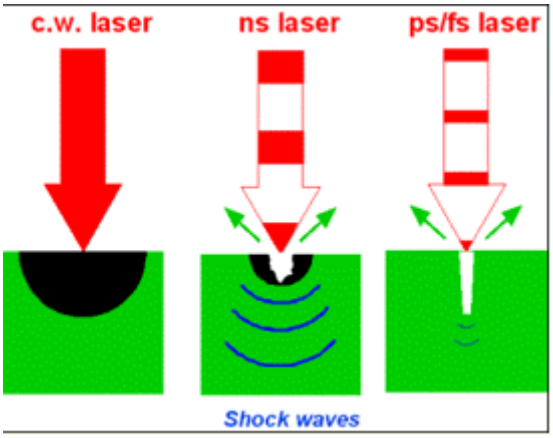

Figure 1: Different effects produced by a laser on the surface of a metal depending on the pulse width.

In order to define other characteristic parameters of a laser treatment we have to define the following parameters. First, it is necessary to calculate the area that the laser beam covers in one pulse, which has two contributions: the area of the laser beam (mm^2) and the area that it is covered due to the displacement of the laser during the pulse width (mm^2);

$$A_{pulse} = (\pi \frac{Diameter\ of\ the\ beam^2}{4}) + (Diameter\ of\ the\ beam \cdot Pulse\ width \cdot Scanning\ speed\ )$$

There are some important parameters that should be considered in this study, which will also play a significant role on the interaction of laser-material. Some of the most important parameters are pulse irradiance, I (kW/cm^2), laser peak power per unit area; and pulse fluence, F(J/cm^2), the energy density per unit area. Both of these magnitudes can be calculated as:

$$F = \frac{P}{fr \cdot A_{pulse}}$$

Where *P* is the average output power and *fr* is the frequency of laser. While irradiance is:

$$I = \frac{P}{(fr.A_{pulse}.t_p)} = \frac{F}{t_p}$$

Where t_p is the pulse width.

Another parameter that should be considered when analyzing the effects of the laser treatment is incubation energy, S (J/mm), the power output divided by the length that has been covered by the spot per second (scanning speed).

When short pulse lasers with high frequencies are used, the overlapping between different pulses along the direction of the laser movement is high and, in consequence, the real irradiance and fluence values are higher than the values that we have just calculated. *S* can be considered as a measure of this overlapping, but when it is too high the analysis will be more complicated.

1.3 Influence of material properties on laser interaction.

The interaction mechanisms between laser radiation and materials are dependent not only on the parameters of the laser beam but also on the physical and chemical properties of the material. The combination of laser parameters and material properties will induce different physicochemical mechanisms that are responsible for different processes such as heating or melting of material, evaporation or plasma formation.

In this context, the material is characterized by its chemical composition and microstructure that determine the type of elementary excitations and the interaction between them. They are responsible for the optical and thermal properties of the material that are also important in the understanding of the different interactions that take place between lasers and materials.

A solid consists countless number of atoms, which were initially separated with each other. When they are close to each other they linked together to form an orderly atomic disposition that can be found in a crystalline material. When atoms are further apart, each of them is independent but when they are closer to each other, electrons are perturbed by the electrons of the adjacent nuclei. This phenomenon causes the combination of the energy levels of individual atoms into many closely spaced electron states to form what is called the electron energy band distribution. Furthermore, gaps may exist between these bands, which normally are not available for electron occupancy. Figure 2 shows the common representation of the electron energy band structure of a solid in an equilibrium interatomic separation.

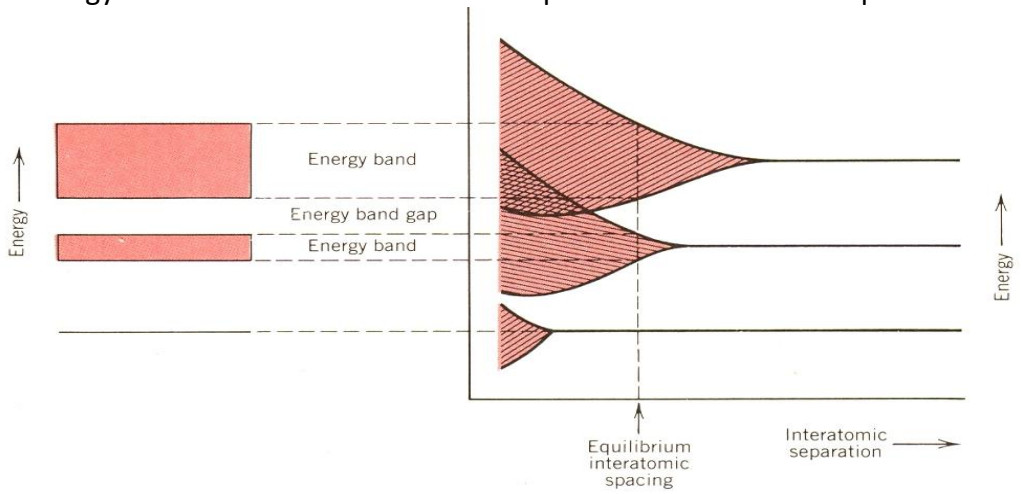

Figure 2: Scheme of the energy bands formation in a solid.

At 0 K, there are four types of energy band structures as shown in Figure 3. The first two structures represent some cases in metallic materials. The band that contains highest-energy

electrons is called valence band. The energy that corresponds to the highest occupied energy state is called Fermi energy, E_f. In some cases, this valence band is partially filled with electrons while for other cases such as the second structure, the valence band is full but it overlaps with conduction band. The conduction band is the next higher energy band which is in most circumstances it is unoccupied by electron. The final two structures correspond to the situation where the valence band is completely filled with electrons but there is an energy gap between this band and the empty conduction band. This is the case for insulators and semiconductors.

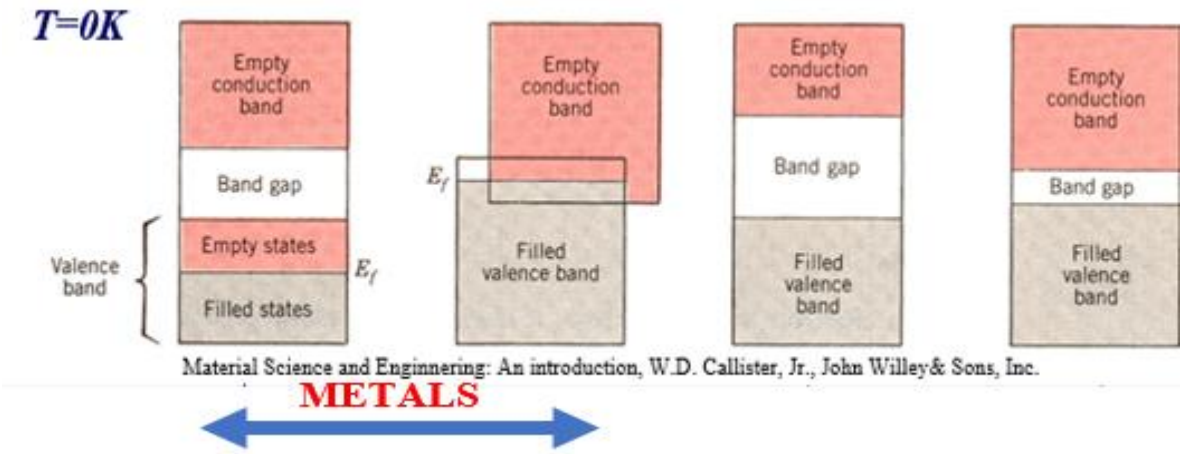

Figure 3: Four types of band structures at T=0K.

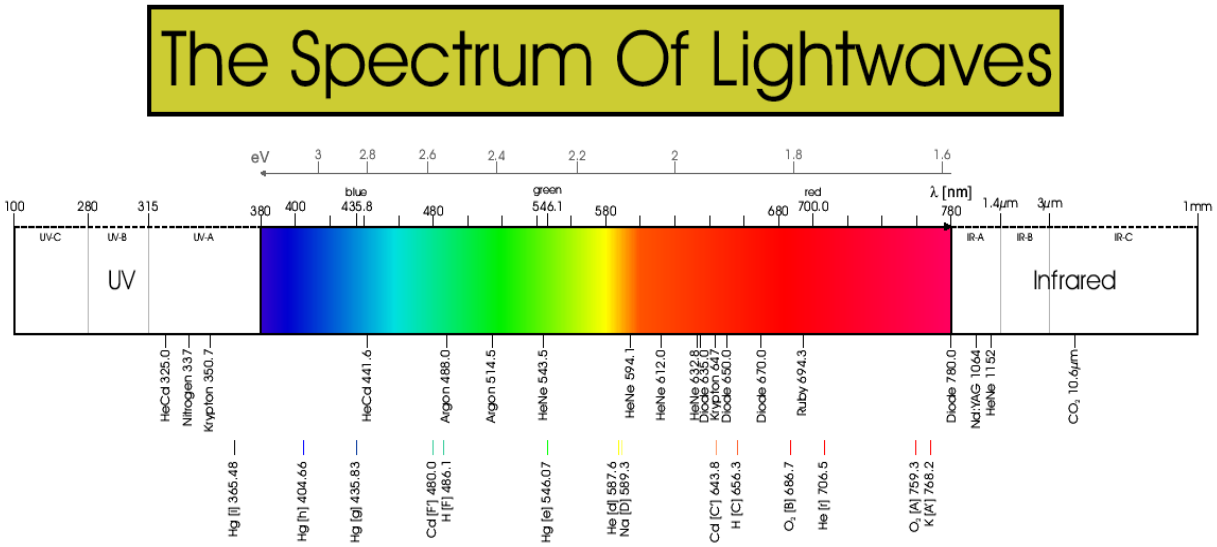

Figure 4: Energy of the photons of a laser depending on its wavelength.

The laser can be considered as a set of photons with a given energy, associated with their wavelength (Figure 4). Obviously, depending on the photon energy induced, interactions will be different depending on the laser used. During this interaction, the electromagnetic waves from the radiation caused the transition of one energy state to another. The most common transitions that occur are electronic, vibrational and rotational transitions.

In most solids, the principal mode of thermal energy assimilation is by the increase in vibrational energy of the atoms. Vibrational waves are also called phonons. Heat is transported by both lattice vibration waves and free electrons. In other words, heat is

transferred by conduction when adjacent atoms vibrate against one another, or as electrons move from atom to atom. In metal, electron mechanism is the most important while in insulators, phonons are the predominant one. This is one of the main mechanisms of interaction when n-IR lasers are used in the processing of materials. If UV radiation are used, the energy of photons is higher and new processes can be induced.

Another point to have in mind is that when a laser radiation interacts with the surface of a material, incident radiation becomes reflected, absorbed, scattered or transmitted, respectively. In metals, most of the absorbed radiation is reemitted from the surface in the form of visible light with the same absorbed wavelength and appears as reflected light. In the range of the electromagnetic spectra associated with the visible light, most of metals have reflectivity around 0.90 and 0.95 due to the small amount of the energy associated with the electron decay is dissipated in the form of heat. Since metals are opaque and have a higher reflectivity, their color is determined by the distribution of radiation that is reflected and not by the absorbed one.

In aluminum, according to the Figure 5, its reflectivity is around 88% to 92% over the visible spectrum and it is almost constant at all wavelengths with only slight changes as the wavelength increase. Hence, resulting in the typical grey color when it is illuminated with white light. This behavior is very similar in the metals that have a grey color (see for instance the spectra of silver in Figure 5). A difference between Ag and Al is that in the case of Al, the reflectivity is very similar when n-IR (λ=1064 nm) or UV (λ=355nm) radiations are used.

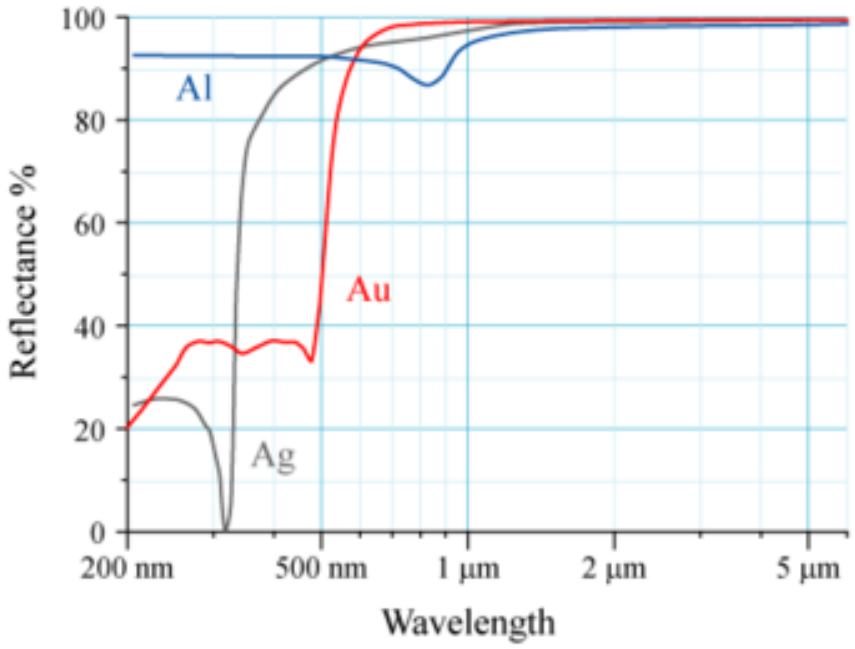

Figure 5: Reflectance of some metals in the range of wavelengths associated with some of the most used lasers.

As we have mentioned before, there are different processes that will occur in the interaction of laser with materials corresponding to its particular physicochemical mechanisms. Absorbed energy leads to rapid heating of the material that results in melting, evaporation or sublimation depending on the amount of absorption (Figure 6). Strong absorption can lead to a rapid heating and ablation that it is caused via acoustic shock wave produced by thermal

expansion. In addition, thermal conductivity and heat capacity are also important physical properties of the materials because they determine the volume of the sample that is affected by laser irradiation and the maximum temperature that is reached.

By definition, thermal conductivity is the amount of heat that passes through a unit area per unit of time when a temperature difference of one degree is established between the two surfaces. While heat capacity is the amount of energy required to raise the temperature of the unit of mass by 1 °C and latent heat of fusion is the energy necessary to change the state from solid to a liquid at constant pressure of the unit mass of material.

Surface heating and melting processes occur when the internal energy of the material increases, typically by the application of heat, which raise the material's temperature to the melting point. This process normally occurs when using low irradiance of the laser. While ablation is the process of removing material from a solid surface by irradiating it with a laser beam. When a high irradiation is used, ablation of materials will result in formation of plasma.

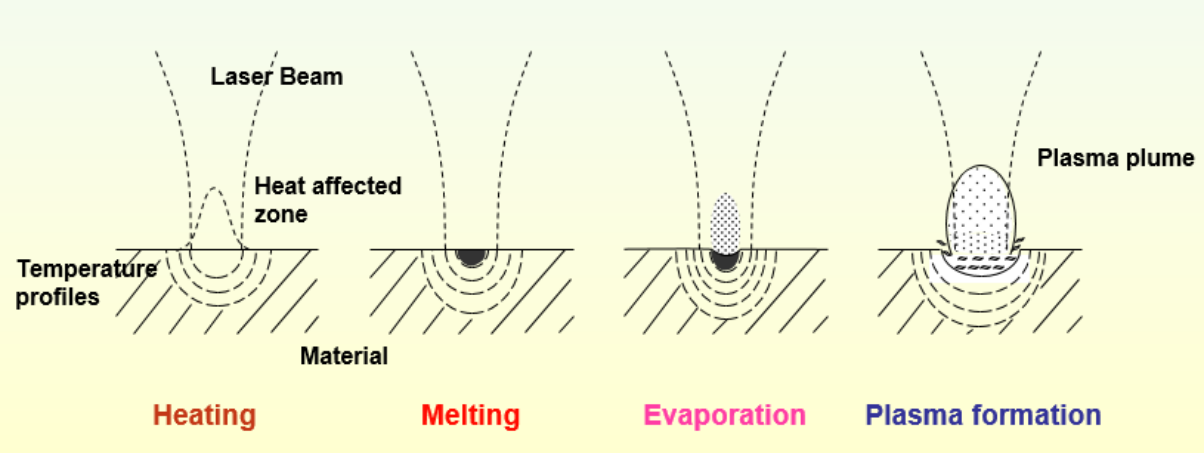

Figure 6: Different processes that are induced in the surface of a material due to laser interaction

1.4 Generation of nanostructures in surfaces

Due to the appearance of short-pulse lasers, new phenomena have appeared. One of those induced processes during laser treatments that aroused interest in many research works is the formation of Laser-induced periodic surface structures (LIPSS), often called *ripples.* These laser-induced periodic surface structures (LIPSS) are generated when a surface is irradiated with a linearly polarized radiation. Some works propose that the formation mechanism is due to the interference of the incident wave with a surface plasmon wave [3]. According to the experiment carried out on Nickel [4] (Figure 7), this periodic pattern can also be produced by using Cylindrical Vector Beams (CVB) (radially polarized radiation) resulting a smaller periodicity of the ripples compared to that obtained by linearly polarized radiation. Most of the investigations about the formation of LIPSS were conducted by using femtosecond laser, where the sample being irradiated at the same spot while varying the number of pulses or pulse durations.

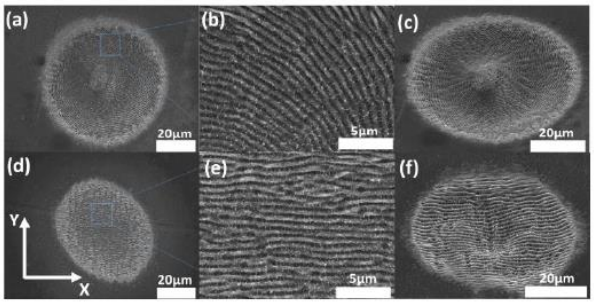

SEM images of surface profiles after fs-irradiation with radial (a)-(c), and linear polarization of the electric field of the incident beam (d)-(f). J=0.36J/cm², τ_P=170fs, NP=200.

Figure 7: Image from article [4] corresponding to the formation of LIPSS by using cylindrical vector beams (CVB).

LIPSS can be generated in almost any surface including metals, semiconductors and dielectrics. There are also new achievements in the attempt to form a highly regular LIPSS, as being elaborate in article [5] . Aluminum exhibits low regularity of LIPSS and only Ti, Mo and steel are able to obtain the high regularity of LIPSS (see Figure 8) but with further decreasing of laser wavelength, it is predicted that majority of analyzed metals in that study can form a LIPSS structure with a high regularity.

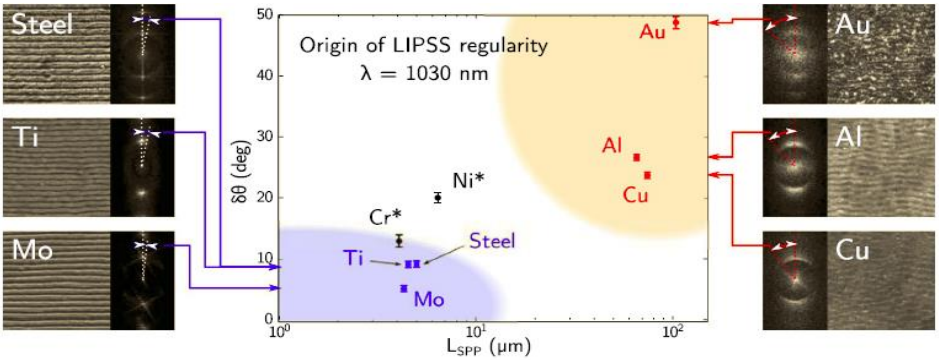

Figure 2. DLOA $\delta\theta$ as a function of the calculated mean free path L_{SPP} of SEW. SEM images obtained with the same magnification are shown for metals studied in this paper (irradiation conditions are given in Table 1) with the corresponding 2D-FT images. Note that the angular sizes displayed on the 2D-FT are comparable to but not as precise as the DLOA used here. Asterisks stand for DLOA $\delta\theta$ data for Cr and Ni, estimated from the images of refs 15 and 26 respectively. Vertical error bars were evaluated from the convergence of the DLOA $\delta\theta$ (see Materials and Methods). The LIPSS fabricated in this work, which exhibit high and low regularities, are marked respectively by blue and pink. Materials located in the blue-colored area (respectively in pink-colored area) are suitable (respectively non-suitable) for the HR-LIPSS formation.

Figure 8: Image of Figure 2 from article [5].

There are two types of LIPSSs forms when a solid material is irradiated by ultrafast laser radiation (Figure 9). The first type is the low-spatial-frequency LIPPS (LSFL), which exhibits periods close to or slightly smaller than the irradiation wavelength. LSFL can be classified into two types of LIPPS, LSFL-I and LSFL-II. LSFL-I usually oriented perpendicular to the laser beam polarization and has periodicity closer to the wavelength. This mechanism occurs on strong absorbing materials, such as semiconductors and metals [6]. While on dielectrics, LSFL-II is formed. These structures are usually oriented parallel to the laser beam polarization and have spatial periods around $\Lambda_{LSFL} = \lambda/n$. The second type of LIPSS is the high-spatial-frequency (HSFL) with periods smaller than half of the irradiation wavelength. HSFL are oriented either parallel or perpendicular to the laser beam polarization depending on the material [6] , and they can be observed in two types of forms. The HSFL-I, which is mainly observed on dielectrics and semiconductors consists of very narrow periodic grooves with widths of a few

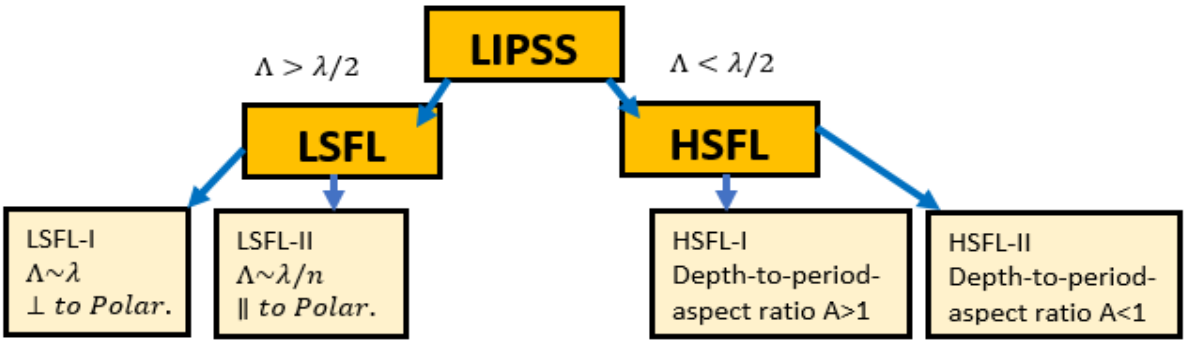

Figure 9 :Classification scheme of fs-laser induced periodic surface structures.

tens nanometer only and the groove depth can reach up to several hundreds of nanometers, resulting in depth-to-period aspect ratio A>1. On the other hands, HSFL-II exhibit groove depth of only a few tens of nanometers along with periods approaching the sub-100 nm range, resulting in a depth to period aspect ratio A<<1. This type of HSFL is mainly observed in metals.

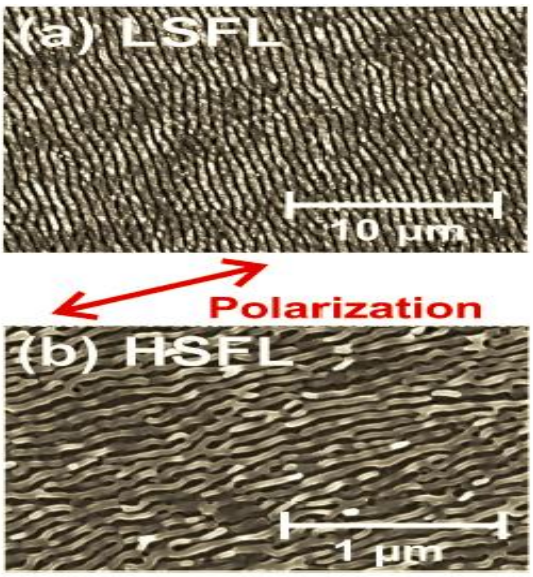

Fig. 2. Scanning electron micrographs of two different types of LIPSS formed on titanium alloy (Ti6Al4V) surfaces after irradiation with fs-laser pulses [30 fs, 800 nm, 1 kHz]. (a) LSFL [$\phi_0 = 0.11$ J/cm^2, $N \sim 56$]; (b) HSFL [$\phi_0 = 0.08$ J/cm^2, $N \sim 560$]. Note the different magnifications.

Figure 10: Figure 2 from article [6] shows the example of LSFL and HSFL formed on titanium alloy after being irradiated with 800 nm,30 fs and 1 kHz of fs-lasers pulses. The LSFL have periods of $\Lambda_{LSFL} \sim (620 \pm 80)$ nm and are formed perpendicular to the laser beam polarization, while the HSFL exhibit periods of $\Lambda_{HSFL} \sim (80\ 20)$ nm only and are oriented parallel to the polarization.

As we mentioned earlier, improving the icephobicity of material used on the aircraft wings can reduce the icing problem in aircraft industry, this can be achieved by forming LIPSS on the material surface. Investigations about LIPSS in article [6] said that the wetting behavior of material can be modified by forming LIPSS on its surface, an increase of surface roughness in nanoscopic scales makes the air remains trapped underneath of the liquid, thus the surface becomes more hydrophobic. Some research also applied this theory in the attempt to mimic the Yarrows spiny lizard (Sceloporus jarrovi) skin that exhibit a hydrophobicity surface with a nanostructure of spikes in the range of about 100 nm [7]. Other technological approach by

using the formation of LIPSS are for generating structural color, manipulating the growth of cell and bacteria film as well as reducing friction in tribological applications [6].

According to previous research works, the characteristics of the obtained LIPSS can vary tremendously depending on various parameters. Even it is often difficult to control the quality of LIPSS formation, it is believed that parameters such as laser fluence, polarization direction, irradiation wavelength, number of pulses, scan speed and spot size are the keys to manipulate the occurrence of LIPSS. The laser fluence has a great impact on the formation of LIPSS, a different value of fluence can create a different type of LIPSS (LSFL or HSFL). According to article [8], ripples are clearly visible at lower fluence values and if the value of fluence is too high, the high occurrence of ablation phenomenon may cause the absence of ripples on the Aluminum surface.

2. EXPERIMENTAL METHODS

2.1 Laser system specification

Experiments were performed with two types of lasers fabricated by Rofin-Sinar, both emitting pulses in the sub-nanosecond regimes, one with a wavelength of 1064 nm (near Infrared (n-IR)) and the second with 355 nm, in the UV region of the light spectra. The infrared laser operates with a maximum output power 8 W, it can achieve a high repetition rate up to 800 kHz, the pulse width is 800 ps and the spot diameter is 25 µm. All the experiments presented in this work have been performed using a lens of 160 mm. Figure 11 shows the infrared laser machine and the calibration curve of this laser for the full range of available frequencies. Additionally, a source of electrical current controls the laser power.

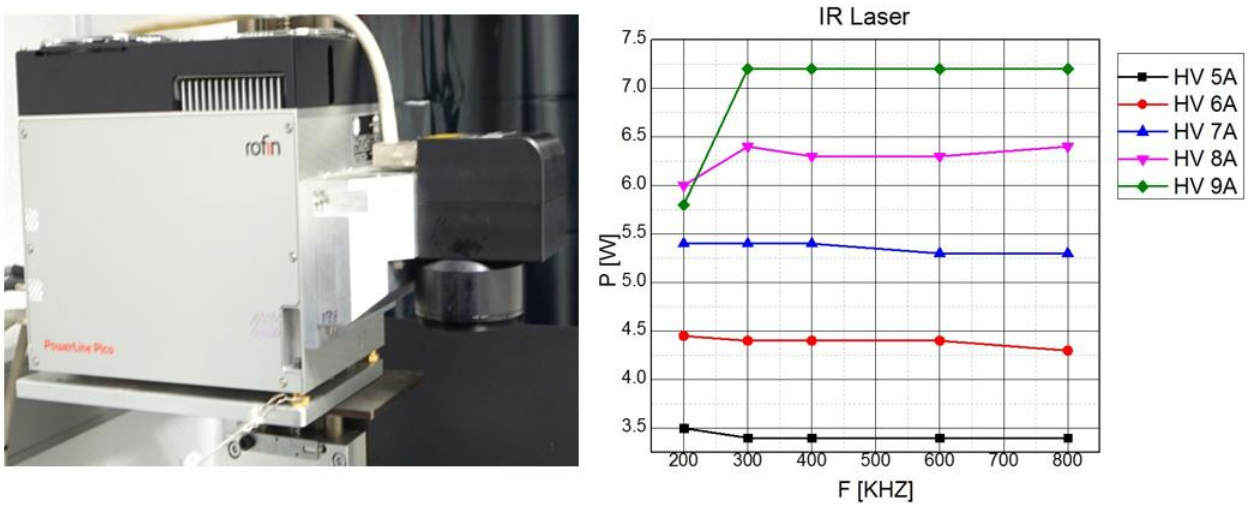

Figure 11: Image on the left is the infrared laser machine; Model: PowerLine Pico 10-1064, while graph on the right shows the variation of IR laser power as frequency increases.

The UV laser is presented in Figure 12. Also fabricated by Rofin-Sinar, the maximum power is 3 W and the highest repetition rate is the same as in the infrared laser, 800 kHz. This laser operates with a spot diameter around 17 µm and with a pulse duration equal to 300 ps. Figure 12 also shows the calibration curve for the different frequencies. In this case the maximum power that can be reached with the laser depends on the frequency. Another difference between both lasers is that in this case, the height adjustment for the focus length of UV laser can be done automatically by software. This possibility increases the level of reproducibility of the different experiments.

Experiments can be done with two different configurations: beam scanning or line scanning. In the first case, the sample is fixed and the laser moves along the surface of the sample. In the second configuration, laser making a line while the sample moves in the perpendicular direction. In this case, one of the incident angles is maintained during the full treatment, obtaining a more uniform laser treatment.

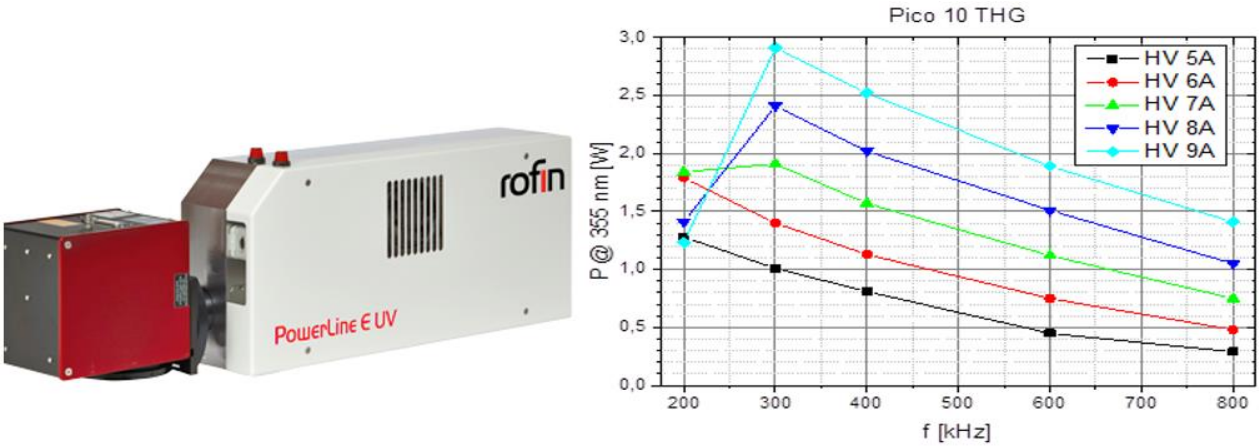

Figure 12: Left: The UV laser machine that was used in this experiment, right: calibration curves of the relation between electrical current and power for the UV laser for different frequencies.

The aluminum sample was positioned perpendicularly to the incident beam and experiments were conducted in two types of atmospheres, in air and/or Argon atmosphere. During the experiment in Ar, we used a special chamber with a quartz glass attached on its lid to allow the penetration of laser radiation. After making sure the lid was securely closed, air molecules inside the chamber were evacuated by pumping Argon molecules into it. The pressure inside of the chamber was being monitored until it reached 0.4 atm over pressure, (e.g. 1.4 atm in Ar atmosphere). Figure 13 shows the chamber that was used in this experiment.

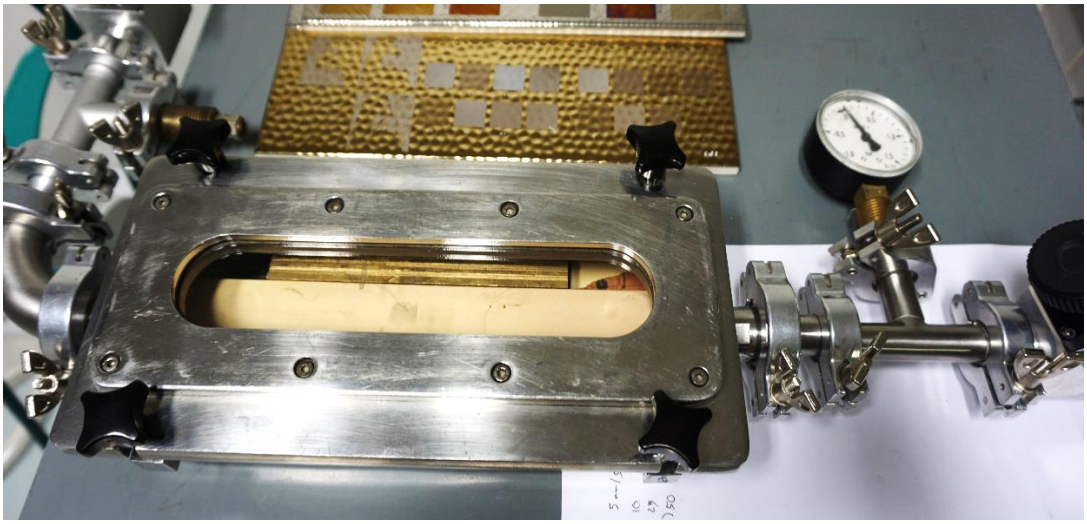

Figure 13:The steel chamber with a pressure gauge attached with it and it was securely closed with its lid.

2.2 Material

The main focus of our experiment is the interaction of laser on the surface of Aluminum 6061. This type of metal is a precipitation-hardened aluminum alloy, containing around 0.8% of Magnesium and 0.4% of Silicon as its major alloying elements. Originally called “Alloy 61S”, it was developed in 1935 [9]. It has good mechanical properties, exhibits good weldability and is very commonly extruded. This 2.7 g/cm^3 metal is one of the most common alloys of aluminum for general-purpose use. The melting point of this metal is approximately 585 °C and its thermal conductivity is between 151 to 202 W/(mK). Another important thermal property are the specific heat capacity and the thermal expansion coefficient, which reach values of about

897 J/ (kg. K) and 2.32 x 10^{-5} K^{-1}, respectively. The thickness of the Aluminum plates used in this work is equal to 3.2 mm (see Figure 14). Before using the sample, it is advised to clean the aluminum surface with ethanol to avoid any interference such as dust or fingerprints during the interaction with laser.

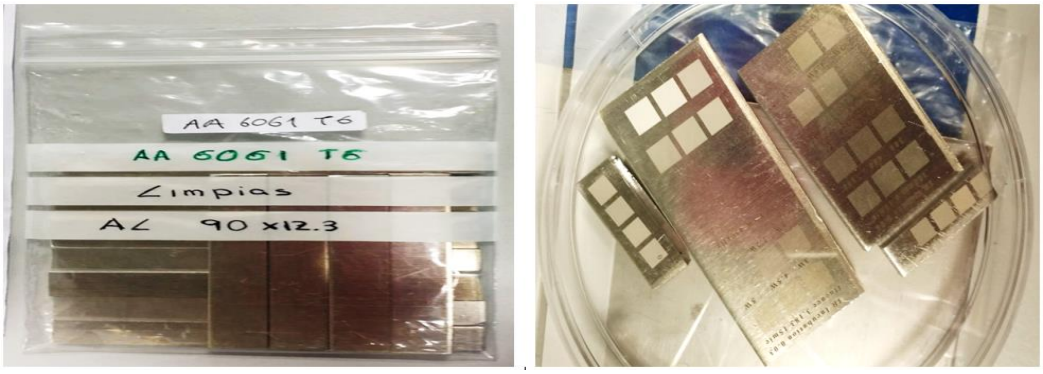

Figure 14 :The example of aluminum samples used to carry out the experiment of this study.

2.3 Field emission scanning electron microscopy

Samples have been analyzed using the Field emission scanning electron microscope (FESEM) that is available at the Servicio de Microscopia Electrónica de Materiales del Servicio General de Apoyo a la Investigación–SAI de la Universidad de Zaragoza. The scanning electron microscope is a technique of electron microscopy, which is capable of producing high resolution images on the surface of the sample by scanning it with a focused electron beam. In the case of non-conductive samples, they are usually coated with a very thin layer of gold or carbon, which gives its conductive properties. The technique is called “sputtering”.

This type of microscope works in vacuum so that the electron moves without interaction with other molecules. The microscope is internally equipped with detectors that collect the energy of the electron and transform it into images. When the surface of the sample is scanned with a beam of energetic electrons, variety of signals are produced. These signals include secondary electrons, backscattered electrons, diffracted backscattered electrons (EBSD), photons, visible light and heat. Secondary electrons and backscattered electron are commonly used for imaging samples, secondary electrons are most valuable for showing morphology and topography on samples while backscattered electron are for illustrating contrast in composition in multiphase sample. EBSD are used to determine crystal structures and orientations of minerals. The important feature of FESEM is the three-dimensional appearance of its images because of its large depth of field. A scanning electron microscope also capable of magnifying objects in the order of 100,000 times, thus, produced a detail three-dimensional image [10] .

3. RESULTS AND DISCUSSION

3.1 Analysis of the influence of the laser wavelength on the structures formed on Aluminum surface.

Figure 15 shows the original surface of Aluminum 6061 sample before the treatment. It can be seen that the surface is not completely smooth; some lines from lamination process are observed on it. The sample did not undergo a further polishing process.

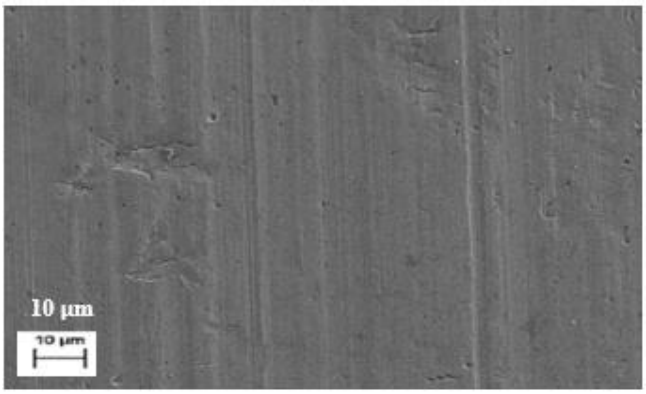

Figure 15 :The FESEM image of non-treated Aluminum surface.

The samples have been treated by using the two lasers that have been previously described. When the n-IR radiation is used, the interaction on the sample is expected to be more thermal, while in the case of the UV radiation, some differences on the results are expected to occur.

3.1.1 Analysis of the changes induced by n-IR radiation

An initial set of experiments has been performed in order to observe the different microstructures that can be obtained in the Al 6061 surface. Figure 16 shows the aspect of the sample after being processed with the n-IR laser by increasing the laser power and maintaining the rest of laser parameters (frequency 800 kHz, laser speed 100 mm/s and distance between lines 15 microns).

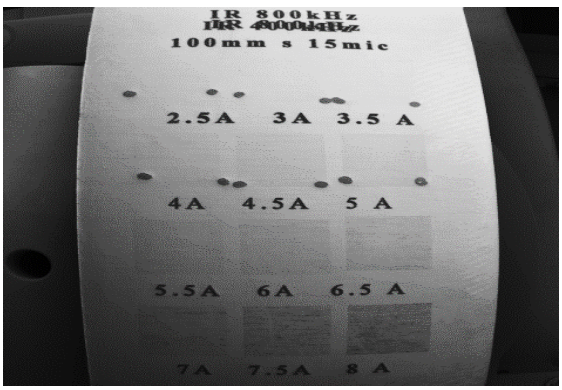

Figure 16: The surface of Aluminum 6061 after being treated with IR irradiation at high repetition rates 800 kHz and scanning speed 100 mm/s.

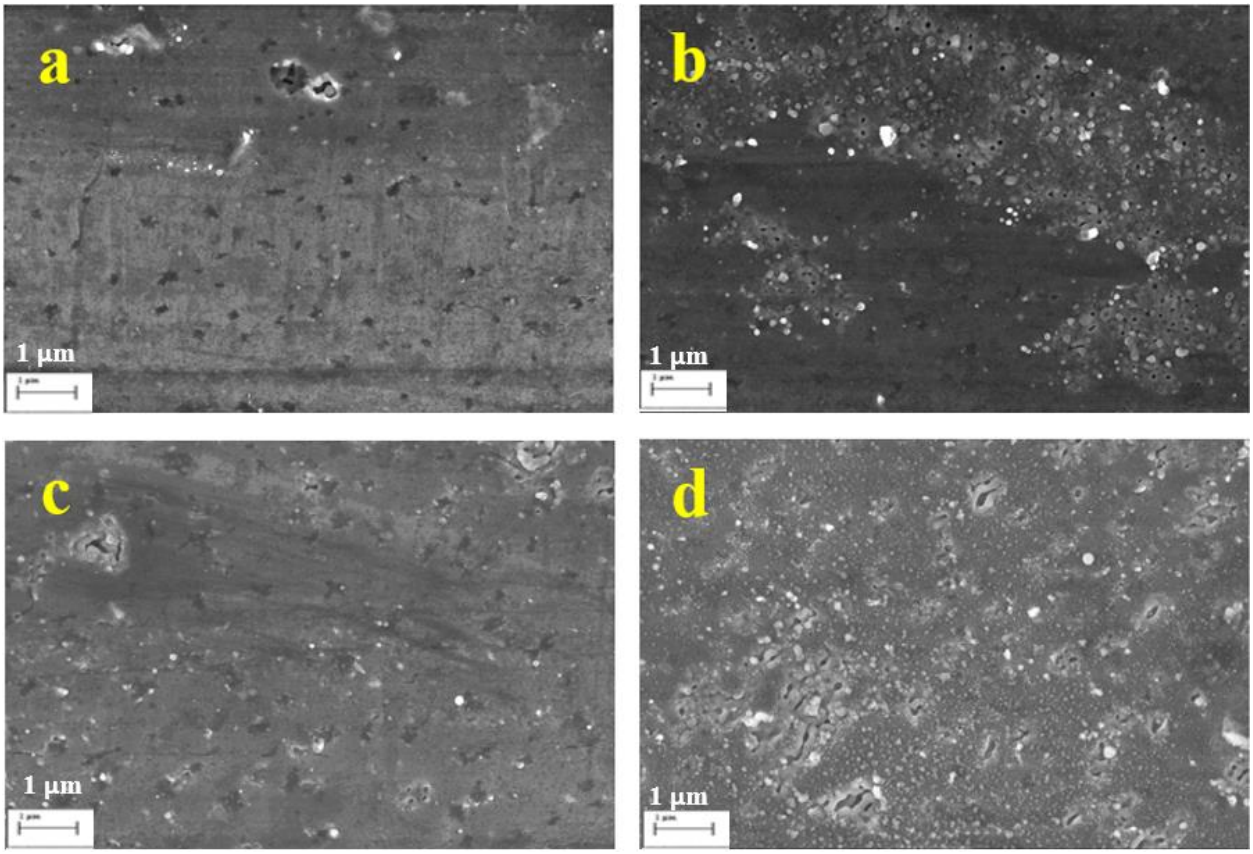

Figure 17: Surface morphologies of samples treated with the n-IR laser at high frequency (800 kHz). Different levels of laser powers have been used: ***(a) 2.965 W, (b) 3.915 W, (c) 5.34 W and (d) 6.29 W.***

Figure 17 shows the surface of the samples processed with a frequency of 800 kHz and with the laser parameters detailed on Table 1 in Annex III. These FESEM micrographs show that at low current values (2.5 A, 3A and 3.5 A), the surfaces are almost unaffected by the laser, and a minimum power of 2.965 W is needed to start to modify the surface. It is observed that the pulse fluence has reached values between 0.76 J/cm^2 and 1.60 J/cm^2 and that in most of the experiments, the surface has been slightly melted. It is also observed that the treatment is not uniform throughout the surface and more effective in the regions that are located close to the defects that are present on the surface, indicating that in these areas, laser absorption is higher.

In order to increase the fluence values, new experiments with a lower frequency (400 kHz) have been repeated (see Fig. 18). In these cases, the amount of molten material is increased, and with the higher fluence values, the laser treatment can modify the full surface. Figure 19 shows a detail image of sample *h* showing the molten material with an aspect of cotton-cloud. This structure covers the full surface and impedes the focalization of the FESEM observation, indicating that it is a non-conductive phase, which is probably Al_2O_3.

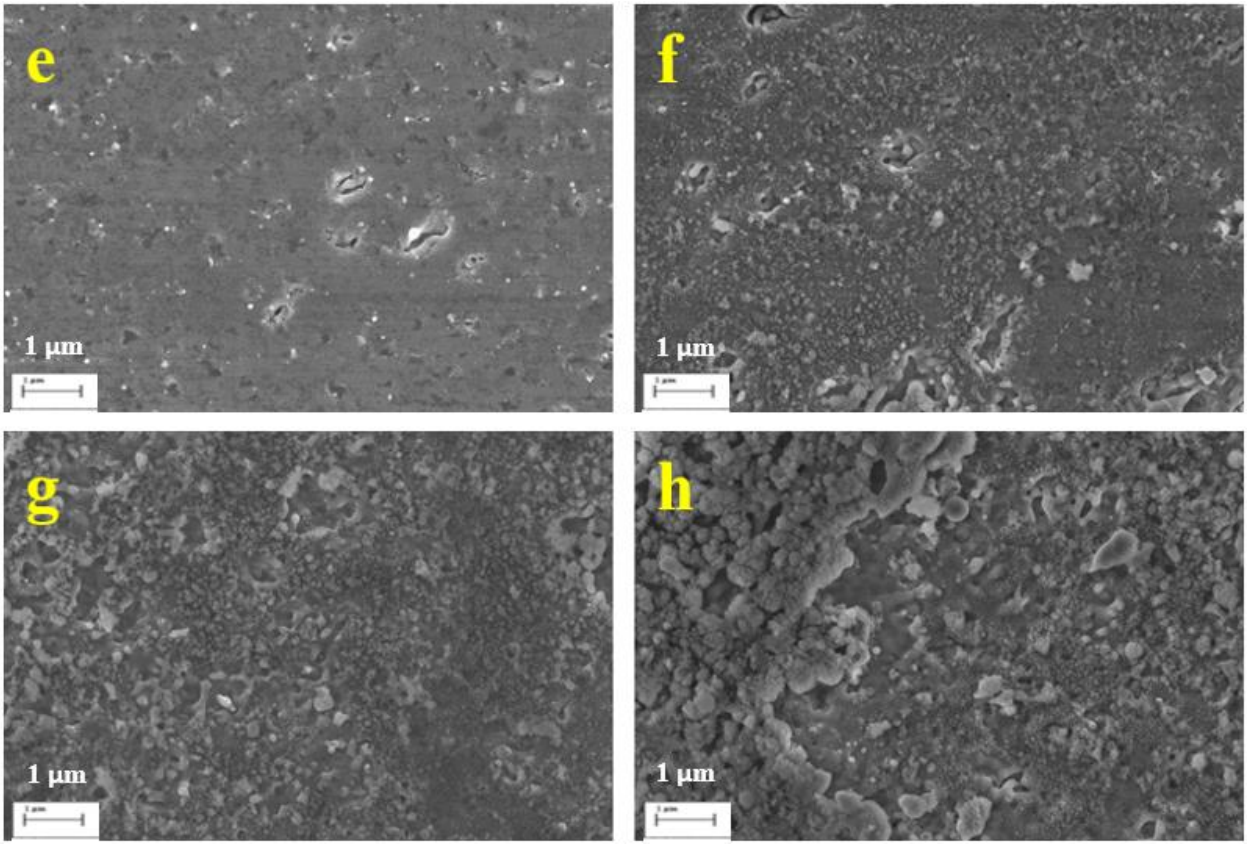

Figure 18: Surface morphologies of samples treated with the n-IR laser at low frequency (400 kHz). Different levels of laser powers have been used: ***(e) 2.965 W, (f) 3.915 W, (g) 4.865 W and (h) 6.29 W****.*

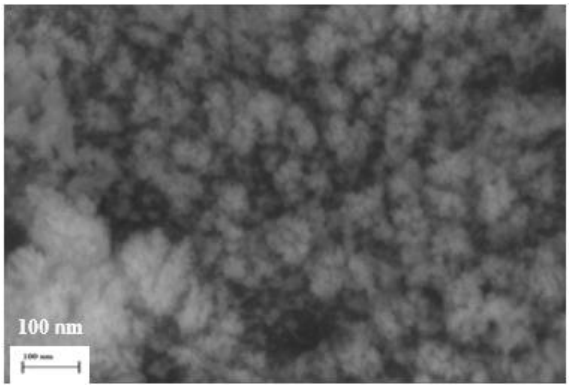

Figure 19: Detail of the surface morphology of sample h treated with the n-IR laser at higher irradiance value (4004.3 MW/cm^2).

In order to explore the possible influence of the different laser processing parameters, we have designed several experiments in which frequency and laser power have been modified but maintaining the fluence and incubation energies values. Figure 20 shows the FESEM images of the treated samples adjusting the laser parameters in order to reach a fluence value of 2.04 J/cm^2 and an incubation energy of 0.03 J/mm. The particular set of parameters in each sample is presented in Table 3 in Annex III. There are only slight differences when the surfaces of the three samples are compared. And in this case, the effects of laser radiation on the regions close to the defects are also more severe compared to the other regions of the surface.

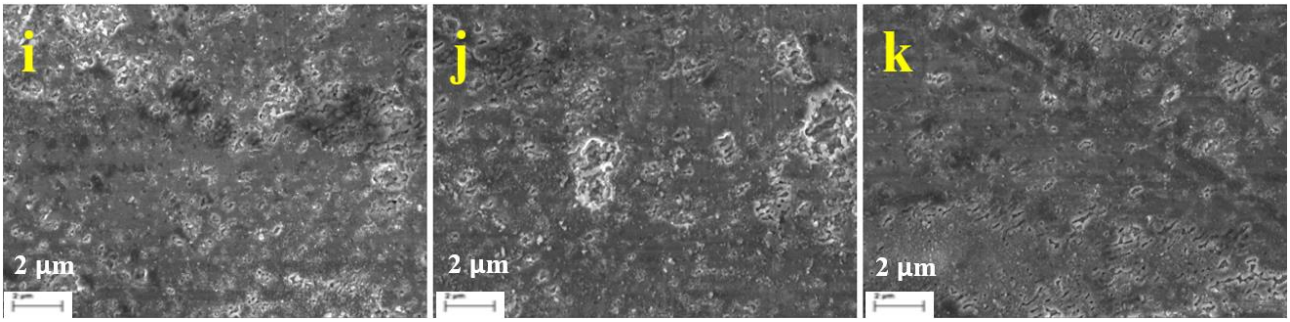

Figure 20: Surface morphologies of samples treated with the same value of fluence 2.04 J/cm² and incubation energy 0.03 J/mm. Samples were treated with different in frequencies, scanning speeds and powers: sample ***(i) 300 kHz, 100 mm/s, 3W, (j) 500 kHz, 167 mm/s ,5W, and (k) 600 kHz, 200 mm/s, 6W.***

Based on the results of all experiments conducted by using n-IR laser, it is proven that the interaction of this laser on Al 6061 surface is more thermal. We can conclude that the main reason of this phenomena is probably due to the wavelength of the IR laser.

3.1.2 Analysis of the changes induced by UV radiation

A similar study has been performed using the UV laser. Figure 21 shows the surface morphologies that have been obtained with two different fluence values: 1.74 and 1.23 J/cm^2. As it can be observed, the aspect of the surface is completely different, inducing modifications in the micro- and nanometric scale. Micrographs with the higher magnification, show that the nanostructure induced on the surface presents some ripples. It is important to mention that the fluence values used in these experiments are smaller than those used with the n-IR laser, and, in consequence, the effect of the UV laser on the surface is much stronger.

If the fluence value is reduced, for instance, by increasing the laser frequency up to 800 kHz, the main effect of the laser is melting process. Figure 22 shows the nanostructures that can be obtained in these surfaces. It is observed that with these conditions a nanodot structure is created and that by controlling the laser parameters it is possible to modify the order of the nanostructure. There is a minimum value of energy to create these structures. For instance, Figure 23 shows the surface morphology of a sample that has been processed with 0.16 J/cm^2. A very thin layer of molten material is obtained, but not enough to induce some order on the metal surface.

According to the results obtained with these experiments, it is obviously showing that a large modification of the fluence values will give a profoundly different nanostructure. For this reason, the rest of the work has been focused in analyzing the effect of the UV radiation on the Al6061 surface.

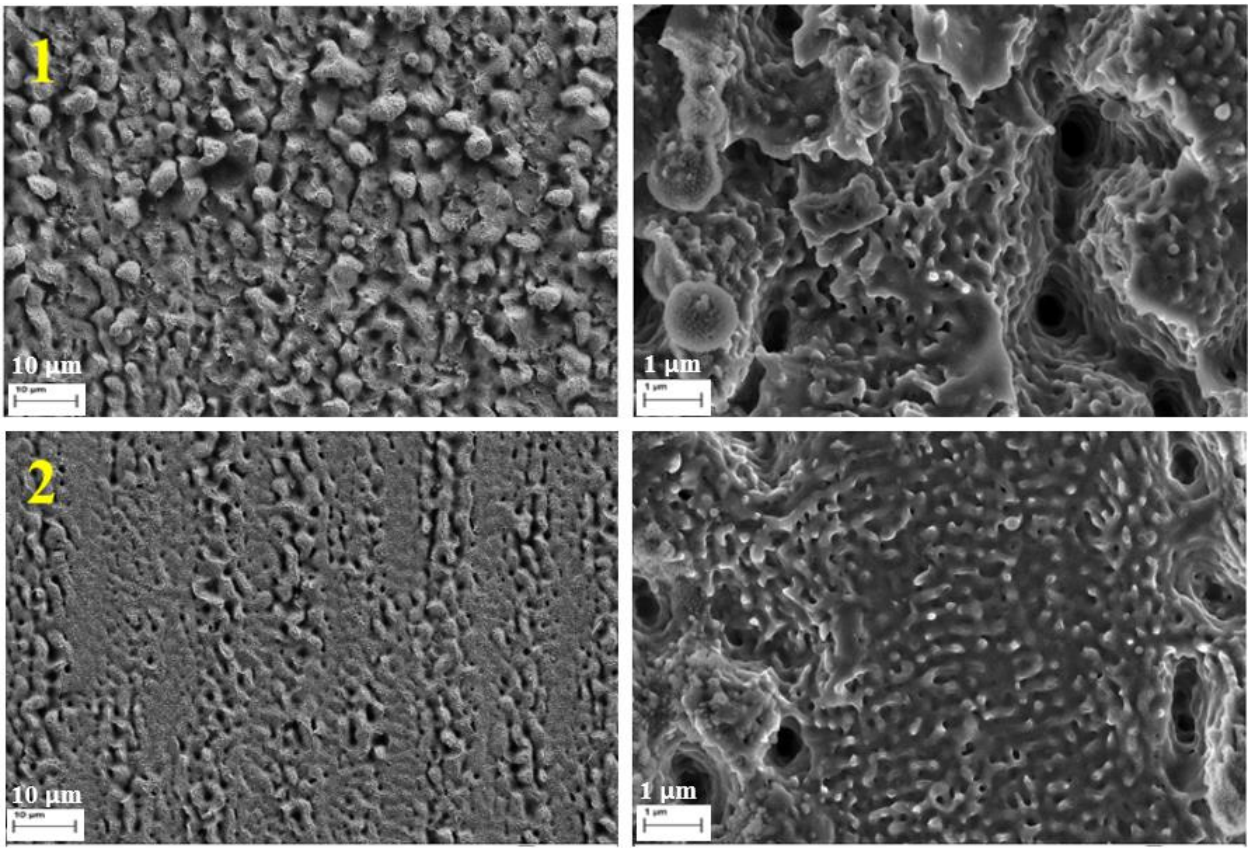

Figure 21: FESEM images of samples treated at low repetition rates of laser, 400 kHz with scanning speed equal to 100 mm/s. Images on the left is taken at magnification of 1000 X while on the right side taken at magnification of 10000 X. Different structures formed at different values of irradiance and fluence; ***(1) 5800.8 MW/cm² , 1.74 J/cm2, (2) 4111.9 MW/cm² ,1.23 J/cm².***

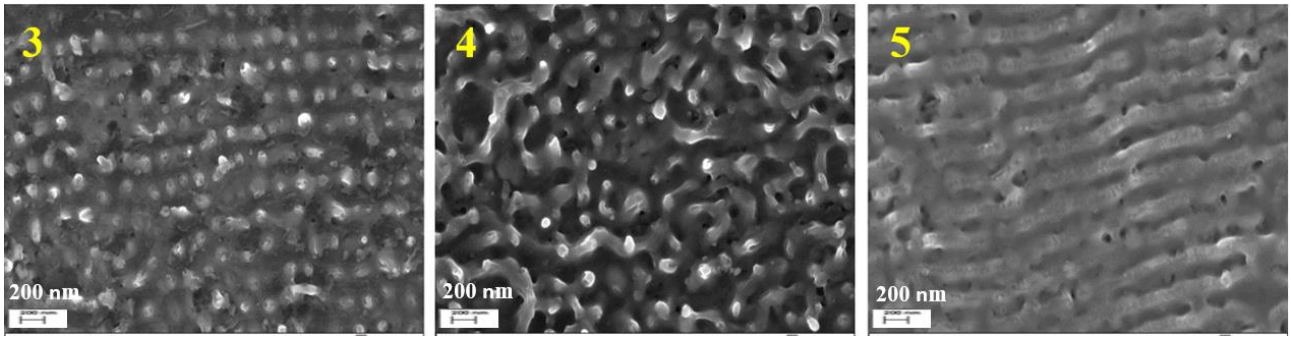

Figure 22: Surface morphologies of samples treated at frequency of 800 kHz with different values of irradiance and fluence; ***(3) 917.8 MW/cm² ,0.275 J/cm², (4)1376.7 MW/cm², 0.41 J/cm², (5) 2569.9 MW/cm², 0.77 J/cm².***

Also, the cross-section of the samples has been analyzed in order to obtain some information about how deep is the laser interaction. The aspect of a sample, which is irradiated by using UV irradiation at 300 kHz with a fluence value equal to 1.43 J/cm² is presented in Figure 24. This fluence value is enough to induce the ablation of the material, generating jagged structures on the treated area (Figure 24 (c)). We can see that these jagged structures are not uniformly formed over the surface, the height of each peak is different to one another. Yet, we cannot see this mechanism from the top view of the sample as the ablated structures are formed randomly on the surface.

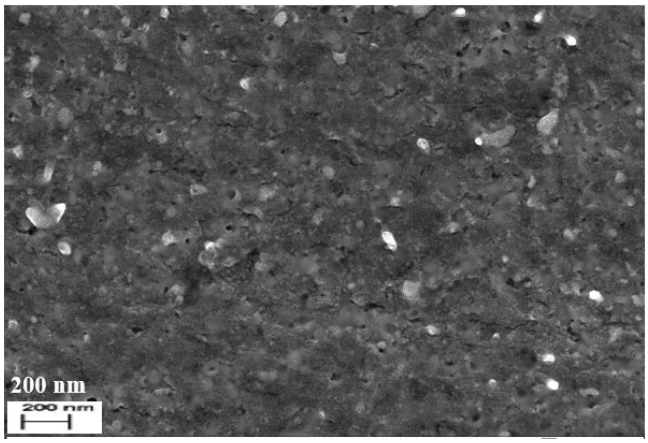

Figure 23: Surface morphology of a sample treated by using UV laser at 800 kHz with irradiance equal to 550.7 MW/cm^2 and fluence value is 0.16 J/cm^2.

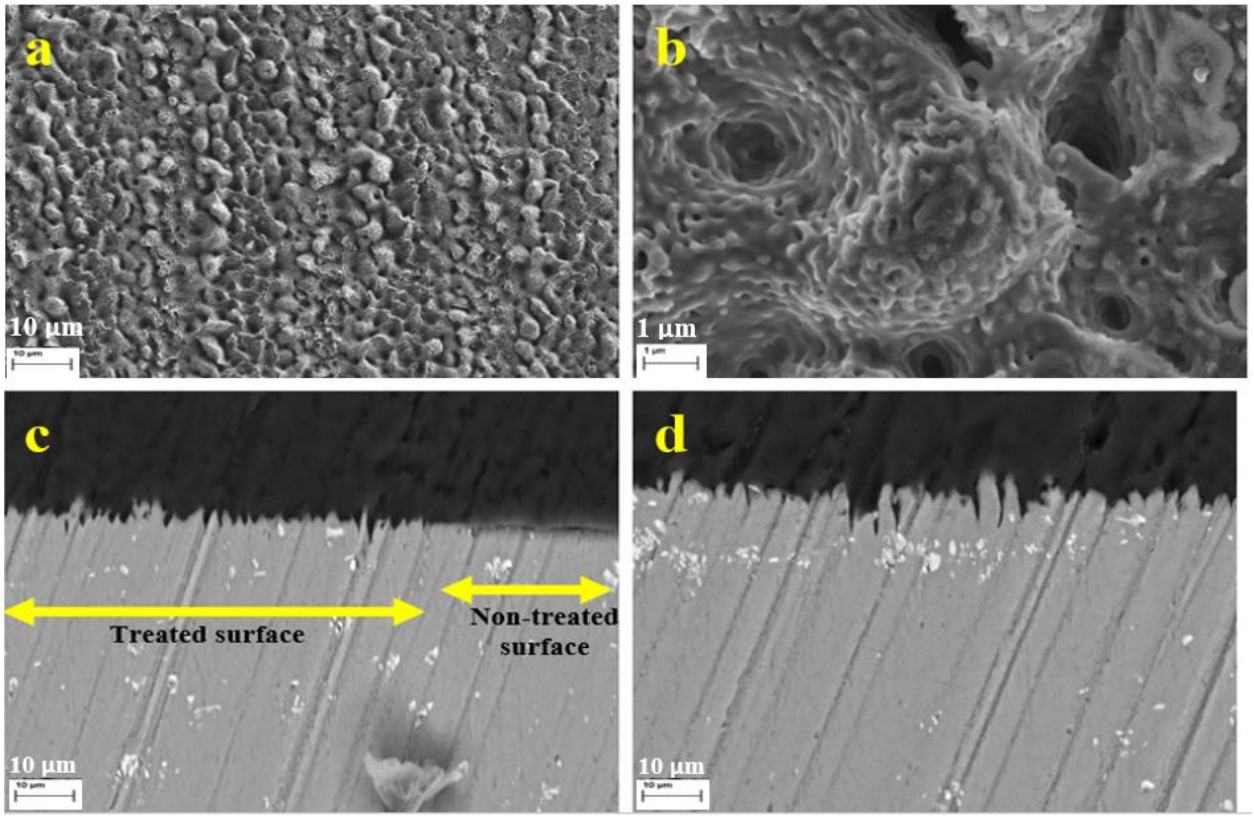

Figure 24 :The FESEM images of a sample treated with UV laser at frequency equal to 300 kHz with fluence value about 1.43 J/cm^2. The first image shows the ablated structures from the top view of the sample, the second image is the view at close distance taken at magnification of 10000 X, while the last two images are from the side view of the sample.

3.2 Influence of fluence values on Aluminum surface

As it has been presented in the previous section, in some conditions, sub-nano UV lasers are capable of generating similar LIPPS structures that are formed by using fs lasers. One of the main laser parameters that determine the formation of structures on the Aluminum 6061 surface is the laser fluence. To analyze the effect of fluence values on the interaction of laser-material, laser fluence was modified by changing the power output while keeping the frequency fixed. The change in fluence value will result in the change of irradiation too, however as the pulse width that we used in this study is fix, both magnitudes are proportional. We classified the results obtained into two types, first, the results obtained using low repetition rates of laser (<400 kHz) and the second one with high repetition rate values (800 kHz).

A. Influence of fluence values at low frequency *(300 kHz and 400 kHz).*

When low frequency values are used, for a given laser power, the energy of each pulse increases and higher fluence values can be reached. The FESEM images of Figure 25 show the evolution of structures formed on the surface due to the ablation process as the fluence values decreases. These experiments were conducted under the influence of Ultraviolet irradiation with a frequency of 400 kHz. From the surface morphologies in Figure 25, we observed that the ablated structures formed on the sample *III* with a fluence value equal to 0.88 J/cm^2 are almost unnoticeable compared to sample *I*. Another aspect that it is observed is that when the fluence increases, the aspect is more uniform (see sample I). When the fluence decreases, the distribution energy of the beam is observed, showing clearly the scanning lines of the laser, that in these experiments were separated by 15 microns. Remember that the beam diameter has been estimated to be 17 microns.

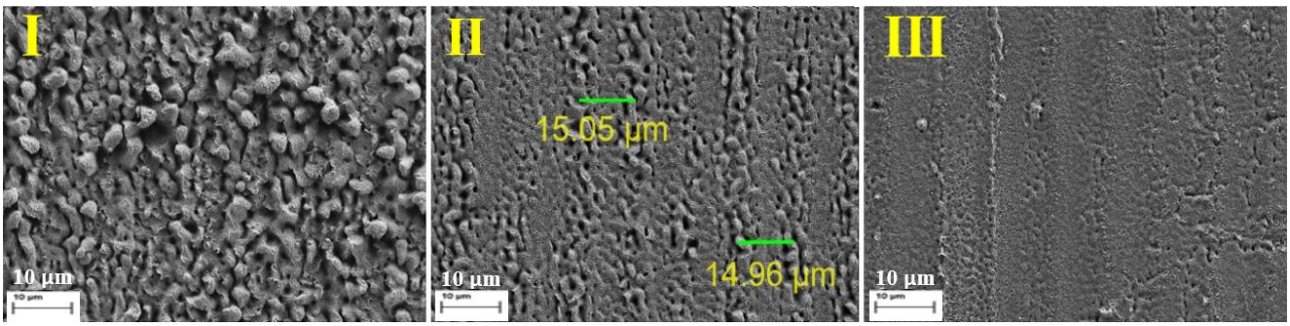

Figure 25: FESEM images of three samples treated with UV radiation at 400 kHz with scanning speed about 100 mm/s. Each of the samples have different level of power and fluence values: ***(I) 1.58W ,1.74 J/cm^2, (II) 1.12 W, 1.23 J/cm^2, and (III) 0.8 W, 0.88 J/cm^2.***

To be able to attend higher fluence values new experiments with a lower frequency (300 kHz) have been performed. Figure 26 shows the results obtained after the laser treatments, we can clearly observe that the size of ablated structures on the surface is increased when fluence value increases. According to table 5 in Annex III, sample IV has the highest energy of pulse compared to other samples and it also exhibits the biggest size of ablated structures.

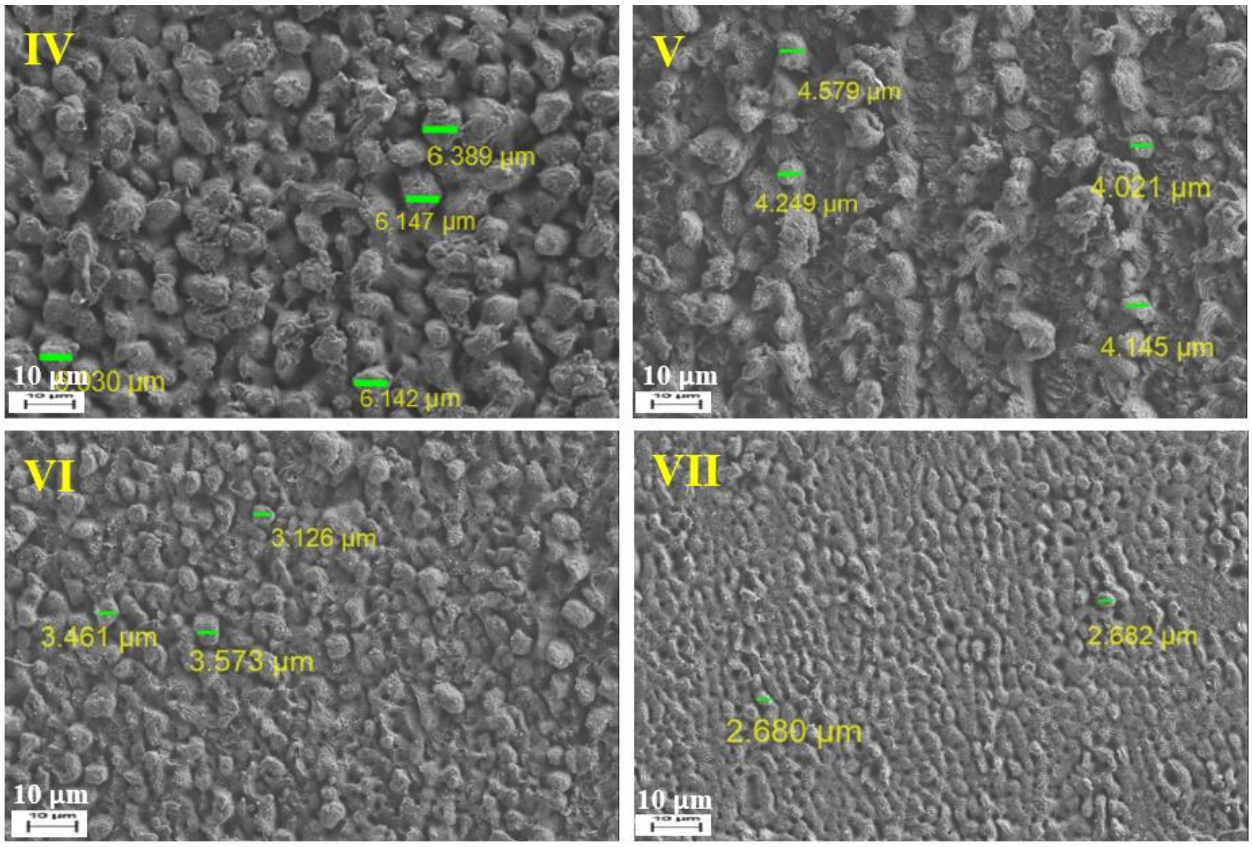

Figure 26: Images of samples treated with UV radiation at 300 kHz and 100 mm/s show the evolution of ablated structures as fluence value increases. The value of power and fluence of each sample are: ***(IV) 2.4 W, 3.52 J/cm², (V) 1.4 W, 2.06 J/cm2, (VI) 1 W, 1.47 J/cm² and (VII) 0.6 W, 0.88 J/cm².***

In addition to melting, these laser parameters produce an important ablation process. Figure 27 shows the same samples that were presented in Figure 26 with a higher magnification. The depth and size of the ablated structures are getting deeper and bigger when fluence value is higher. Therefore, we can conclude that when the fluence value increases, energy of pulse also increases, and this causes the ablation depth on the treated surface to increase. Figure 27 shows that on top of these microstructures, there are also nanostructures with characteristics similar to those obtained at low fluence values.

On the other hand, when fluence value is lower, the ablation process is less important and some nanostructures with different levels of order will start to form on the sample associated to surface fusion processes. Figure 28 shows that the affected surface was characterized by the formation of ripples when fluence value is low (see areas indicated by the circles B and D). In this figure, we compare the nanostructure obtained using a fluence value of 0.44 J/cm^2 and that presented in sample *III* of Figure 25, where a fluence value of 0.88 J/cm^2 was used. The main difference in comparison with the high fluence experiments is that only nanostructures are formed on the sample surface, with the formation of ripples. As the distance between the scanning lines is 15 microns and the laser beam diameter is 17 microns, the overlapping between two scanning lines is very small and the energy distribution of the laser beam is reflected in different levels of interaction on the sample surface, it is being more evident on the sample processed with a fluence of 0.88 J/cm^2, although they can also be observed in the lowest fluence one. Ripples are more ordered in the areas where the laser energy seems to be lower (areas B and D in the photographs).

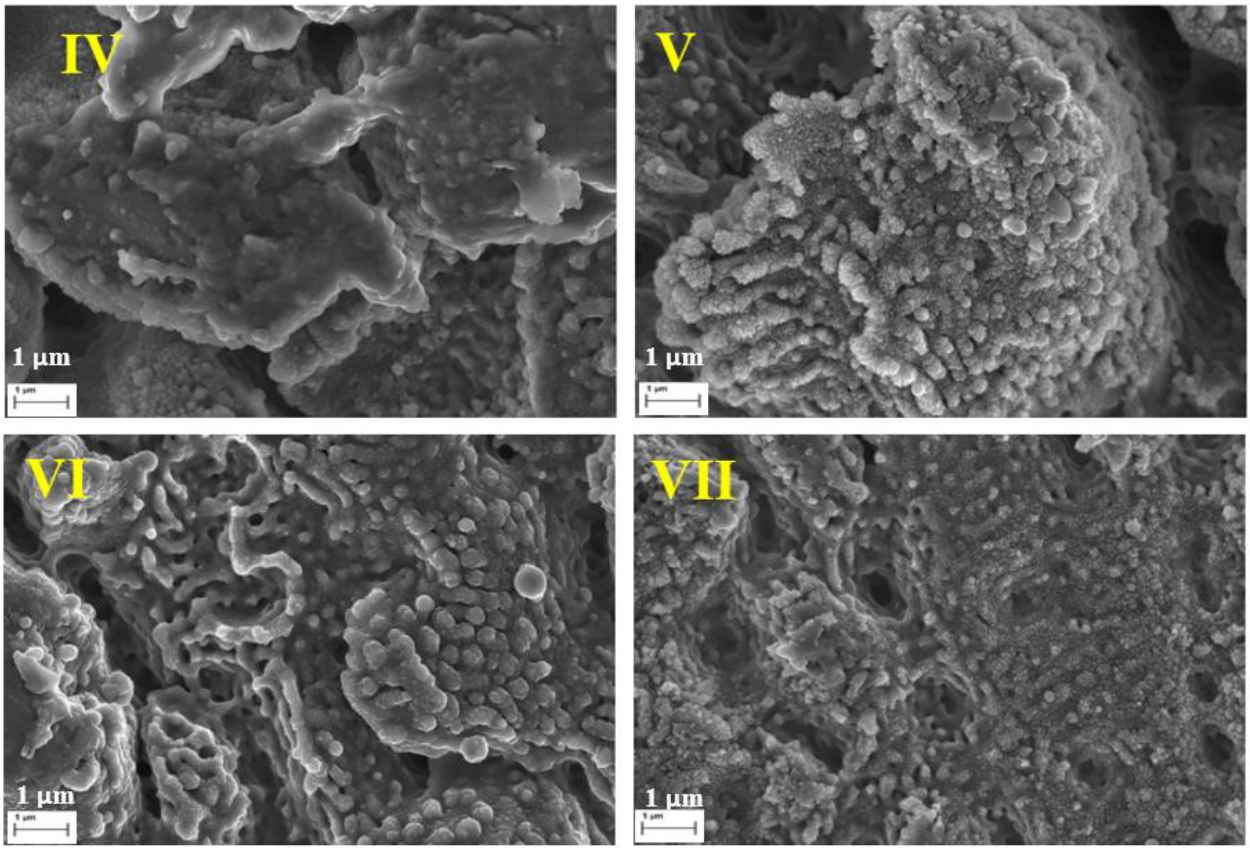

Figure 27: The detail images of results in Fig 26 which show a clear aspect of the ablated structures that formed on the sample surface.

Also, nanodots are formed in the area A, being more evident that this region has been treated with the lowest energies. In sample 1 with fluence equal to 0.44 J/cm^2 shows that in circle A, the distance between nanodots is close to the irradiation wavelength (355 nm), and in both of the samples (1 and 2), the periodicity of the ripples formed in circle B and D is also close to the irradiation wavelength. Therefore, we can conclude that, at these values of fluence, ripples are formed. And they can induce some order in the generation of nanodots and according to the theory, the ripples that formed are probably LSFL-I. If a more uniform structure is desired, the overlapping between laser scanning lines should be higher in order to reduce the differences in local fluence values between different regions of the surface. This will be confirmed in the next section.

In addition, the microstructure of the regions with a higher energy (area C) shows that between the ripples, a new nanostructure appears and it fills the background of the ripples. When the value of fluence increases, the size of amorphous on the background also increases. Further increase in fluence at this region will cause the formation of ablated structures (see yellow circle in the Figure 29).

However, as we can see in the right image of Figure 29, ripples are still formed despite the occurrence of this ablation process. In conclusion, we can say that the reason of the formation of these two regions on the same surface is that the amount of energy intensity received during laser irradiation is different due to the Gaussian energy distribution in the laser beam.

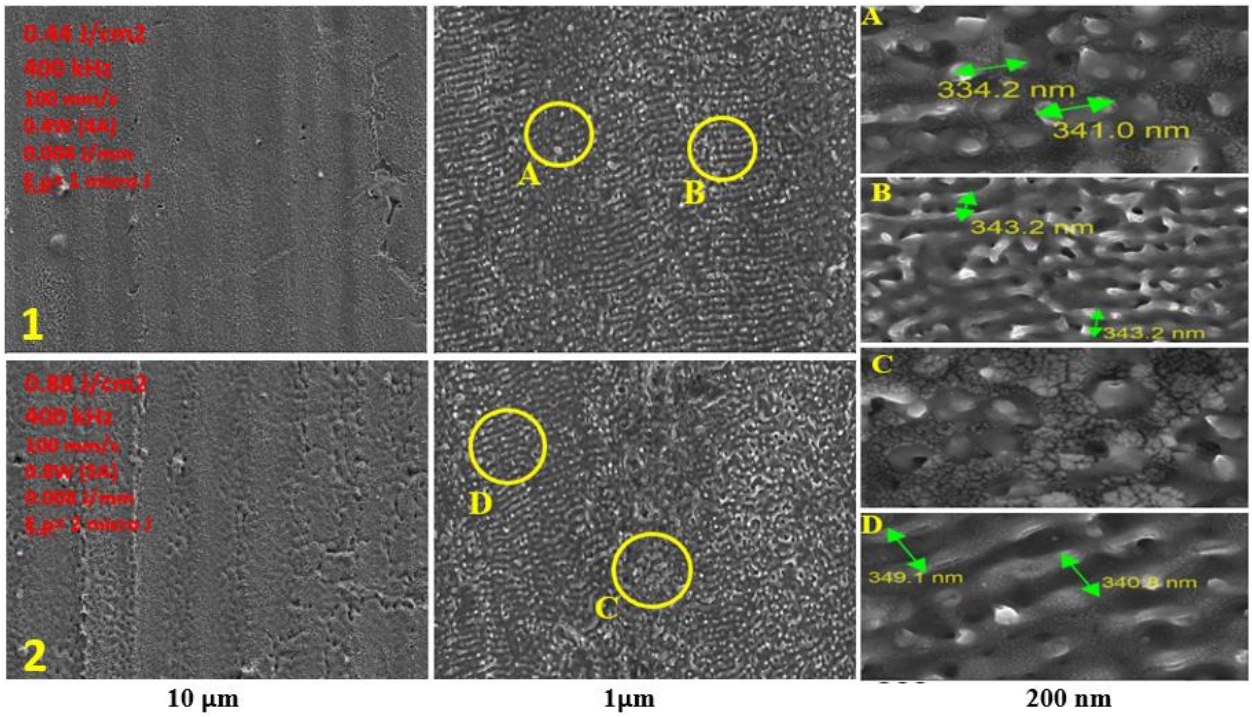

Figure 28: FESEM images of two samples after being treated with UV irradiation. Both of these samples are used to compare the ripples formation at low repetition rates of laser. Magnification of circle A, B, C and D can be observed at the third column of this figure where the structures in the circle B and D exhibit the formation of ripples and A and C exhibit the formation of nanodots with amorphous background.

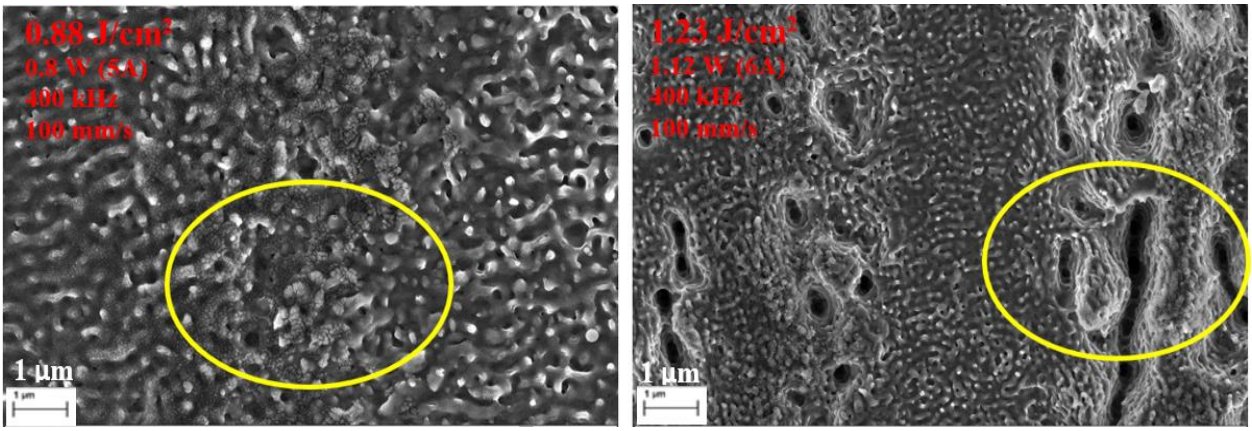

Figure 29: The FESEM images of experiments at the same frequency and scanning speed. (400 kHz and 100 mm/s) but with different value of fluence. The yellow circle shows that along the scanning lines of laser, the chaotic amorphous structure change to ablated structures when fluence value increases.

The sequence of these structures formed as energy intensity increases is: With the lowest fluence values, the main nanostructure are nanodots, which associated in the beginning of the generation of ripples as it can be deduced from the order that has been detected in some conditions. The second structure is the formation of well-defined ripples and finally the ablated structures which are similar to the spikes structures that obtained with fs lasers [7]. In the sample 1 from Figure 28, that are processed with a low fluence value; 0.44 J/cm^2, the scanning lines of laser results in formation of ripples (see circle B), while the area between the scanning lines, nanodots with amorphous background is produced as the energy is not sufficient for the complete formation of a well-defined ripples (see circle A). But it can be

detected that these nanodots are ordered in lines that follow the orientation of the ripples. By contrast, in sample 2 with a fluence equal to 0.88 J/cm^2, along the scanning lines of laser, ripples were destroyed due to high intensity of energy received on the surface, hence resulting in the formation of a chaotic amorphous structure (see circle C), whereas at the area between the scanning lines, due to the energy applied is lower, the energy of plasmon on this area is not too high for the ablation process however it is still sufficient for the formation of ripples (see circle D). This occurrence normally happens in the intermediate value of fluence.

B. Influence of fluence values at high frequency *(800 kHz).*

Considering the available laser parameters, the experiments at high frequency (800 kHz) provide additional information of the low fluence values regimen. The maximum fluence value that can be produced at 800 kHz is only 0.78 J/cm^2. However, as we mentioned earlier, if the fluence value is too low, less effect of radiation can be observed on the surface. Figure 30 shows the aspect of the surface when a fluence of 0.16 J/cm^2 has been used. The structure of ripples is not clearly defined, only a small number of ripples and some nanodots are observed.

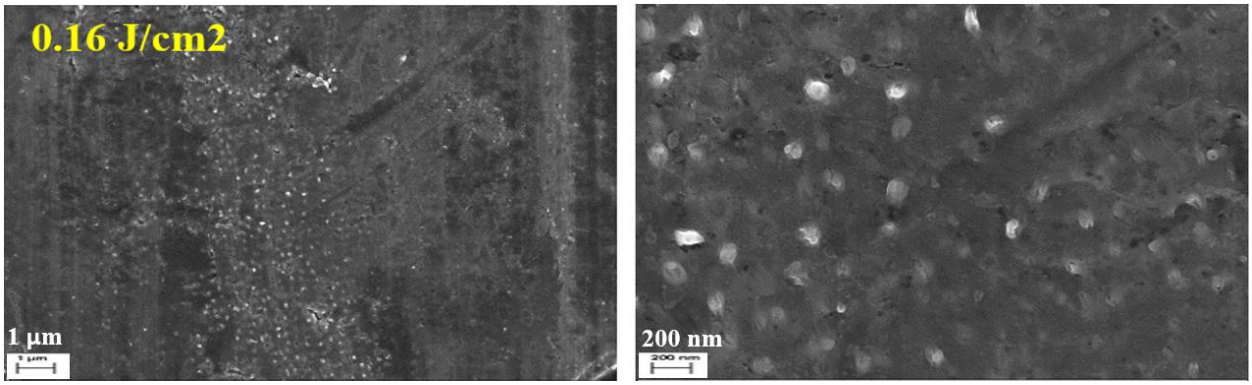

Figure 30: A sample treated with UV laser at 800 kHz and scanning speed of 100 mm/s and a fluence of 0.16 J/cm^2.

Figure 31 clearly shows the evolution of the nanostructure when fluence value increases from 0.27 J/cm^2 to 0.78 J/cm^2. In this case, the distance between laser scanning lines is also 15 microns and the energy gradient in the laser beam is also reflected in the distribution of nanostructures that have been created on the metal surface. Figure 31 shows the aspect of three samples processed with 0.27 J/cm^2 ,0.41 J/cm^2 and 0.78 J/cm^2. In the second column, details at higher magnification of the more affected areas (center of the laser beam) are presented and in the third column we include the regions that have been less affected by the laser (border of the laser beam). According to the second column, we observe that when fluence values increase, the arrangement of nanostructures starts to form ripples-like structures before the chaotic amorphous ones are formed at the highest fluence value (see sample 3). Similar to the results in the previous section, where further increase of fluence at this region will result in the formation of ablated structures. It is observed that nanostructures on sample 2 in the second column tried to form LSFL-1 ripples as the periodicity of the ripples formed is close to the wavelength of UV laser. On the other hand, the surface morphologies in the third column of Figure 31, we can observe that on sample 1, the structures formed on

the sample surface are almost absent and as we can see in samples 2 and 3, the surfaces start to develop more structures with further increase of fluence value.

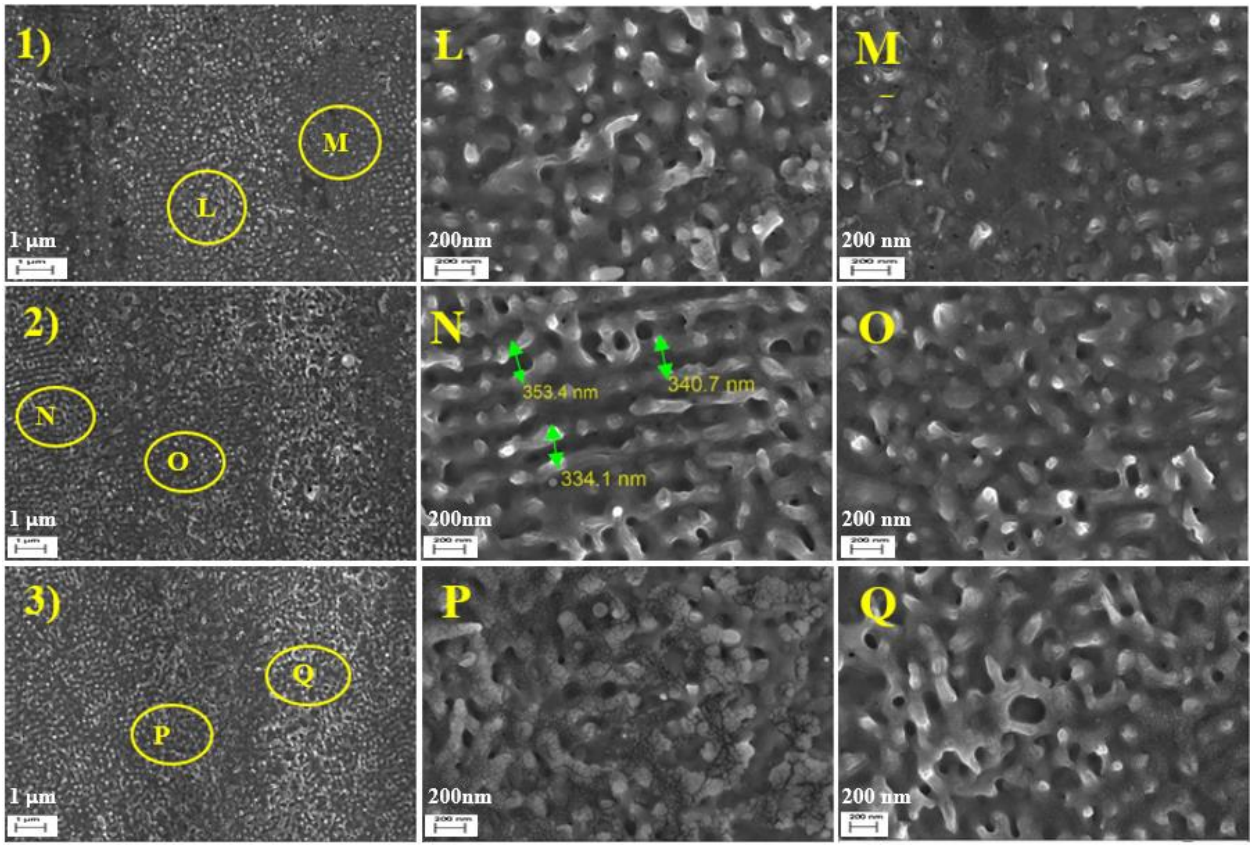

Figure 31: Three samples of experiments which were carried out by using UV irradiation at high repetition rates,800 kHz. Different power levels and fluence values are used: ***Sample (1) 0.5 W,0.27 J/cm², (2) 0.75 W, 0.41 J/cm² and (3) 1.42 W, 0.78 J/cm².***

As it can be observed in these experiments, energy gradients perpendicular to the scanning direction produce an inhomogeneous structure. In order to have a more uniform distribution of nanostructures over the whole area, we have performed additional experiments by reducing the distance between laser scanning lines up to 5 microns. With this geometry, the real fluence value increases but it is more uniform throughout the surface. Figure 32 shows an estimation of the energy distribution over the sample surface for different scanning lines distances. This is an approximation one because the distribution of Gaussian energy has been considered. The energy distribution of the laser beam is a Gaussian distribution, however, due to the overlapping between spots along a line, the energy distribution perpendicular to a line is not exactly a Gaussian distribution.

Experiments performed with a distance between scanning lines of 5 microns have allowed the formation of more uniform nanostructures on the sample surface. Results obtained with pulse fluence of 0.27 J/cm^2 and 0.41 J/cm^2 with a scanning speed of 750 mm/s are presented in Figure 33. In the first sample, a uniform nanodots and ripples structures are formed, while in the second one, the energy has increased excessively and the order is lost, thus resulting a more irregular nanostructures all over the surface. The images on the right are the detail image of each sample. Due to the increase of fluence associated with the overlapping between lines, the microstructures obtained over the surface are very closed to those

measured with the twice value of the fluence of the beam. Micrographs also show that the nanostructure can have a high order over distances of several microns. Distances between ripples and nanodots are similar to those measured in the previous section.

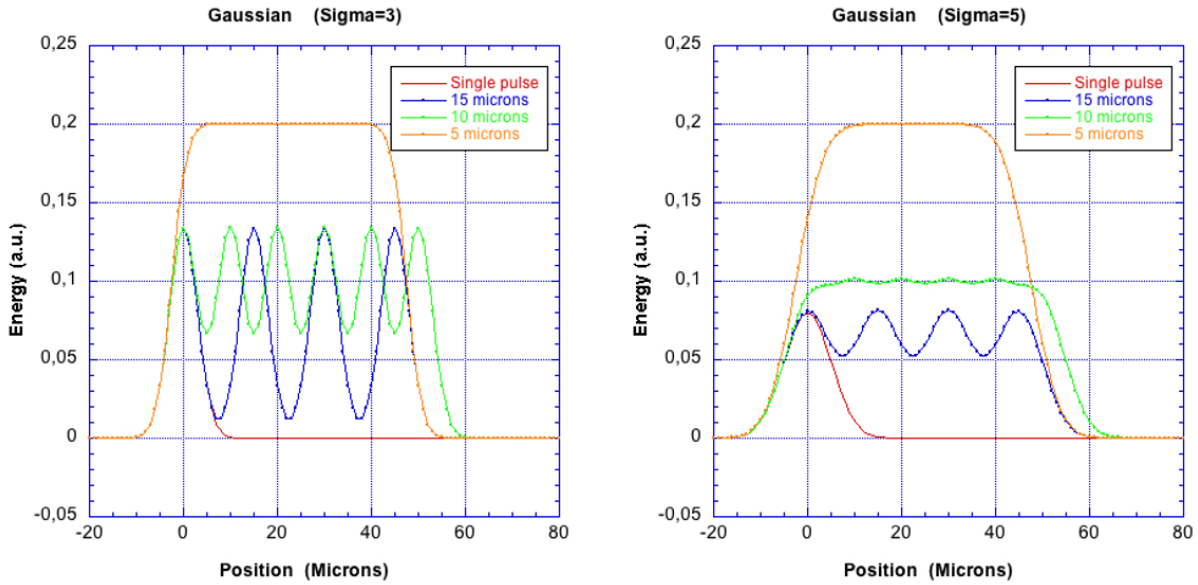

Figure 32: Estimation of the energy distribution over the sample surface for different distances of scanning lines. Image on the left with standard deviation σ of 3 and image on the right with standard deviation of 5, both of the images show a similar phenomenology of the energy distribution when overlapping increases.

Finally, we can conclude that with intermediate values of fluence, it favors the formation of nanostructures, while at high value of fluence, ablation process is more likely to occur. Moreover, to obtain a uniformly distributed nanostructures on the surface it is recommended to decrease the distance between each scanning lines in order to obtain a more uniform energy distribution over the surface.

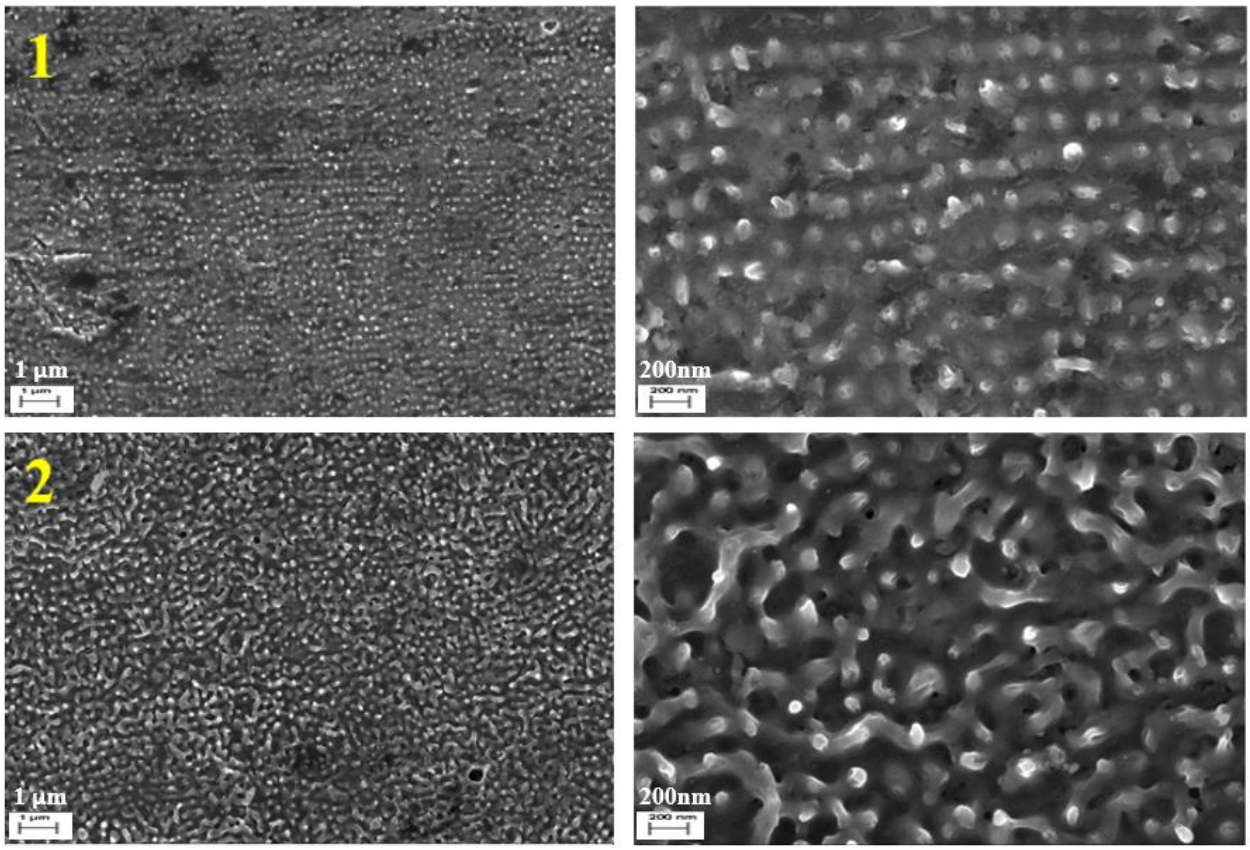

Figure 33: Two samples of Al 6061 treated with UV laser at frequency of 800 kHz and scanning speed of 750 mm/s. Nanodots are formed on the sample 1 while irregular structures are formed on sample 2. Fluence value and power for each sample are: ***(1) 0.27 J/cm², 0.5W and (2) 0.41 J/cm², 0.75 W.***

3.3 Influence of incubation energy

In the previous section, we have analyzed how the peak fluence value can influence in the generation of micro- and nanostructures on the surface. It is important to take into account that due to high frequency of the used lasers, there is always an overlapping in the direction of the laser movement. For instance, when a frequency of 800 kHz is used the distance between two laser dots is 0.125 microns for a laser speed of 100 mm/s, and 2.5 microns if this speed increases up to 2000 mm/s. These distances increase up to 0.33 (100 mm/s) and 6.7 microns (2000 mm/s) if the frequency is reduced up to 300 kHz. The magnitude that we have called incubation energy can be considered as a measure of this effect.

In order to evaluate which magnitude is more important (laser beam fluence or the incubation energy), several experiments have been designed in which the laser parameters are selected in order to maintain one of the magnitudes while the other is modified. To modify the incubation energy, while keeping constant the fluence values, we modified the scanning speed while keeping the frequency fixed. For these experiments, we also classified the results obtained according to its repetition rates.

In the first set of samples, the fluence value has been maintained constant at 1.42 J/cm^2 with a frequency of 300 kHz, the laser speed and its power have been combined to explore a lower incubation values regimen, from 0.010 J/mm to 0.002 J/mm. The microstructures of the samples are presented in Figure 34. Due to high value of fluence, ablated structures are formed on these samples. It is clearly shown that all of the samples (A, B and C) exhibit the same structures on its surface. However, it is hard to notice any changes on the samples as the incubation energy decreases. These results seem to indicate that the fluence value plays a more important role in the generation of microstructures.

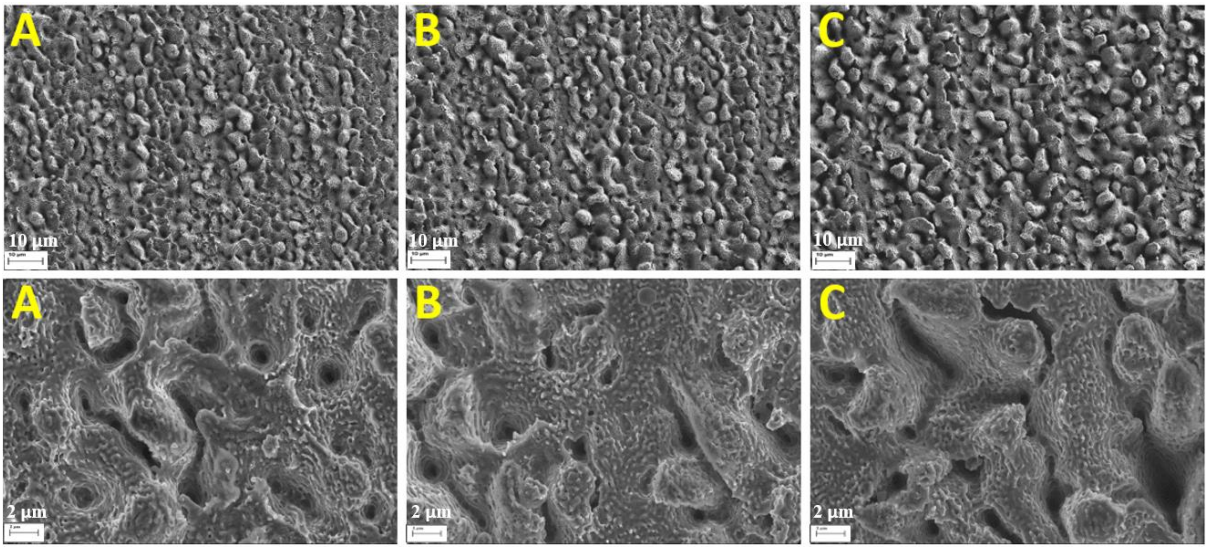

Figure 34: FESEM images taken at two magnification, the images above at 1000 X and below at 5000 X. Experiments were conducted under UV irradiation at the same frequency and fluence, (300 kHz and 1.42 J/cm^2). Each of the samples has different incubation energy; ***(A) 0.010 J/mm, (B) 0.003 J/mm, and (C) 0.002 J/mm.***

This conclusion has also been confirmed with an additional set of experiments performed at high frequency, 800 kHz, with two different values of fluence, 0.27 J/cm^2 and 0.41 J/cm^2. As

we have observed in the previous section, with this level of fluence, nanostructures are formed on the surface due to fusion process. Photographs presented in Figures 35 and 36 show the microstructures obtained using four sets of laser speeds (750 mm/s, 1500 mm/s, 2000 mm/s and 2500 mm/s) with the same laser power and fluence values. In these experiments, the distance between scanning lines is 5µm.

Figure 35 is the set of experiment when the fluence is equal to 0.27 J/cm^2, where it can be observed that nanodots are uniformly formed all over the surface. The scanning speed used for these four samples is different and, in consequence, the incubation energy has been increased by more than three times.

Similar experiments have been repeated with a fluence value equal to 0.41 J/cm^2 and the results are shown in Figure 36. In this case, with a sufficient amount of energy, nanostructures start to form some irregular ripples. However, this formation is slightly reduced when incubation energy decreases. It seems that nanostructures on sample H have a slightly more order compared to sample K.

From the results of these experiments, we can conclude that the change in incubation energy has less effect than fluence in the generation of micro and nanostructures in both processes: ablation and melting.

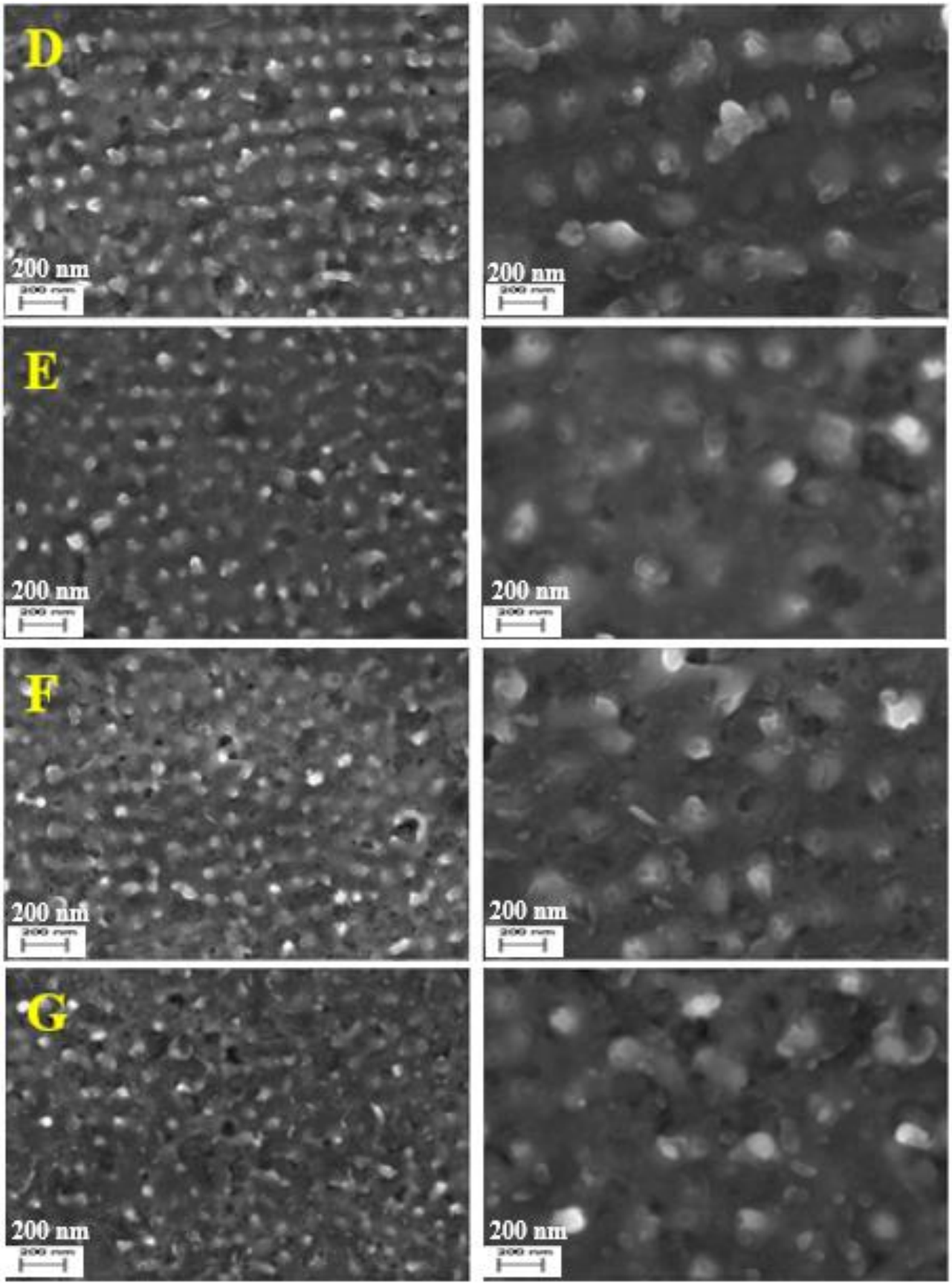

Figure 35:Surface morphologies of samples treated with fluence value equal to 0.27 J/cm2 at frequency of 800 kHz. Incubation energy of each sample is: ***(D) 0.00067 J/mm, (E) 0.00033 J/mm, (F) 0.00025, and (G) 0.00020 J/mm.***

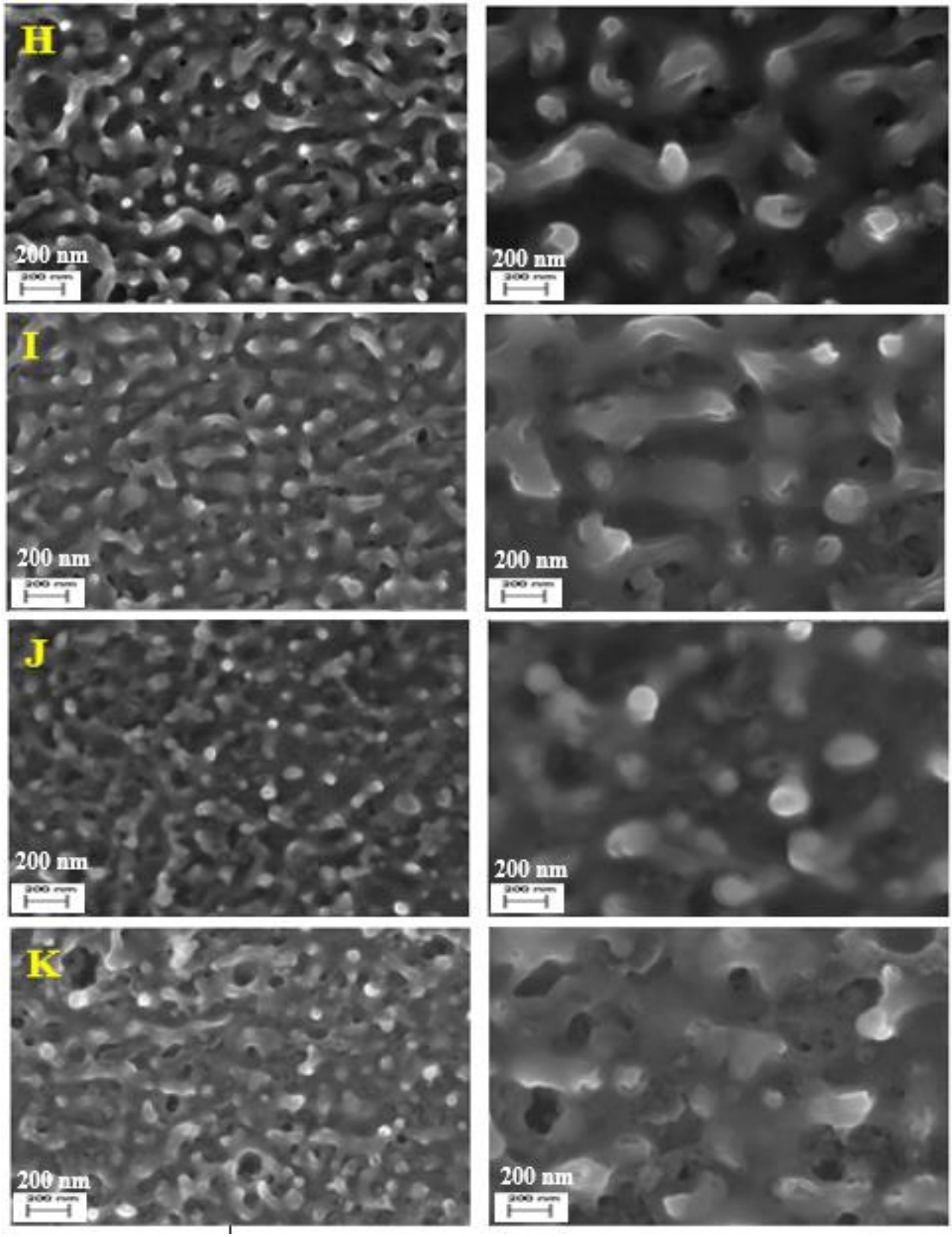

Figure 36:Surface morphologies of samples treated with fluence value equal to 0.41 J/cm2 at frequency of 800 kHz. Incubation energy of each sample is: ***(H)0.00100 J/mm, (I)0.00050 J/mm, (J)0.00038, and (K)0.00030 J/mm.***

3.4 Influence of the laser angle between laser scanning and polarization direction.

For any experiments conducted by using laser, polarization is one of the most important parameters that should be carefully considered. We do not have any information about the polarization of the laser that has been used in this work. But previous works have shown that in the nanostructures induced by laser radiation, ripples tend to be ordered in the direction perpendicular to the laser polarization. To study this effect, several experiments in which the polarization direction was modified have been performed. Figure 37 shows the microstructures observed on the surface using the UV laser at 300 kHz with a scanning speed of 100 mm/s and a fluence value equal to 1.47 J/cm^2. At this high value of fluence, the process of ablation is relevant and apart from nanostructures, spikes microstructures are also created. In this case, configuration of beam scanning is used and the distance between each scanning line is 15 microns. Figure 37 shows the FESEM images of the treated samples at different scanning directions: 0°, 90°, 180°, and 270°. The angle has been measured taking as a reference the horizontal line on the paper. It can be observed that the microstructures that are formed on the samples are oriented vertically and independently with the scanning direction. These results indicate that the laser has a linear polarization. And by considering to the ripples that formed are oriented perpendicular to the laser polarization, we can conclude that the laser polarization is very close to the scanning direction of 90º.

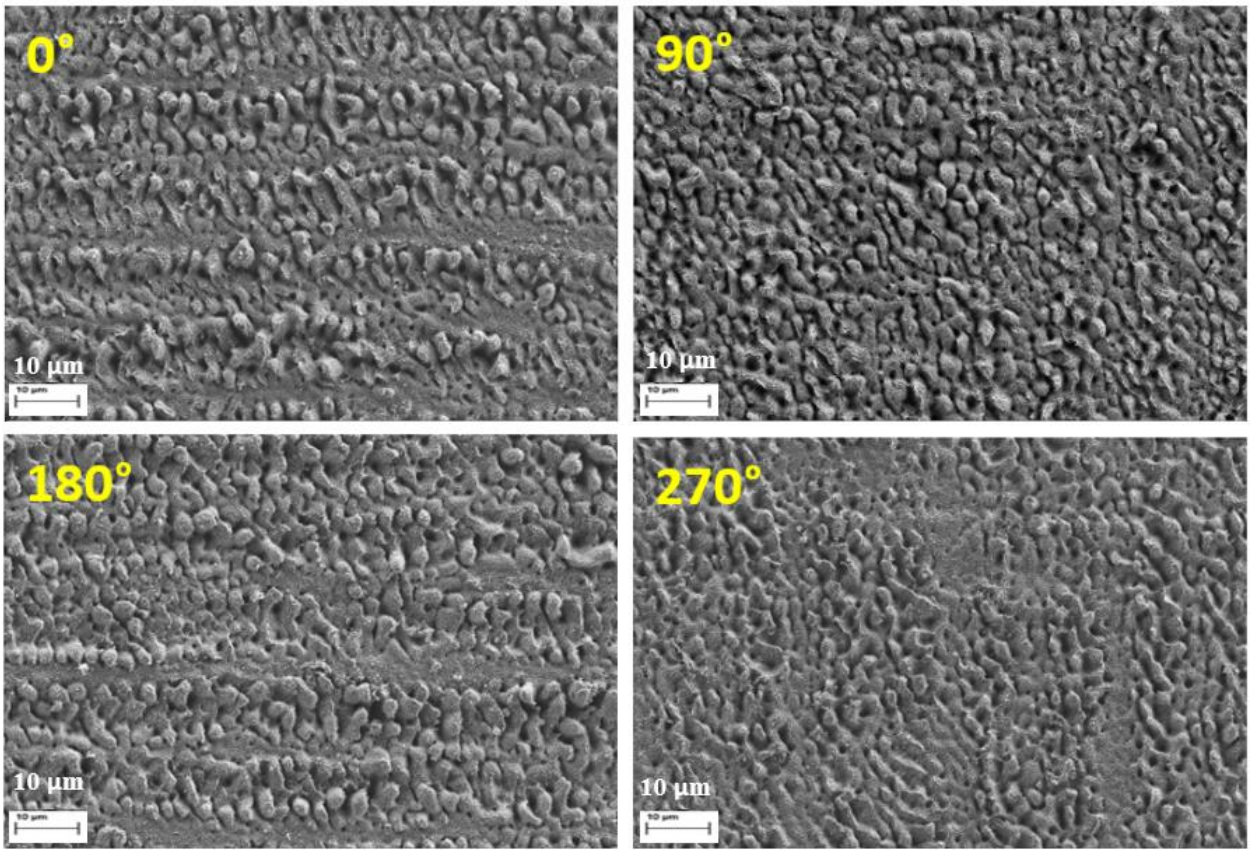

Figure 37: FESEM images of four samples which were treated under the influence of UV irradiation (300 kHz, 100 mm/s) taken at magnification of 1000 X. Samples were treated at different scanning direction of 0°,90°,180° and 270° respectively.

Previous results also seem to indicate that the interaction of the laser with the metallic surface is stronger when laser beam makes the scanning in the direction of the polarization and besides all this, we have also identified that the interaction is stronger on the defects of the sample surface. In order to separate both contributions, new set of experiments has been performed with a completely different set of laser parameters and using the line-scanning configuration. In this configuration laser moves in a line and the scanning over the surface takes place when the sample moves below this line (see Figure 38). In the first configuration, laser movement takes place in the 0º configuration, with the laser moving in the perpendicular direction with respect to its polarization direction. Also, this laser movement is parallel to the mechanical lamination direction of the sample. In the second configuration, laser movement has been performed in the configuration of 90º (parallel to the polarization direction) but the sample has also rotated 90º in order to maintain the orientation with respect to the mechanical lamination and avoiding differences that are associated with lamination mechanical defects. Micrographs presented in Figure 39 show the aspect of the samples after being irradiated at 800 kHz and a fluence of 0.413 J/cm^2. The differences between the samples are associated to the laser speed (100 mm/s, 300 mm/s and 750 mm/s) (see Table 12 in Annex III). Table speed has also been adapted to maintain the overlapping between lines during processing.

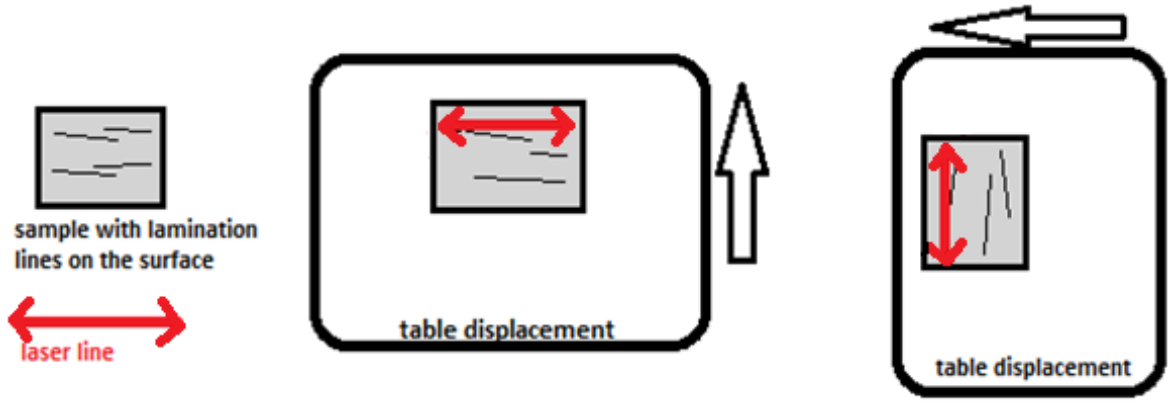

Figure 38: The first image shows the red line of laser scanning is in the configuration of 0° while the second image shows the red line of laser scanning is in the configuration of 90°.

It is observed that samples that have been processed at 90º (parallel to the polarization direction) are more affected than those that were processed at 0º (perpendicular to the polarization direction). These results confirm the initial results that were obtained in the experiments performed with the beam-scanning configuration, in which the scanning direction was modified without moving the sample. By analyzing the microstructures obtained with the three laser speeds, it is observed that more differences are obtained in the case of the 90º configuration, while in the other case, effects are more similar on the three samples. As a conclusion of all these results, in order to analyze the influence of the different laser processing parameters, it is highly recommended to use a 90º configuration, with the laser moving parallel to the laser polarization direction.

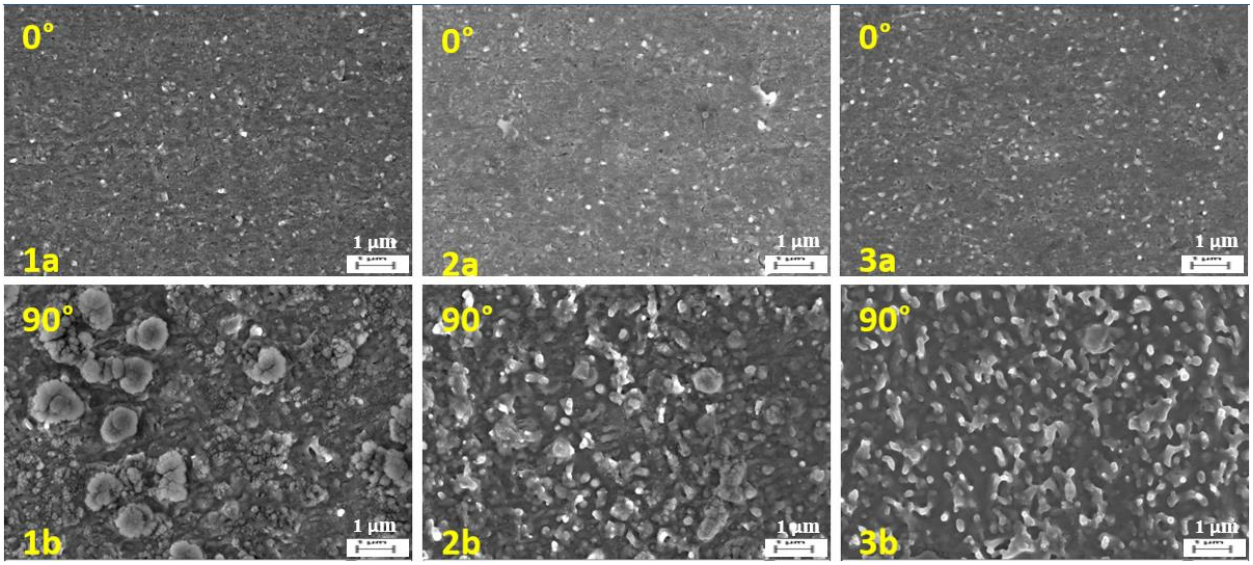

Figure 39: Surface morphologies of treated samples at different scanning angles and speeds. ***Images in the first row: Sample (1a) 0° ,100 mm/s, (2a) 0°,300 mm/s, and (3a) 0°, 750 mm/s.*** *Images in the second row:* ***(1b) 90° ,100 mm/s, (2b) 90°,300 mm/s, and (3b) 90°, 750 mm/s.***

3.5 Influence of atmosphere during laser treatment.

The atmosphere during laser treatment can also modify these nanostructures. In this work we have checked what happens if these experiments are performed in Argon atmosphere. They were carried out by using the UV laser with a frequency of 800 kHz and with the laser line scanning configuration. The scanning lines were separated by 5 µm distance and the speed of table displacement used is depending on the scanning speed of laser. As we mentioned earlier, experiments in Argon were carried out by using a chamber with a quartz glass attached on its lid, the pressure inside of the chamber is 0.4 atm over pressure, particularly at 1.4 atm of Argon atmosphere. The real fluence values acting on the sample surface in this condition are lower than in air because a percentage of the laser energy is absorbed in the quartz glass. In order to observe the interaction of laser on Al 6061 at different conditions, we have designed several experiments in which the results obtained for each condition are compared according to the incubation energy and fluence values respectively. Fluence values are modified by changing the power output whereas incubation energy values are modified by using different scanning speeds. The particular laser parameters that have been used in these experiments are presented in Tables 13 and 14 in Annex III.

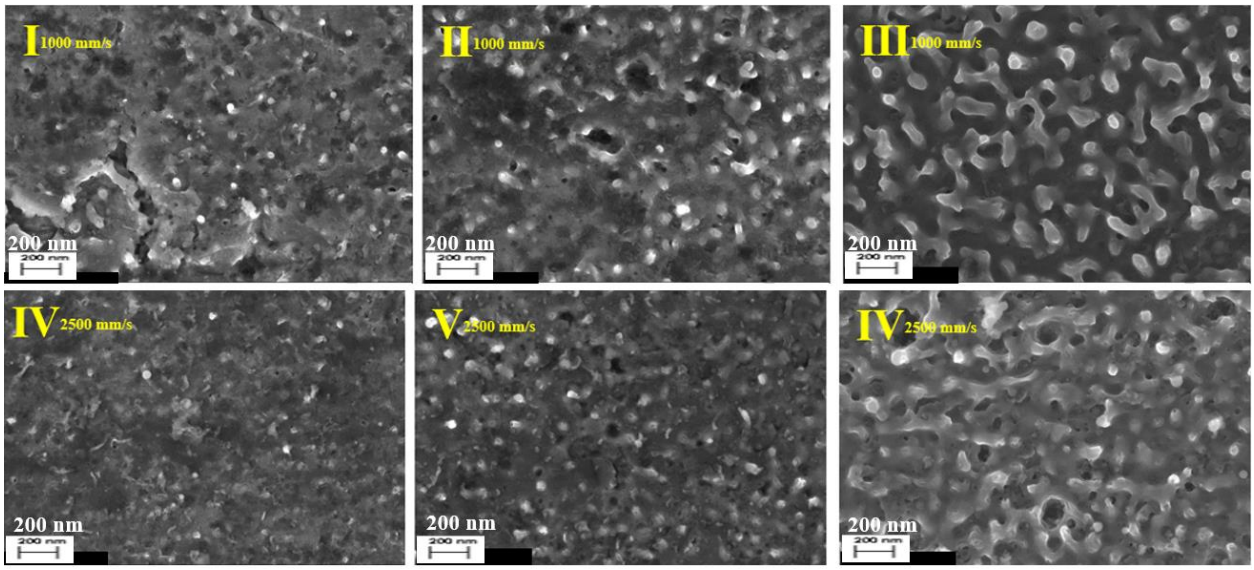

Figure 40: FESEM images of 6 samples treated by laser in Air with frequency of 800 kHz. Different speeds and powers are applied for each sample: ***Sample (I) 1000 mm/s, 0.3 W, (II) 1000 mm/s, 0.5 W, (III) 1000mm/s, 0.75 W, (IV) 2500 mm/s, 0.3 W, (V) 2500 mm/s, 0.5 W and (IV) 2500 mm/s, 0.75 W.***

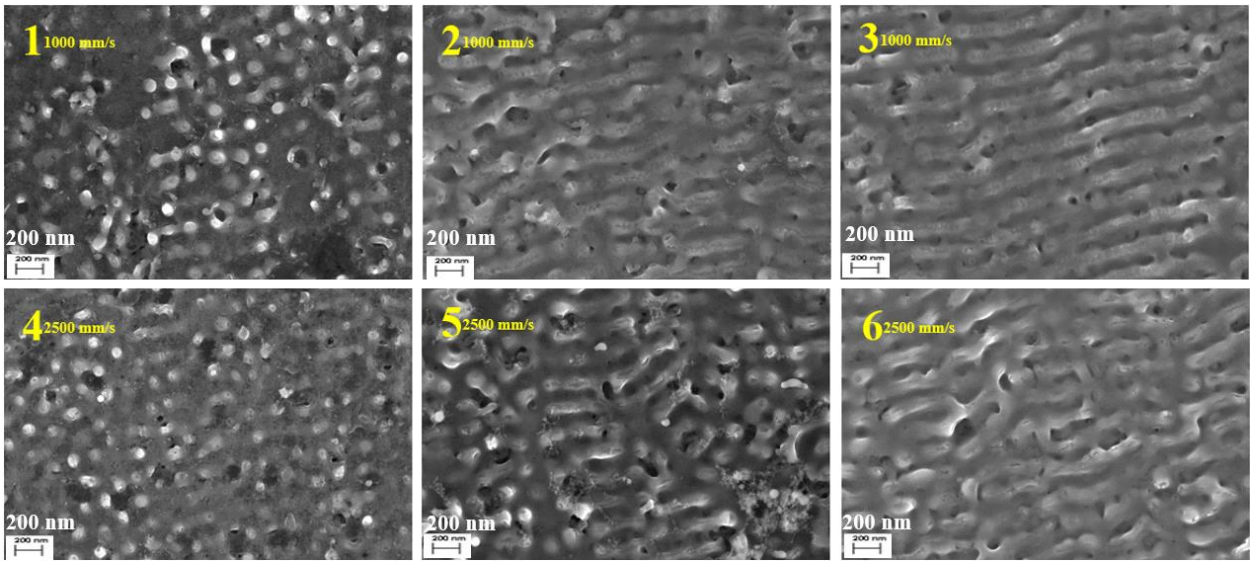

Figure 41: FESEM images of 6 samples treated by laser in Argon with frequency of 800 kHz. Different speeds and powers are applied for each sample: ***Sample (1) 1000 mm/s, 0.75 W, (2) 1000 mm/s, 1.05 W, (3) 1000mm/s, 1.4 W, (4) 2500 mm/s, 0.75 W, (5) 2500 mm/s, 1.05 W and (6) 2500 mm/s, 1.4 W.***

Figures 40 and 41 show the comparison of nanostructures that have been obtained in the experiments of both atmospheres. In these cases, the frequency values are high, and in consequence, the fluence values correspond to the range between 0.16 J/cm^2 and 0.41 J/cm^2 for the experiments performed in air and in the range 0.41 J/cm^2 and 0.77 J/cm^2 when the experiments were performed in Ar. In each Figure, the first row corresponds to the samples that have been processed with the lower speed (1000 mm/s) and the second row with 2500 mm/s. In both atmospheres, the processing parameter conditions lead to the formation of nanostructures on the surface, but the main difference is that in the case of the samples treated in Ar atmosphere, a higher level of order has been attained. For the different fluence values, it is observed that the orientation of the ripples is very similar, as it was expected because the orientation of the sample with the laser polarization direction has been maintained throughout the experiments. In conclusion, working in the condition with low-oxygen atmospheres reduces the amount of Al_2O_3 that can be formed during the laser treatment and this improves the order of nanostructure that is obtained on the surface.

With the low fluence values (0.41 J/cm^2), nanodots are created on the top of the ripples structures. Figure 42 shows the surface morphologies of sample 1 and 3 from Figure 41 with a higher magnification. It has been measured that the ripples wavelength is very close to 355 nm, similar to the laser wavelength. Also, the distance of the nanodots is of the same order of magnitude, indicating the importance of the laser wavelength in the formation of these nanostructures. We can conclude that the ripples structures that are formed are probably the LSFL-I as the result obtained is similar to what is described in the theory.

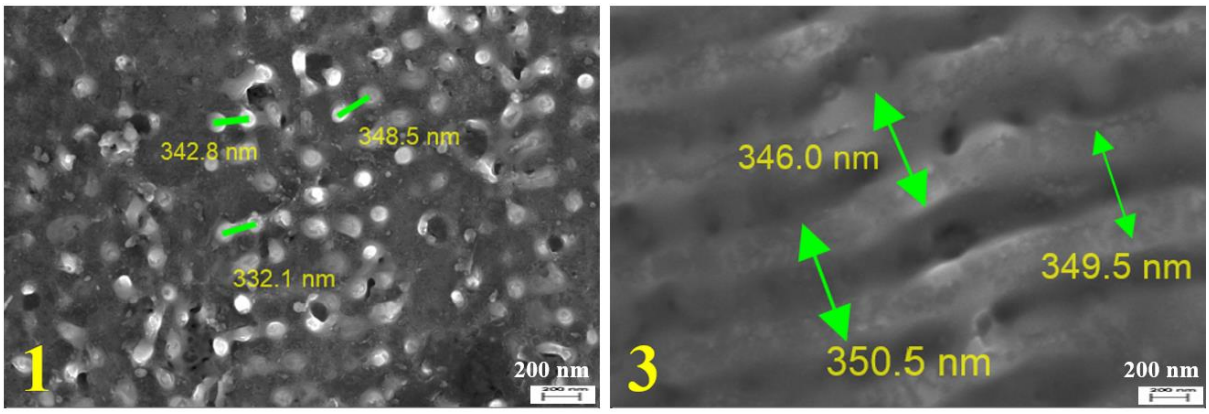

Figure 42: FESEM images of sample 1 and 3 in Figure 41 in Argon atmospheres at closer distance. Nanodots and ripples exhibits a distance and periodicity close to the wavelength of ultraviolet spectrum, 355 nm.

Another observation on the results obtained after being treated with laser in Argon is that the sample surface exhibits some colors and that they are modified when the illumination angle is changed. Figure 43 shows the example of colors that have been obtained with four different illumination-observation angles. This behavior is due to the formation of well-ordered nanostructures on the surface creating a diffraction lattice that provides some colors to the sample depending on the illumination angle.

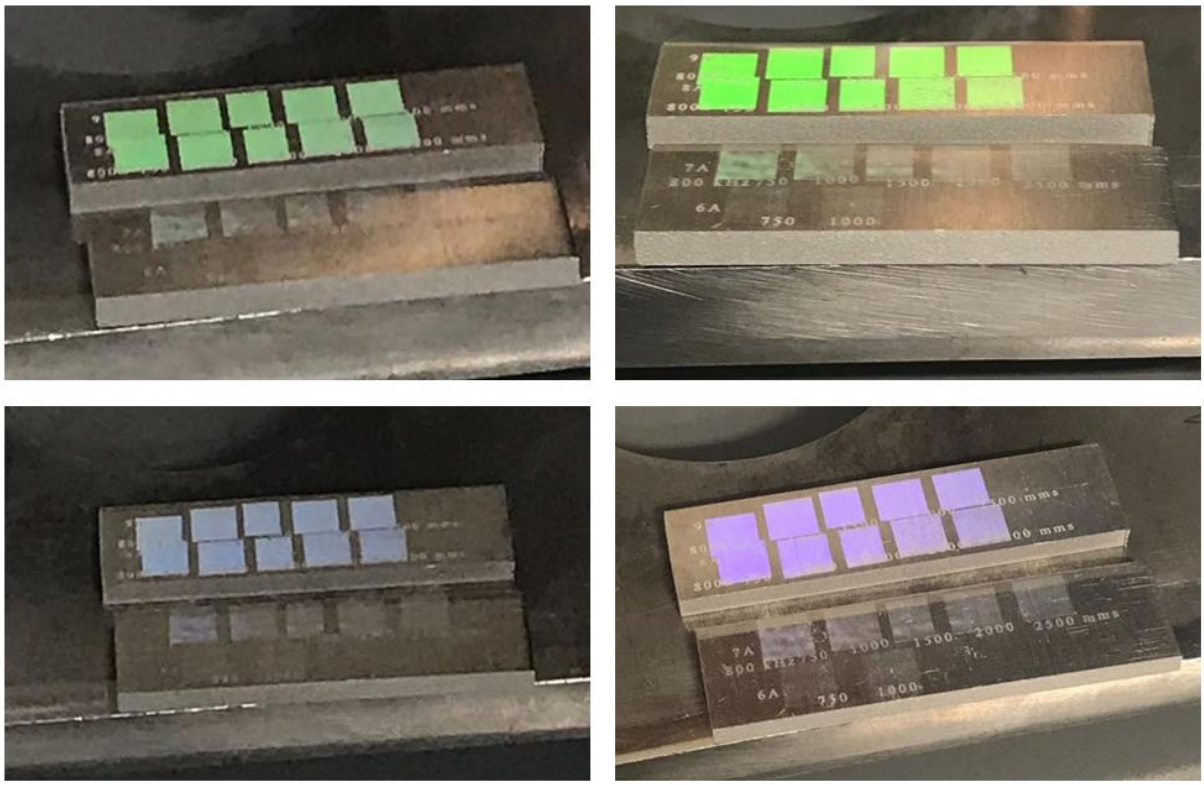

Figure 43: The images show four different positions of sample after being irradiated with UV laser in Argon atmosphere, where it illuminates colors such as green, blue and purple.

4. CONCLUSIONS

In this study, the interaction of short pulses (sub-nano) lasers on Aluminum 6061 was investigated experimentally by using Ultraviolet radiation and Infrared radiation. The main objective is to analyze the generation of nano- and microstructures on the metal surfaces.

The results obtained from all of the experiments that were conducted under the influence of Infrared radiation with a pulse duration of 800 ps and a wavelength of 1064 nm show that the interaction that occurs on the Al6061 is mainly thermal. The only change that is observed in this study when we modify laser parameters is that, the amount of melting material increases as fluence value increases. With a sufficient amount of fluence, melting takes place covering full surface.

While for experiments that were carried out by using the Ultraviolet laser, there are two mechanisms that occurs on the sample such as ablation and melting process. It has been observed that the fluence value is the main parameter that determines the modifications induced on the surface. For a sufficient level of fluence, micro and nanostructures are started to form on the sample. However, if the fluence value is too low, only a very thin layer of molten material is obtained. Moreover, observation on the cross-section of the sample shows that jagged structures are formed due to the ablation process that occurs on the surface. The results from the study by using Ultraviolet laser caused the formation of different process and structures, hence the rest analysis on the interaction of laser-material had been focused on the ultraviolet radiation.

High values of fluence can be obtained by using low frequency as the energy per pulse is higher, while low values of fluence can be obtained by using high frequency. It is found that at high value of fluence, the ablation process is more likely to occur and the higher the value of fluence, the bigger the ablated structure formed and the deeper the ablation depth. While for intermediate values of fluence, nanostructures such as ripples and nanodots started to form on the sample. The distance between nanodots and the periodicity of ripples that are formed is close to the wavelength of laser irradiation, which indicates that the generated ripples can be classified as a LSFL-I structure. Also, it has been established that by controlling the overlapping between the scanning lines in order to homogenize the energy distribution in the perpendicular direction of the laser movement, it is possible to obtain some homogeneous structures over a long range of areas on the surface. This has been proved experimentally when the scanning lines distance is reduced up to 5 microns. In order to define the real fluence or irradiance values over a given area of the surface, it is important to bear in mind the overlapping between laser spots in both directions.

We have also studied the influence of incubation energy on Aluminum surface. The effect of incubation energy is associated with the distance between two laser dots depending on the speed scanning and frequency used. The lower the frequency and the higher the scanning speed used, the higher the distance between two dots of laser. Results from this study show that incubation energy has much less affect than fluence in the generation of micro and nanostructures in the ablation and melting process. Therefore, we can conclude that the most important parameter in the laser treatment is fluence value as the modification of fluence

induced a different process and structures on the sample surface while incubation energy only effects the order of the nanostructures.

Another important aspect to consider in laser treatment is polarization direction of laser. To explore the effect of polarization, analysis of influence of the laser angle between laser scanning and polarization direction is done. The results obtained indicate that the interaction is stronger when laser moves parallel to the direction of polarization. To confirm this, a set of experiment is done by using line configuration with scanning angle of 0° and 90°. The results obtained are more affected when the scanning angle is aligned parallel to the polarization direction (90°). Therefore, in order to analyze the influence of the different laser processing parameters, it is highly recommended to use a 90º configuration, with the laser moving parallel to the laser polarization.

The influence of atmosphere during laser treatments also plays an important role in the interaction of laser and material. In Argon atmosphere, the nanostructures formed are more oriented and well ordered, this creates a diffraction lattice that provides colors to the sample. We can observe different colors on the sample depending on the illumination angle. This occurrence will encourage a new idea for improvements involving the appearance of Aluminum applications. Furthermore, by using a suitable value of fluence, the high regular ripples can be form in this condition as there is no interference of Aluminum oxide during its formation on the sample surface.

In consequence, the use of sub-nano UV lasers opens new opportunities in the development of nanostructures in surface metals. It opens new research lines that can cover the analysis of their use in different applications: hydrophobicity, icephobicity, decoration, antibacterial applications, etc. In addition, research efforts are also required to scale these treatments to big samples in order to define how to transfer the laser parameters that have been found in the small samples to big areas.

The results of this work were presented at the Congreso Nacional de Materiales, 4 to 6 July 2018 as an oral presentation: Nanostructures in Al surfaces induced by interaction with UV ps-lasers; Z. Binti-Haron, J.A. Rojo, L.A. Angurel, G.F. de la Fuente, R. Navarro.

5. BIBLIOGRAPHY

1. https://www.skybrary.aero/bookshelf/books/659.pdf .
2. Charles H. Townes. *"The First laser"*. *A Century of Nature: Twenty-One Discoveries that Changed Science and the World.*
3. G. D. Tsibidis, M. Barberoglou, P. A. Loukakos, E. Stratakis, And C. Fotakis. (2012). *"Dynamics of ripple formation on silicon surfaces by ultrashort laser pulses in subablation conditions". PHYSICAL REVIEW B 86, 115316.*
4. George D. Tsibidis, Evangelos Skoulas, Emmanuel Stratakis. *"Ripple formation on Nickel irradiated with radially polarized polarized femtosecond beams".*
5. Iaroslav Gnilitskyi, Thibault J.-Y. Derrien, Yoann Levy, N6adezhda M. Bulgakova, Tomáš Mocek, Leonardo Orazi. (2017). *"High-speed manufacturing of highly regular femtosecond laser induced periodic surface structures: physical origin of regularity". Scientific Reports.*
6. Jorn Bonse, Sandra Hohm, Sabrina V. Kirner, Arkadi Rosenfeld, and Jorg Kruger, (2016). *"Laser Induce Periodic Surface Structures -A Scientific Evergreen*". *IEEE Journal of Selected Topics in Quantum Electronics, Vol. 23, No. 3, May/June 2017*.
7. U. Hermens, S.V. Kirner, C. Emonts, P. Comanns, E. Skoulas, A. Mimidis, H. Mescheder, K. Winands, J. Krüger, E. Stratakis, J. Bonse. (2016). *"Mimicking lizard-like surface structures upon ultrashort laser pulse irradiation of inorganic materials". Applied Surface Science 418 (2017) 499–507.*
8. P. Bizi-bandoki, S. Valette, E. Audouard, S. Benayoun. (2013). *"Time dependency of the hydrophilicity and hydrophobicity of metallic alloys subjected to femtosecond laser irradiations." Applied Surface Science ,Volume 273, 15 May 2013, Pages 399-407 http://dx.doi.org/10.1016/j.apsusc.2013.02.054.*
9. Robert E. Sanders, Jr. (2001). *"Technology Innovation in Aluminum Products"*. JOM. 53(2): 21–25. *Bibcode*:*2001JOM....53b..21S*. *doi*:*10.1007/s11837-001-0115-7*.
10. Barbara H. Stuart. (2017). "*Analytical techniques in materials conservation*."

ANNEX

ANNEX I: SAFETY STANDARDS

In most industrial situations, laser activity is conducted inside of the laser safety cabin. This cabin is designed to absorb the laser power by using a special walls and roof. For our study, experiments were carried out in the laser laboratory of Aragon Materials Science Institute (joint research centre of the CSIC and the University of Zaragoza). To ensure the safety of people who may be exposed to the photo-chemical effect of laser, a warning sign is placed on the door during laser working to inform that the use of goggles is compulsory.

Figure A- 1:Warning label that indicates laser is on and protective eyewear is required.

Thermal effects are the main cause of laser radiation injury, however photo-chemical effects can also be one of the concerns for specific wavelengths of laser radiation. Thermal effects cause damage to the retina while photochemical caused the laser light to trigger the chemical reaction in the biological tissues. Photochemical damage occurs mostly with Ultraviolet laser light while thermal damage mainly caused by Infrared laser light. Protective eyewear in the form of appropriately filtering optics can protect the eyes from visible and invisible wavelength of laser radiation. Eyewear must be selected for the specific type of laser, to block and filter the appropriate wavelength range. Normally, the protective eyewear is designed according to its particular wavelengths of laser and the details for the specific use are printed on the goggles. Figure A-2 shows the safety equipment that were used during laser experiments.

Additionally, during the engraving operation of laser, the ablation and melting processes causes the generation of smoke and nanoparticulate as the engraving material is being vaporized by the laser, therefore it is necessary to turn on the exhaust ventilation system for a safety precaution.

Figure A- 2: Example of goggles that were used throughout the experiment and the exhaust ventilation system used in the laser laboratory.

ANNEX II: CONTROL SOFTWARE OF LASER AND TABLE DISPLACEMENT

Both laser systems are coupled to an optical steering system, which allows user to sketch any types of drawing on the material surface. With the adequate software, it is possible to draw the design that wants to be transferred to the surface. Most of experiments performed in this work have been performed covering a square region 5 x 5 mm^2 such shown in Figure A-3. Laser makes a line of 5mm that moves in the perpendicular direction with steps in the range between 2 µm to 15 µm. The control software allows modifying the processing parameters of this laser treatment. They include the frequency, power, overlap, direction, hatching type (either by using unidirectional or bidirectional) etc.

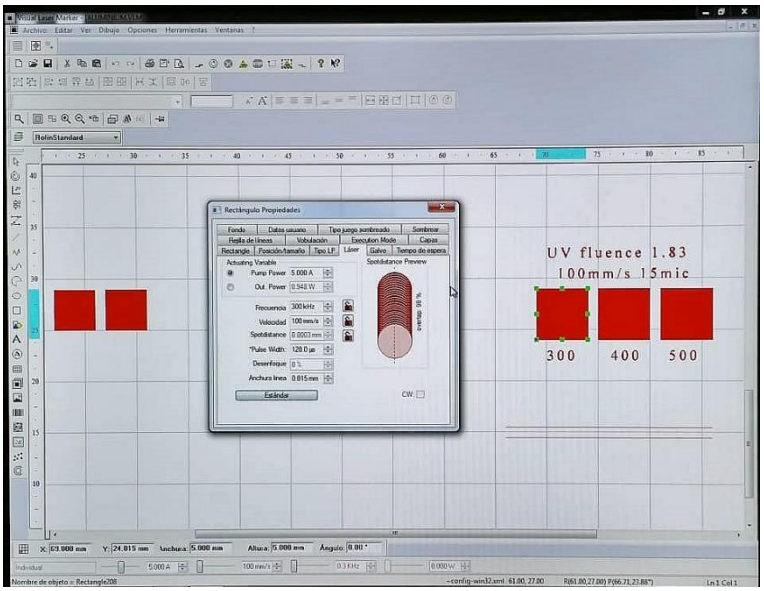

Figure A- 3: Control software application in both types of laser.

Experiments can be done with two different configurations: beam scanning or line scanning. In the first case, the sample is fixed and the laser moves along the surface of the sample. In the second configuration, laser making a line while the sample moves in the perpendicular direction. In this case, one of the incident angles is maintained during the full treatment, obtaining a more uniform laser treatment. In the case of the laser line configuration, a displacement table was used during the experiment to combine the sample movement with laser scanning. By controlling the speed of the sample and the speed of the laser, it is possible to control the laser overlapping during the treatment. Figure A-4 shows the software that has been used to control the displacement table. Symbol A in the figure show the range of motion of the table, B shows the distance moved by the table and C is the control parameters of the table displacement.

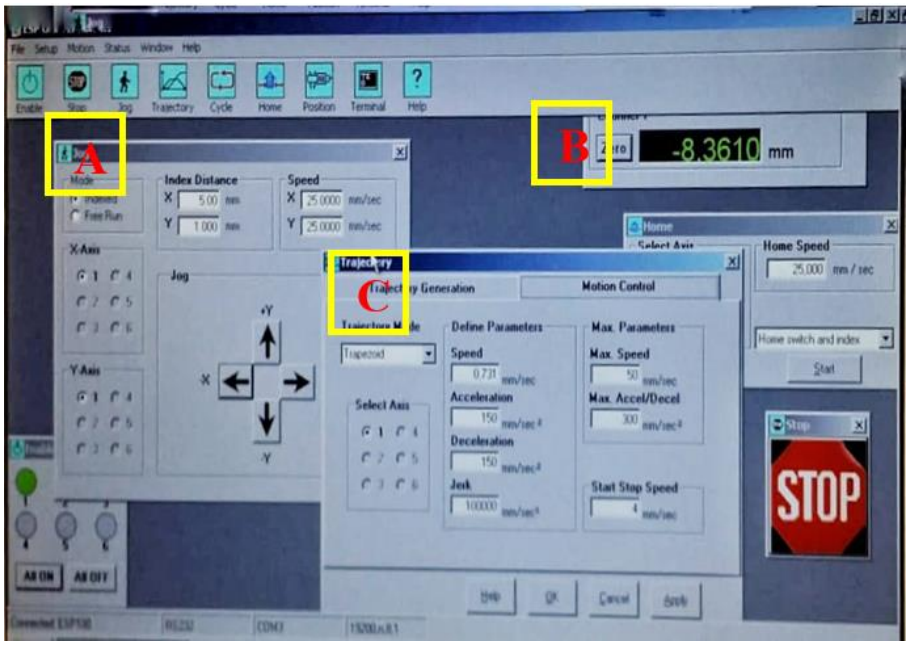

Figure A- 4: The control application for table displacement.

The difference between Infrared and Ultraviolet laser machine is that in the second case the height adjustment to focus the laser can be done automatically by software, while in the case of the n-IR laser it has to be done manually by the user. The automatic adjustment can increase the level of reproducibility of the different experiments.

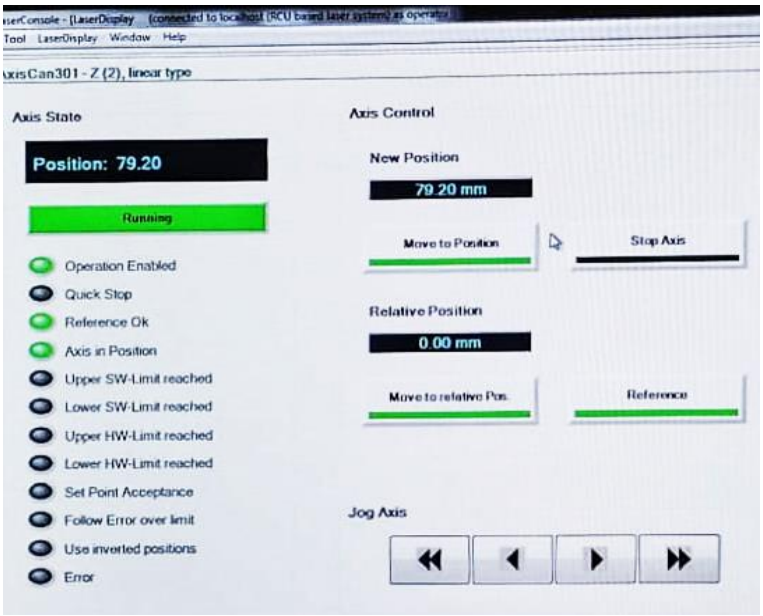

Figure A- 5: The adjustment of height of UV laser can be done by entering the total height in the new position above.

ANNEX III: TABLE OF PARAMETERS FOR LASER PROCESSING

In this annex III, we present the table of the laser parameters used in all the experiments that have been presented in this work.

3.1 Analysis of the influence of the laser wavelength on the structures formed on Aluminum surface.

3.11 Analysis of the changes induced by n-IR radiation.

Table 1 for Figure 17:

Figure 17: Sample	***a***	***b***	***c***	***d***
Ø beam (µm)	*25*	*25*	*25*	*25*
Pulse width (ps)	*800*	*800*	*800*	*800*
Power (W)	*2.965*	*3.915*	*5.34*	*6.29*
Current (A)	*4.5*	*5.5*	*7*	*8*
Frequency (kHz)	*800*	*800*	*800*	*800*
Scanning speed (mm/s)	*100*	*100*	*100*	*100*
Fluence (J/cm^2)	***0.76***	***0.996***	***1.36***	***1.60***
Irradiance (MW/cm^2)	*943.8*	*1246.1*	*1699.8*	*2002.1*
Incubation energy (J/mm)	*0.0297*	*0.0391*	*0.0534*	*0.0629*
E_{pulse} (µ J)	*3.70*	*4.89*	*6.67*	*7.86*

Table 1: Laser parameters used to process the samples presented in Fig. 17.

Table 2 for Figure 18:

Figure 18: Sample	***e***	***f***	***g***	***h***
Ø beam (µm)	*25*	*25*	*25*	*25*
Pulse width (ps)	*800*	*800*	*800*	*800*
Power (W)	*2.965*	*3.915*	*4.865*	*6.29*
Current (A)	*4.5*	*5.5*	*6.5*	*8*
Frequency (kHz)	*400*	*400*	*400*	*400*
Scanning speed (mm/s)	*100*	*100*	*100*	*100*
Fluence (J/cm^2)	***1.51***	***1.99***	***2.48***	***3.20***
Irradiance (MW/cm^2)	*1887.6*	*2492.3*	*3097.1*	*4004.3*
Incubation energy (J/mm)	*0.0297*	*0.0391*	*0.0486*	*0.0629*
E_{pulse} (µ J)	*7.41*	*9.79*	*12.16*	*15.72*

Table 2: Laser parameters used to process the samples presented in Fig. 18.

Table 3 for Figure 20:

Figure 20: Sample	***i***	***j***	***k***
Ø beam (µm)	*25*	*25*	*25*
Pulse width (ps)	*800*	*800*	*800*
Power (W)	*3*	*5*	*6*
Current (A)	*4.5*	*6.6*	*7.7*
Frequency (kHz)	*300*	*500*	*600*
Scanning speed (mm/s)	*100*	*167*	*200*
Fluence (J/cm^2)	*2.04*	*2.04*	*2.04*
Irradiance (MW/cm^2)	*2549.0*	*2545.4*	*2544.5*
Incubation energy (J/mm)	*0.03*	*0.03*	*0.03*
E_{pulse} (µ J)	*10*	*10*	*10*

Table 3: Parameters used for experiments in the Figure 20.

3.2 Influence of fluence values on Aluminum surface

A. Influence of fluence values at low frequency. *(300 kHz and 450 kHz)*

Table 4 for Figure 25:

Figure 25: Sample	***I***	***II***	***III***
Ø beam (µm)	*17*	*17*	*17*
Pulse width (ps)	*300*	*300*	*300*
Power (W)	*1.58*	*1.12*	*0.8*
Current (A)	*7*	*6*	*5*
Frequency (kHz)	*400*	*400*	*400*
Scanning speed (mm/s)	*100*	*100*	*100*
Fluence (J/cm^2)	***1.74***	***1.23***	***0.88***
Irradiance (MW/cm^2)	*5800.8*	*4111.9*	*2937.1*
Incubation energy (J/mm)	*0.016*	*0.011*	*0.008*
E_{pulse} (µ J)	*3.95*	*2.8*	*2*

Table 4: Parameters used in the study of effects of fluence under UV irradiation at 400 kHz laser frequency.

Table 5 for Figure 26:

Figure 26: Sample	***IV***	***V***	***VI***	***VII***
Ø beam (µm)	*17*	*17*	*17*	*17*
Pulse width (ps)	*300*	*300*	*300*	*300*
Power (W)	*2.4*	*1.4*	*1*	*0.6*
Current (A)	*8*	*6*	*5*	*4*
Frequency (kHz)	*300*	*300*	*300*	*300*
Scanning speed (mm/s)	*100*	*100*	*100*	*100*
Fluence (J/cm^2)	***3.52***	***2.06***	***1.47***	***0.88***
Irradiance (MW/cm^2)	*11748.4*	*6853.3*	*4895.2*	*2937.1*
Incubation energy (J/mm)	*0.024*	*0.014*	*0.010*	*0.006*
E_{pulse} (µ J)	*8*	*4.67*	*3.33*	*2*

Table 5: Parameters used in the study of effects of fluence under UV irradiation at 300 kHz.

Table 6 for Figure 28:

Figure 28: Sample	***1***	***2***
Ø beam (µm)	*17*	*17*
Pulse width (ps)	*300*	*300*
Power (W)	*0.4*	*0.8*
Current (A)	*4*	*5*
Frequency (kHz)	*400*	*400*
Scanning speed (mm/s)	*100*	*100*
Fluence (J/cm^2)	***0.44***	***0.88***
Irradiance (MW/cm^2)	*1468.5*	*2937.1*
Incubation energy (J/mm)	*0.004*	*0.008*
E_{pulse} (µ J)	*1*	*2*

Table 6: Parameters used for experiments on samples 1 and 2 in Figure 28.

B. Influence of fluence values at high frequency. *(800 kHz)*

Table 7 for Figure 31:

Figure 31: Sample	***1***	***2***	***3***
Ø beam (µm)	*17*	*17*	*17*
Pulse width (ps)	*300*	*300*	*300*
Power (W)	*0.5*	*0.75*	*1.42*
Current (A)	*6*	*7*	*9*
Frequency (kHz)	*800*	*800*	*800*
Scanning speed (mm/s)	*100*	*100*	*100*
Fluence (J/cm^2)	***0.27***	***0.41***	***0.78***
Irradiance (MW/cm^2)	*917.8*	*1376.8*	*2606.7*
Incubation energy (J/mm)	*0.0050*	*0.0075*	*0.0142*
E_{pulse} (µ J)	*0.625*	*0.937*	*1.775*

Table 7 :Parameters used for the studies on samples 1,2 and 3 under the influence of UV irradiation.

Table 8 for Figure 33:

Figure 33: Sample	***1***	***2***
Ø beam (µm)	*17*	*17*
Pulse width (ps)	*300*	*300*
Power (W)	*0.5*	*0.75*
Current (A)	*6*	*7*
Frequency (kHz)	*800*	*800*
Scanning speed (mm/s)	*100*	*100*
Fluence (J/cm^2)	***0.27***	***0.41***
Irradiance (MW/cm^2)	*917.8*	*1376.8*
Incubation energy (J/mm)	*0.00067*	*0.00100*
E_{pulse} (µ J)	*0.625*	*0.937*

Table 8: Parameters used for experiment in the Fig 33.

3.3 Influence of incubation energy.

Table 9 Figure 34:

Figure 34: Sample	***A***	***B***	***C***
Ø beam (µm)	*17*	*17*	*17*
Pulse width (ps)	*300*	*300*	*300*
Power (W)	*0.97*	*0.97*	*0.97*
Frequency (kHz)	*300*	*300*	*300*
Scanning speed (mm/s)	*100*	*300*	*500*
Fluence (J/cm^2)	*1.42*	*1.42*	*1.42*
Irradiance (MW/cm^2)	4748.3	4748.3	4748.3
Incubation energy (J/mm)	***0.010***	***0.003***	***0.002***
E_{pulse} (µ J)	*3.23*	*3.23*	*3.23*

Table 9: Table of parameters used for the studies on samples A, B and C in Figure 34.

Table 10 for Figure 35:

Figure 35: Sample	***D***	***E***	***F***	***G***
Ø beam (µm)	*17*	*17*	*17*	*17*
Pulse width (ps)	*300*	*300*	*300*	*300*
Power (W)	*0.5*	*0.5*	*0.5*	*0.5*
Current (A)	*6*	*6*	*6*	*6*
Frequency (kHz)	*800*	*800*	*800*	*800*
Scanning speed (mm/s)	*750*	*1500*	*2000*	*2500*
Fluence (J/cm^2)	*0.27*	*0.27*	*0.27*	*0.27*
Irradiance (MW/cm^2)	*917.8*	*917.8*	*917.8*	*917.8*
Incubation energy (J/mm)	***0.00067***	***0.00033***	***0.00025***	***0.00020***
E_{pulse} (µ J)	*0.625*	*0.625*	*0.625*	*0.625*

Table 10: Table of parameters used for the experiments on samples D, E, F, and G in Figure 35.

Table 11 for Figure 36:

Figure 36: Sample	***H***	***I***	***J***	***K***
Ø beam (µm)	*17*	*17*	*17*	*17*
Pulse width (ps)	*300*	*300*	*300*	*300*
Power (W)	*0.75*	*0.75*	*0.75*	*0.75*
Current (A)	*7*	*7*	*7*	*7*
Frequency (kHz)	*800*	*800*	*800*	*800*
Scanning speed (mm/s)	*750*	*1500*	*2000*	*2500*
Fluence (J/cm^2)	*0.41*	*0.41*	*0.41*	*0.41*
Irradiance (MW/cm^2)	*1376.7*	*1376.7*	*1376.7*	*1376.7*
Incubation energy (J/mm)	***0.00100***	***0.00050***	***0.00038***	***0.00030***
E_{pulse} (µ J)	*0.9375*	*0.9375*	*0.9375*	*0.9375*

Table 11: Table of parameters used for the experiments on samples H, I, J, and K in Figure 36.

3.4 Influence of the laser angle between laser scanning and polarization direction.

Table 12 for Figure 39:

Figure 39: Sample	***1 a&b***	***2 a&b***	***3 a&b***
Ø beam (µm)	*17*	*17*	*17*
Pulse width (ps)	*300*	*300*	*300*
Power (W)	*0.75*	*0.75*	*0.75*
Current (A)	*7*	*7*	*7*
Frequency (kHz)	*800*	*800*	*800*
Scanning speed (mm/s)	*100*	*300*	*750*
Fluence (J/cm^2)	*0.413*	*0.413*	*0.413*
Irradiance (MW/cm^2)	1376.7	1376.7	1376.7
Incubation energy (J/mm)	***0.0075***	***0.0025***	***0.0010***
E_{pulse} (µ J)	*0.9375*	*0.9375*	*0.9375*
Speed table (mm/s)	***0.094***	***0.271***	***0.589***

Table 12: Table of parameters used for both scanning angle in the Figure 39.

3.5 Influence of atmosphere during laser treatment.

Table 13 for Figure 40:

Figure 40: Sample	***I***	***II***	***III***	***IV***	***V***	***VI***
Ø beam (µm)	*17*	*17*	*17*	*17*	*17*	*17*
Pulse width (ps)	*300*	*300*	*300*	*300*	*300*	*300*
Power (W)	*0.3*	*0.5*	*0.75*	*0.3*	*0.5*	*0.75*
Current (A)	*5*	*6*	*7*	*5*	*6*	*7*
Frequency (kHz)	*800*	*800*	*800*	*800*	*800*	*800*
Scanning speed (mm/s)	*1000*	*1000*	*1000*	*2500*	*2500*	*2500*
Fluence (J/cm^2)	***0.16***	***0.27***	***0.41***	***0.16***	***0.27***	***0.41***
Irradiance (MW/cm^2)	*550.7*	*917.8*	*1376.7*	*550.7*	*917.8*	*1376.7*
Incubation energy (J/mm)	***0.00030***	***0.00050***	***0.00075***	***0.00012***	***0.00020***	***0.00030***
E_{pulse} (µ J)	*0.375*	*0.625*	*0.9375*	*0.375*	*0.625*	*0.9375*
Speed table (mm/s)	***0.731***	***0.731***	***0.731***	***1.309***	***1.309***	***1.309***

Table 13: Parameters used for the experiments in Air.

Table 14 for Figure 41:

Figure 41: Sample	***1***	***2***	***3***	***4***	***5***	***6***
Ø beam (µm)	*17*	*17*	*17*	*17*	*17*	*17*
Pulse width (ps)	*300*	*300*	*300*	*300*	*300*	*300*
Power (W)	*0.75*	*1.05*	*1.4*	*0.75*	*1.05*	*1.4*
Current (A)	*7*	*8*	*9*	*7*	*8*	*9*
Frequency (kHz)	*800*	*800*	*800*	*800*	*800*	*800*
Scanning speed (mm/s)	*1000*	*1000*	*1000*	*2500*	*2500*	*2500*
Fluence (J/cm^2)	***0.41***	***0.58***	***0.77***	***0.41***	***0.58***	***0.77***
Irradiance (MW/cm^2)	*1376.7*	*1927.4*	*2569.9*	*1376.7*	*1927.4*	*2569.9*
Incubation energy (J/mm)	***0.0008***	***0.0011***	***0.0014***	***0.0003***	***0.0004***	***0.0006***
E_{pulse} (µ J)	*0.9375*	*1.3125*	*1.75*	*0.9375*	*1.3125*	*1.75*
Speed table (mm/s)	***0.731***	***0.731***	***0.731***	***1.309***	***1.309***	***1.309***

Table 14: Parameters used for the experiments in Argon.

ANNEX IV: RESUMEN EXTENDIDO EN ESPAÑOL.

A1. INTRODUCCIÓN

La formación de hielo en los puntos críticos del cuerpo de un avión es uno de los problemas que la industria de la aviación está estudiando. Esta formación de hielo modifica el flujo del aire, aumenta el arrastre y disminuye la capacidad del avión para crear sustentación. Además, el hielo también puede provocar que algunos sensores den una lectura incorrecta a los pilotos. Para ello, los fabricantes de la industria de la aviación han decido investigar y crear diseños específicos para resolver este problema. Uno de ellos es mejorar la hielofobicidad del material utilizado en las alas de los aviones. Para llevar a cabo esta idea, el tratamiento con láseres de pulso corto es uno de los métodos más efectivos para modificar la superficie del material usado a escala nano- y microscópica. La tecnología láser se utiliza principalmente en la ingeniería de superficie gracias a la alta densidad de energía que genera un aumento de la temperatura superficial en poco tiempo y con la mínima alteración de las propiedades físicas y dimensiones en el interior del material. En los últimos anos, ha habido una gran cantidad de trabajos teóricos y experimentales para comprender la interacción del láser en los materiales y, utilizando esta comprensión modificar el efecto de interacción para desarrollar aplicación especifica. Sin embargo, una de las principales limitaciones en la aplicación de la tecnología de láser es cómo transferir los resultados obtenidos en áreas pequeñas (como se hace en la mayoría de los estudios académicos) a un área más extensa, tal como se requiere en estas aplicaciones aeronáuticas.

Las aleaciones de aluminio son frecuentemente utilizadas en aplicaciones aeronáuticas por su baja densidad y por esta razón es interesante analizar las posibilidades de la tecnología láser puede conseguir en la modificación de la superficie de estos materiales. En particular, es importante explorar el uso de los nuevos sistemas de láser de pulso corto.

A1.1 Fundamentos del láser.

El término LASER es un acrónimo que significa *Light Amplification by Stimulated Emission of Radiation*. Básicamente, el láser es un dispositivo electró-optico que transforma la energía que se genera por las transiciones electrónicas de un medio activo en un haz de luz mono direccional, donde todas las ondas tienen la misma frecuencia (monocromática) y están en fase (luz coherente). La alta coherencia espacial lograda con los láseres permite un enfoque extremo y conseguir una alta densidad de energía. La monocromaticidad del láser permite controlar la profundidad del tratamiento térmico o la excitación selectiva dentro del material o de las moléculas simplemente cambiando su longitud de onda.

Un láser puede operar en modo continuo o en modo pulsado. Durante la operación en modo continuo la potencia es constante a lo largo del tiempo. Este láser se conoce como de onda continua (CW) y frecuentemente se inducen procesos de calentamiento o fusión. En el funcionamiento del láser en modo pulsado, la energía se emite en forma pulsos a una cierta frecuencia. La energía de cada pulso puede alcanzar valores de energía extremadamente altos y también es posible inducir procesos de ablación. En los últimos años, la tecnología ha evolucionado para producir láseres que emiten pulsos muy cortos, con anchuras de pulso

inferiores a nanosegundos. En este estudio, estábamos más interesados en la operación de modo pulsado donde la radiación de laser interactúa con la superficie en una corta duración con pulsos altamente energéticos. Los pulsos cortos maximizan la energía que actúa sobre la capa superficial, reduciendo el calor que se transfiere al sustrato. Además, la entrega de energía rápida y la reducción de las áreas afectadas por el calor son las ventajas más importantes de la técnica en comparación con los efectos inducidos por pulsos más largos. Por esta razón, este método es una herramienta potencial para la fabricación de estructuras superficiales en micro y nano escalas.

Para caracterizar los tratamientos de láser, se pueden definir varios parámetros. La tasa de repetición de los pulsos también llamada frecuencia del láser, describe la cantidad de los pulsos emitidos por segundo. La energía del pulso se puede calcular dividiendo el promedio de la potencia por el número de pulsos por segundo (frecuencia).

$$E_{pulse} = \frac{power\ (watt)}{laser\ frequency\ (Hz)}$$

En consecuencia, la energía de un pulso es una función de la tasa de repetición. Por lo tanto, una tasa de repetición más alta disminuye la energía de un pulso si se utiliza la misma potencia.

Aparte de eso, también es necesario considerar la duración del pulso, también llamado anchura del pulso, porque cuanto más corta es la duración del pulso, más alta es la intensidad máxima de potencia que se aplica, y por lo tanto se produce una onda de choque más fuerte. Dependiendo del material tratado, los pulsos cortos pueden tener una potencia máxima que puede dañar el sustrato, aunque puede evitar la acumulación de calor en el sustrato. La duración del pulso del láser puede variar entre milisegundos (ms) y femtosegundos (fs). Para la duración de pulsos entre ms-ns, la cantidad de calor involucrado en el proceso es importante y los procesos de fusión son relevantes, incluso si se induce algún proceso de ablación. Por el contrario, al operar con pulsos ps-fs, no hay tiempo para que ocurra el proceso de calentamiento y el efecto principal está asociado a la ablación. Por lo tanto, es absolutamente necesario elegir la duración óptima del impulso para desarrollar el proceso de superficie deseado.

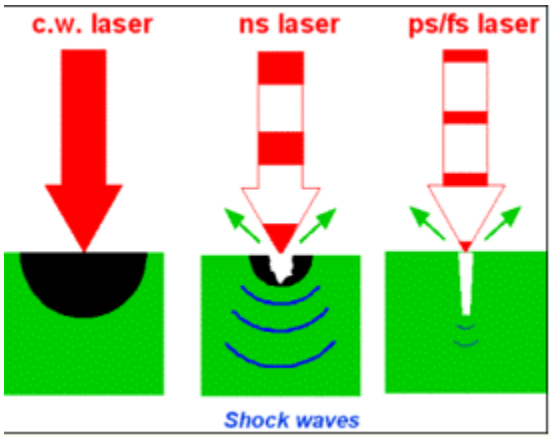

Figura 1: Se produce los efectos diferentes con el láser en la superficie del metal dependiendo de la duración del pulso.

Para definir otros parámetros característicos de un tratamiento de láser, debemos definir las siguientes variables. Primero, es necesario calcular el área que cubre el haz láser durante un pulso, que tiene dos contribuciones: el área del haz láser (mm^2) y el área que cubre debido al desplazamiento de láser durante el ancho del pulso (mm^2):

$$A_{pulse} = (\pi \frac{Diameter\ of\ the\ beam^2}{4}) + (Diameter\ of\ the\ beam \cdot Pulse\ width \cdot Scanning\ speed\ )$$

Hay otros parámetros importantes que deben considerarse en este estudio y que también jugarán un papel importante en la interacción del material con el láser. Algunos de los parámetros más importantes son la irradiancia del pulso, I (kW/cm^2), la potencia máxima del láser por unidad de área y la fluencia del pulso, F (J/cm^2), la densidad de energía por unidad de área. Ambas magnitudes se pueden calcular como;

$$F = \frac{P}{fr \cdot A_{pulse}}$$

Donde P es la potencia de salida y fr es la frecuencia del láser. Mientras que la irradiancia es;

$$I = \frac{P}{(fr.A_{pulse}.t_p)} = \frac{F}{t_p}$$

Donde t_p es la anchura del pulso.

Otro parámetro que debe considerarse al analizar los efectos del tratamiento láser es la energía de incubación, S(J/mm), que mide la energía de salida dividida por la longitud que ha cubierto el pulso por segundo. (velocidad de escaneo de láser).

Cuando se usan láseres de pulsos cortos con altas frecuencias, la superposición entre diferentes pulsos a lo largo de la dirección del movimiento del láser es alta y, en consecuencia, los valores reales de irradiancia y fluencia son más altos que los valores que acabamos de calcular. Se puede considerar S como una medida de esta superposición, pero si el valor es demasiado alto, el análisis será más complicado.

A1.2 Influencia de las propiedades del material en la interacción de láser

Los mecanismos de interacción entre la radiación de láser con los materiales dependen no solo de los parámetros del láser sino también de las propiedades físicas y químicas del material. La combinación de los parámetros del láser y las propiedades del material inducirá diferentes mecanismos físico-químicos que son responsables de diferentes procesos como el calentamiento o la fusión del material, la evaporación o la formación de plasma.

El material se caracteriza por su composición química y microestructura que determina el tipo de excitaciones elementales y la interacción entre ellas. Ellos son responsables de las propiedades ópticas y térmicas del material que también son importantes para comprender las diferentes interacciones que tiene lugar entre los láseres y los materiales.

Un sólido consiste en un gran número de átomos, que se unen para formar una disposición atómica ordenada, y crear el material cristalino. Cuando los átomos están separados, cada uno de ellos es independiente, pero si los átomos se aproximan unos a otros, los electrones

empiezan a interaccionar con los electrones de los núcleos adyacentes. Este fenómeno provoca que el nivel de energía de los átomos individuales se divide en muchos estados de electrones con energía muy próximas, que es lo que se llama la banda de energía de electrones. Además, pueden existir intervalos prohibidos entre estas bandas, que normalmente no pueden ser ocupados por electrones.

A 0K, hay cuatro tipos de estructuras de bandas de energía como se muestra en la Figura 2. Las primeras dos estructuras representan algunos casos en materiales metálicos. La banda que contiene electrones de mayor energía se llama banda de valencia. La energía que corresponde al estado de energía más alta se llama energía de Fermi, E_f. En algunos casos, esta banda de valencia está parcialmente llena de electrones, mientras que, en otros casos, como la segunda estructura, la banda de valencia está llena, pero se solapa con la banda de conducción. La banda de conducción es la siguiente banda de mayor energía que en la mayoría de los casos, está desocupada por el electrón. Las dos estructuras finales corresponden a la situación en que la banda de valencia está completamente llena de electrones, pero hay un espacio de energía entre esta banda y la banda de conducción. Este es el caso para los aislantes y semiconductores.

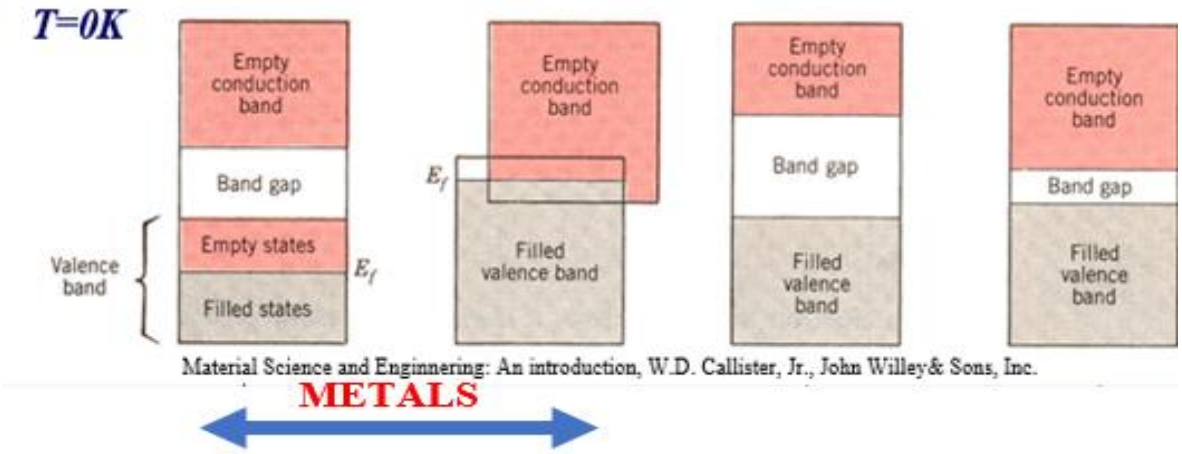

Figura 2: Cuatro tipos de la estructura de banda a T= 0K.

El láser se puede considerar como un conjunto de fotones con una energía dada asociada con su longitud de onda. Obviamente, dependiendo de la energía de los fotones las interacciones serán diferentes dependiendo del láser que se utilice. Durante esta interacción, las ondas electromagnéticas de la radiación causan la transición de un estado de energía a otro estado. Las transiciones más comunes que ocurren son transiciones electrónicas, vibracionales y rotacionales.

En la mayoría de los sólidos, el modo principal de absorber la energía térmica es mediante el aumento de la energía vibratoria de los átomos. Las ondas vibratorias también se llaman fonones. El calor se transporte por vibración de la red y por los electrones libres. En otras palabras, el calor se transfiere por conducción cuando los átomos adyacentes vibran uno contra el otro, o cuando los electrones se mueven de un átomo a otro. En metales, el mecanismo electrónico es el más importante, mientras que, en los aislantes, los fonones son los predominantes. Este es uno de los principales mecanismos de interacción cuando los láseres n-IR se utilizan en el procesado de materiales. Si se usa la radiación de UV, la energía de los fotones es más alta y se inducen nuevos procesos.

Otro punto a tener en cuenta es que cuando una radiación láser interactúa con el material, la radiación incidente se refleja, se absorbe, se dispersa o se transmite, respectivamente. En los metales, la mayor parte de la radiación absorbida se reemite desde la superficie en forma de luz visible con la misma longitud de onda absorbida y aparece como luz reflejada. En el rango de los espectros electromagnéticos asociados con la luz visible, la mayoría de los metales tienen una reflectividad alrededor de 0.90 y 0.95 y una pequeña cantidad de energía se disipa en forma de calor. Como los metales son opacos y tienen una alta reflectividad, su color está determinado por la distribución de la radiación que se refleja y no por la absorbida.

En aluminio, según la Figura 3, su reflectividad es alrededor de 88% a 92% sobre el espectro visible y es casi constante en todas las longitudes de onda con ligeros cambios cuando aumenta la longitud de onda. Este hecho explica el típico color grisáceo que se observa cuando se ilumina con luz blanca. Este comportamiento es muy similar en los metales que tienen un color de gris (ver por ejemplo el espectro de la plata en la Figura 3). Una diferencia entre Ag y Al es que, en el caso de Al, la reflectividad es muy similar cuando se usan radiaciones de n-IR (l=1064 nm) o UV (l=355nm).

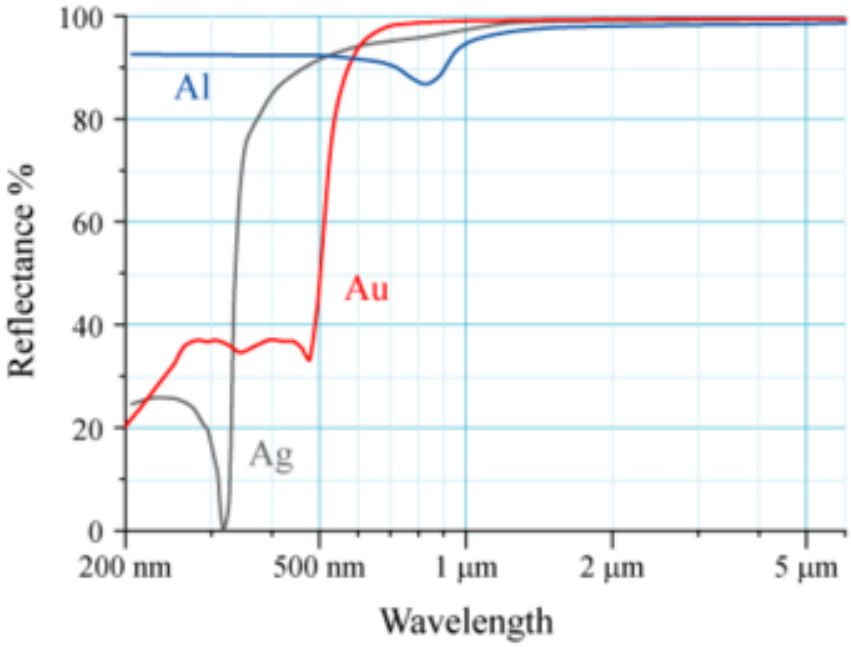

Figura 3: Reflectividad de algunos metales en el rango de longitud de onda asociada con algunos láseres más usado.

A1.3 Generación de las nanoestructuras en la superficie.

Debido a la aparición de los láseres de pulso corto, han surgido nuevos fenómenos. Uno de estos procesos inducidos durante los tratamientos con láser que despertaron el interés en muchos trabajos de investigación es la formación de las estructuras superficiales periódicas inducidas por láser (LIPSS, “Laser-induced periodic surface structures”). Las estructuras superficiales periódicas inducidas por láser (LIPSS) se generan cuando en una superficie se incide con radiación láser del pulso corto polarizada linealmente. Algunas investigaciones proponen que la formación de este mecanismo se debe a la interferencia de la onda incidente con una onda de plasmón superficial [3]. De acuerdo con el experimento llevado a cabo en

Nickel [4], este patrón periódico también se puede producir mediante el uso de radiación radialmente polarizada que produce una menor periodicidad de las ondas en comparación con la obtenida por la radiación polarizada linealmente. La mayoría de las investigaciones sobre la formación de LIPSS se han llevado a cabo usando láseres de femtosegundo, en una configuración en donde la muestra se irradia en un punto mientras se varía el número de pulsos o su duración.

Se puede generar LIPSS en casi cualquier superficie, incluidos metales, semiconductores y dieléctricos. Hay dos tipos de LIPSS que se forman cuando se aplica la radiación de laser ultra rápida a la superficie del material sólido. El primer tipo es el LIPSS de baja frecuencia espacial (LSFL," low-spatial-frequency"), que muestra periodos cercanos o ligeramente más pequeños que la longitud de onda de irradiación. LSFL se puede clasificar en dos tipos de LIPSS, LSFL-I y LSFL-II. LSFL-I normalmente se orienta perpendicularmente a la polarización del haz láser y tiene una periodicidad muy cercana a la longitud de onda. Este mecanismo ocurre en materiales que absorben la radiación, como semiconductores y metales [6]. En los dieléctricos se forman LSFL-II. Estas estructuras generalmente están orientadas en paralelo a la polarización del haz láser y tienen periodos espaciales de $\Lambda_{LSFL} = \lambda/n$. El segundo tipo de LIPSS es el de alta frecuencia espacial (HSFL," high-spatial-frequency") con un periodo inferior a la mitad de la longitud de onda de la irradiación. Los HSFL están orientados en paralelos o perpendiculares a la polarización del haz láser dependiendo del material [6] y, se pueden observar en dos tipos de formas. El HSFL-I que se observa principalmente en dieléctricos y semiconductores y genera ranuras periódicas muy estrechas con anchuras de unas pocas decenas de nanómetros y la profundidad de la ranura puede alcanzar varios cientos de nanómetros, lo que da como resultado una relación de aspecto profundidad-periodo A>1. Por otro lado, HSFL-II presenta una profundidad de ranura de solo unas pocas decenas de nanómetros junto con periodos que se aproximan al rango de menos de 100 nm, lo que da como resultado una relación de aspecto de profundidad a periodo A<<1. Este tipo de HSFL se observa principalmente en metales.

Como hemos mencionado anteriormente, mejorar la hielofobicidad del material utilizado en las alas de avión puede reducir el problema de formación del hielo en la industria aeronáutica. Esto se puede lograr formando LIPSS en la superficie del material. Las investigaciones sobre LIPSS en el artículo [6], muestran que el comportamiento humectante del material puede modificarse formando LIPSS en su superficie con un aumento de la rugosidad superficial en escalas nanoscopicas logrando que el aire quede atrapado por debajo del líquido, por lo que la superficie se hace más hidrófoba. Otras aplicaciones tecnológicas basadas en la generación de LIPSS es la generación de color estructural, manipular el crecimiento de películas de células y bacterias, así como reducir la fricción en aplicaciones tribológicas [6]. De acuerdo con las investigaciones previas, la formación de LIPSS obtenida puede variar enormemente dependiendo de varios parámetros.

A2. RESULTADOS Y DISCUSIÓN

A2.1 Análisis de la influencia de la longitud de onda del láser sobre las estructuras formadas en la superficie del Aluminio.

En este trabajo se han utilizado dos sistemas láser emitiendo con pulsos en el rango de centenares de picosegundos; uno emitiendo pulsos de 800 ps con una longitud de onda de 1064 nm (n-IR) y otro que emite pulsos de 300 ps en el rango del UV (355 nm). La figura 4 muestra la superficie original de la muestra de Aluminio 6061 antes del tratamiento. Se puede ver que la superficie no es completamente lisa; algunas líneas del proceso de laminación se observan en la superficie. La muestra no se ha sometido al proceso de pulido adicional.

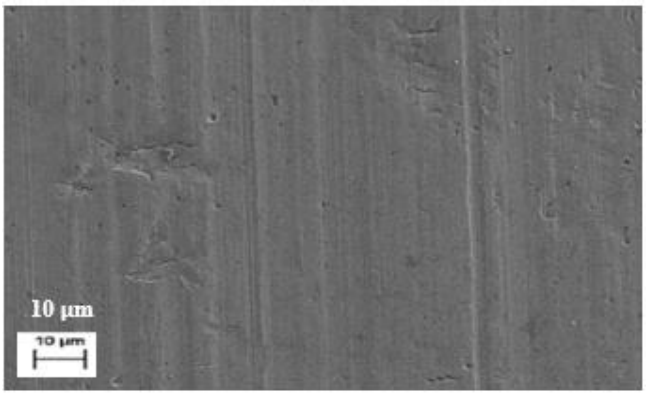

Figura 4: Imagen de FESEM de la superficie original de aluminio.

A2.1.1 Análisis de los cambios inducidos por la radiación n-IR.

Se realizó un conjunto inicial de experimentos para observar las diferentes microestructuras que se pueden obtener en la superficie de Al 6061. Los primeros resultados se han obtenido con una frecuencia 800 kHz, una velocidad del láser 100 mm/s y una distancia entre líneas de 15 micras. La Figura 5 muestra la superficie de estas muestras procesadas con los parámetros de láser detallados en la Tabla 1 del Anexo III. Estas micrografías de FESEM muestran que a bajos valores de corriente (2.5 A, 3 A, 3.5 A), las superficies casi no se ven afectadas por el láser, y se necesita una potencia mínima de 2.965 W para comenzar a modificarla. Se observa que la fluencia del pulso ha alcanzado valores entre 0.76 J/cm^2 y 1.60 J/cm^2 y que, en la mayoría de los experimentos, la superficie se ha fundido ligeramente. También se observa que el tratamiento no es uniforme en toda la superficie y es más eficaz en las regiones que se encuentran cerca de los defectos que están presentes en la superficie, lo que indica que, en estas áreas, la absorción del láser es mayor.

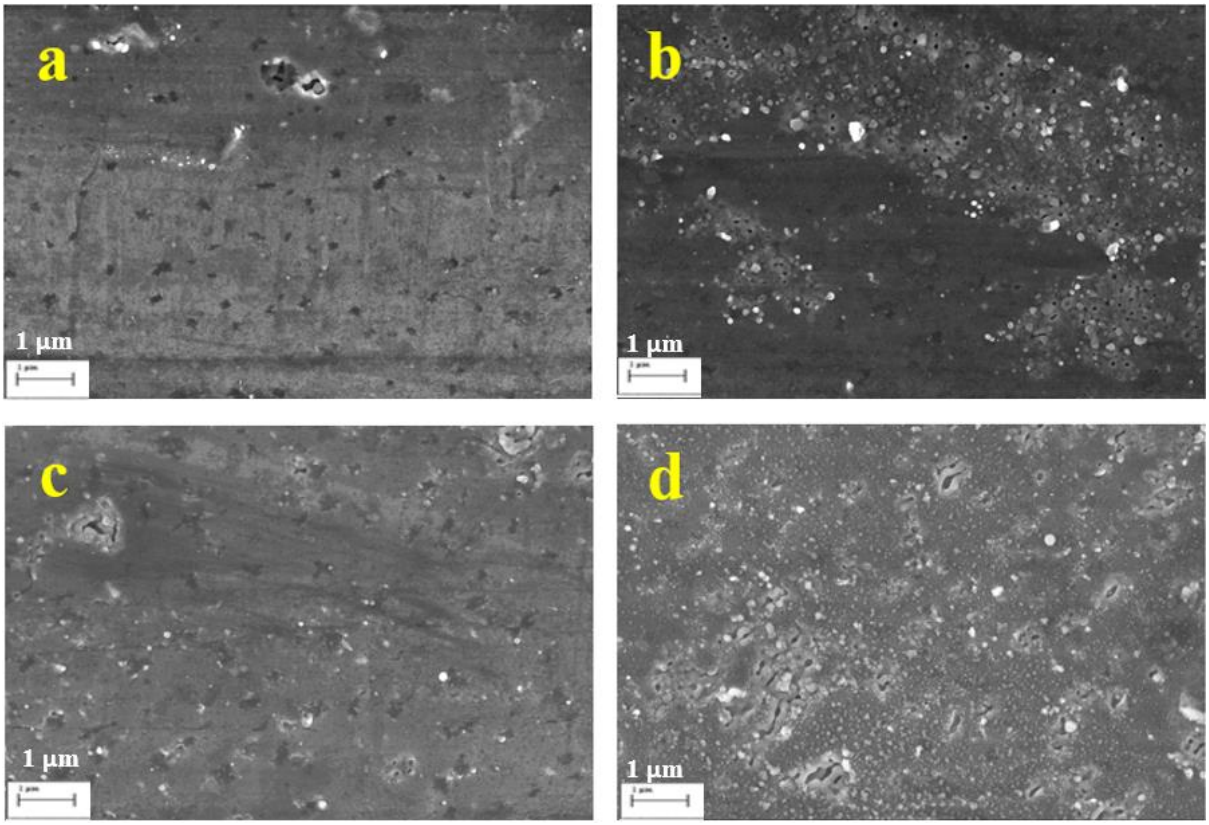

Figura 5: Las morfologías de las muestras después del tratamiento de n-IR láser en alta frecuencia (800 kHz). Se han usado diferentes niveles de potencia ***(a) 2.965 W, (b) 3.915 W, (c) 5.34 W and (d) 6.29 W.***

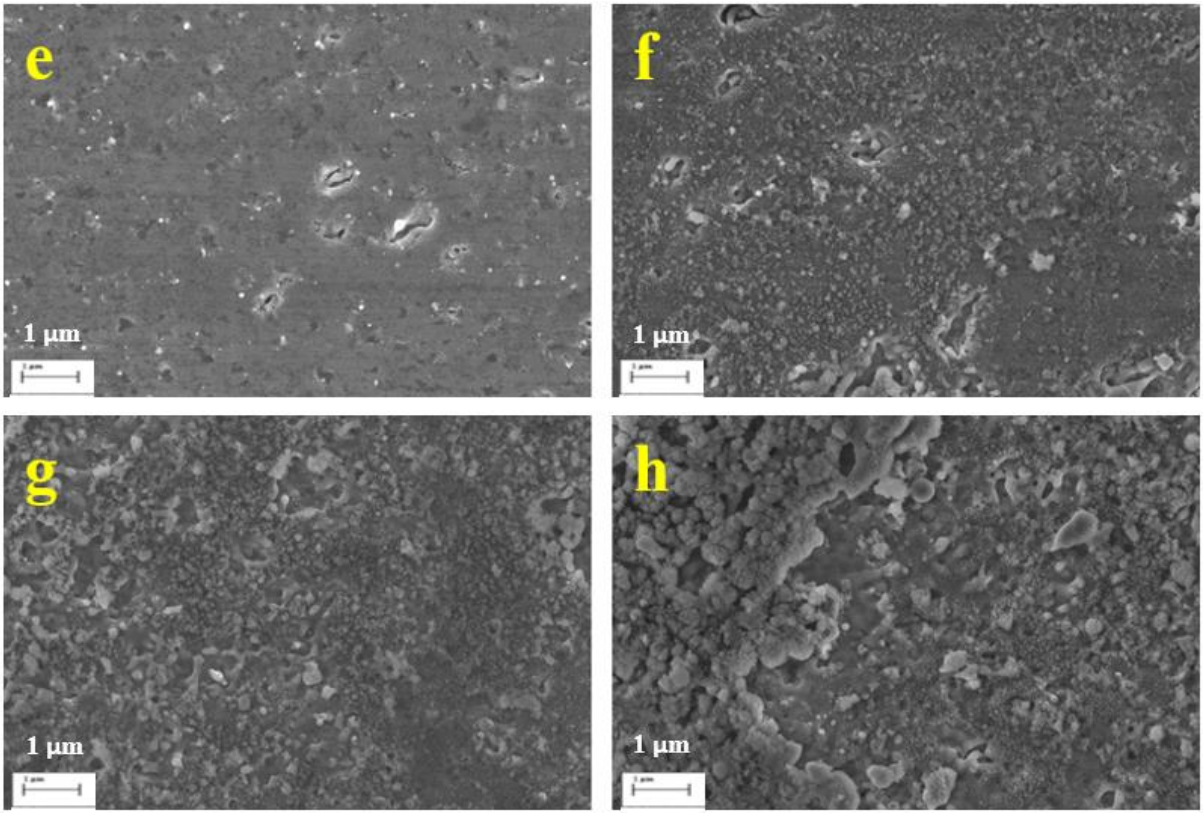

Figura 6: Las morfologías de las muestras después del tratamiento de n-IR láser en baja frecuencia (400 kHz). Se han usado diferentes niveles de potencia del láser: ***(e) 2.965 W, (f) 3.915 W, (g) 4.865 W and (h) 6.29 W.***

Para aumentar los valores de fluencia, se han repetido nuevos experimentos con una frecuencia más baja (400 kHz) (véase la Figura 6). En estos casos, la cantidad de material fundido aumenta, y con los valores de fluencia más altos, el tratamiento llega a modificar toda la superficie. La figura 7 muestra una imagen detallada de la muestra h que muestra el material fundido con un aspecto de nube de algodón. Esta estructura cubre toda la superficie e impide la focalización de la observación de FESEM, indicando que se trata de una fase no conductora, que probablemente sea Al_2O_3.

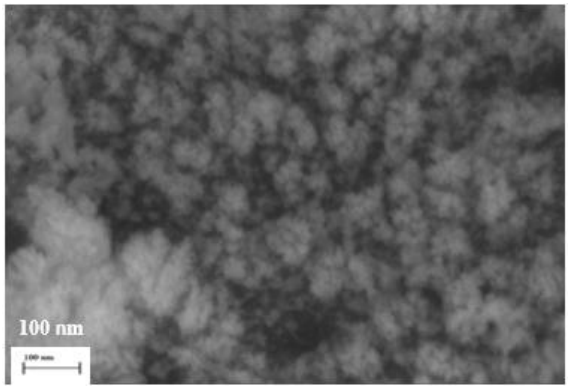

Figura 7: El detalle de la superficie de la muestra h con irradiancia de 4004.3 MW/cm2.

Según a los resultados de todos los experimentos realizados utilizando el láser n-IR, se ha demostrado que la interacción del láser en la superficie Al 6061 es más térmica.

A2.1.2 Análisis de los cambios inducidos por la radiación de UV.

Se realizó un estudio similar usando el láser UV. La Figura 8 muestra las morfologías de superficie que se han obtenido con dos valores de fluencia diferentes: 1.74 J/cm^2 y 1.23 J/cm^2. Como se puede observar, el aspecto de la superficie es completamente diferente, induciendo modificaciones en la escala micro y nanométrica. Las micrografías con grandes aumentos, muestran la nanoestructura inducida en la superficie. Es importante mencionar que los valores de la fluencia usados en estos experimentos son más pequeños que los que se utilizan con el láser n-IR, y, en consecuencia, el efecto del láser UV sobre la superficie es mucho mayor.

Si se reduce el valor de fluencia, por ejemplo, al aumentar la frecuencia del láser hasta 800 kHz, el láser comienza a generar estructuras de fusión en la superficie. La figura 9 muestra las nanoestructuras que se pueden obtener en estas superficies. Se observa que con estas condiciones se obtiene la estructura de nano-puntos y que al controlar los parámetros del láser es posible modificar el orden de la nanoestructura. Hay un valor mínimo de energía para crear estas estructuras. Por ejemplo, la Figura 10 muestra la morfología de la superficie de una muestra que se ha procesado con 0.16 J/cm^2. Se obtiene una capa muy delgada de material fundido, pero no lo suficiente para inducir un cierto orden en la superficie del metal.

De acuerdo con los resultados obtenidos en estos experimentos, obviamente está demostrando que una gran modificación de los valores de fluencia dará una nanoestructura profundamente diferente. Por esta razón, el resto de trabajo se ha centrado en analizar el efecto de la radiación de UV en la superficie de Al6061.

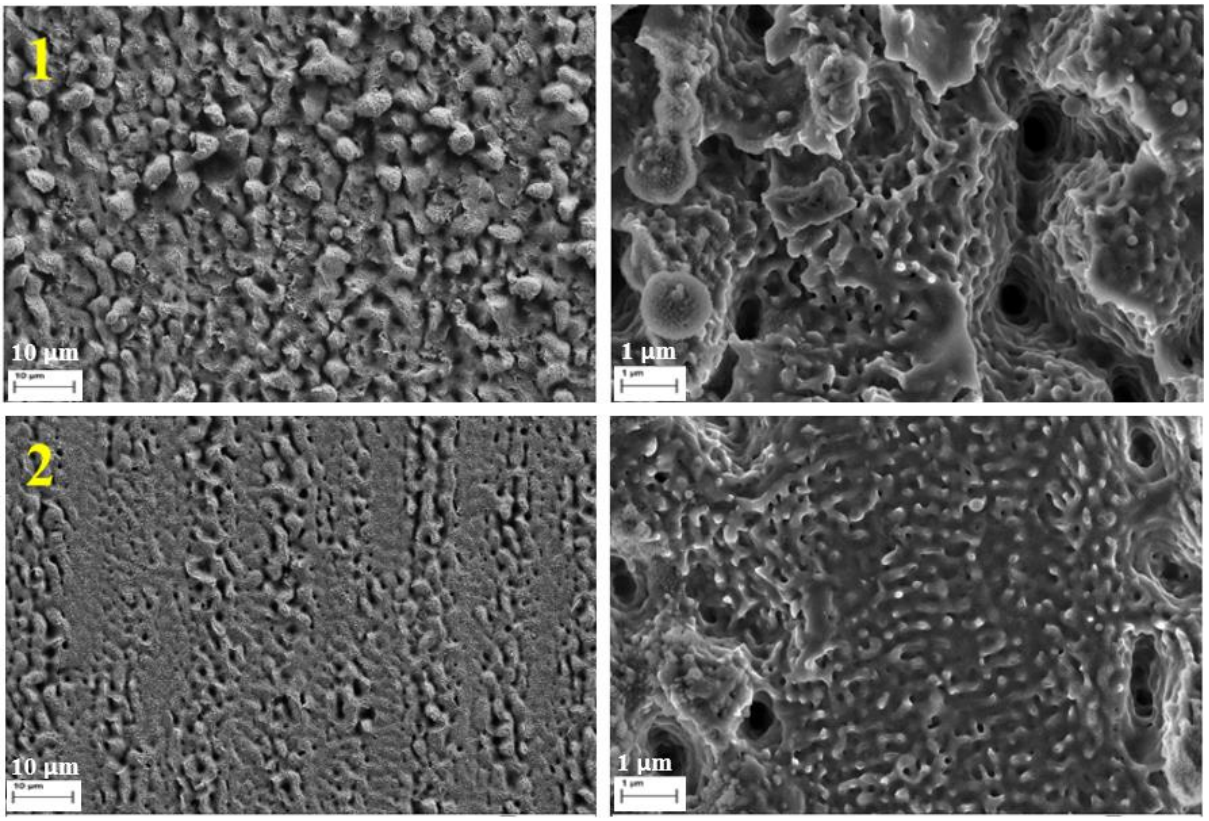

Figura 8: Imágenes de FESEM de las muestras tratadas a bajas tasas de repetición de láser, 400 kHz con velocidad de escaneo igual a 100 mm/s. Las imágenes de la izquierda se toman con un aumento de 1000 X mientras que en el lado derecho se toman con un aumento de 10000 X. Diferentes estructuras formadas a diferentes valores de irradiancia y fluencia; ***(1) 5800.8 MW/cm², 1.74 J/cm2, (2) 4111.9 MW/cm² ,1.23 J/cm².***

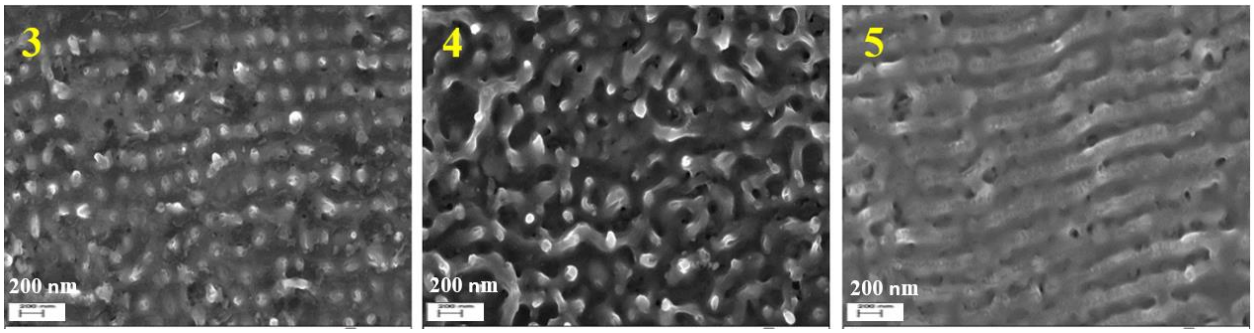

Figura 9: Las morfologías superficiales de las muestras tratadas con frecuencia de 800 kHz y diferentes niveles de irradiancia y fluencia; ***(3) 917.8 MW/cm2 ,0.275 J/cm2, (4)1376.7 MW/cm2, 0.41 J/cm2, (5) 2569.9 MW/cm2, 0.77 J/cm2****.*

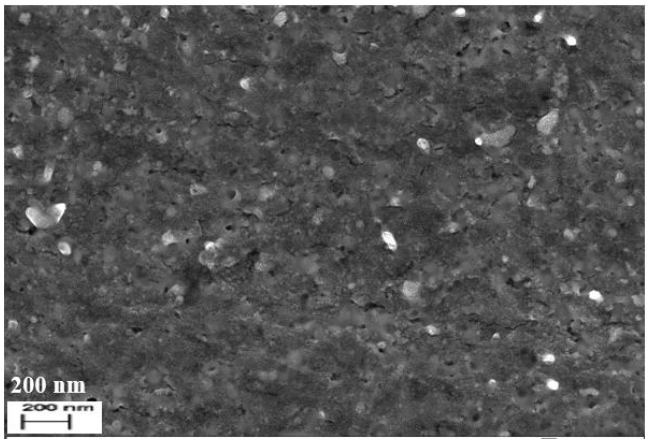

Figura 10: La morfología superficial de una muestra tratada con láser UV a 800 kHz con una irradiancia igual a 550.7 MW / cm² y un valor de fluencia de 0.16 J / cm².

A2.2 La influencia de la fluencia en la superficie de Aluminio.

Como se ha presentado en la sección anterior, en algunas condiciones, el láser de sub-nano UV es capaz de generar estructuras LIPSS similares a las que se forman utilizando láseres de fs. Uno de los parámetros principales del láser que determina la formación de estructuras en la superficie del Aluminio 6061 es la fluencia del láser. Para analizar el efecto de los valores de fluencia en la interacción de laser con material, la fluencia se modificó cambiando la potencia de salida mientras se mantenía la frecuencia fija. El cambio en el valor de la fluencia también produce un cambio de irradiancia. Sin embargo, como la anchura de pulso que utilizamos en este estudio es fija, ambas magnitudes son proporcionales. Clasificamos los resultados obtenidos en dos tipos: primero, los resultados obtenidos usando bajas tasas de repetición de láser (<400 kHz) y el segundo con altas frecuencias (800 kHz).

A. La influencia de los valores de fluencia a baja frecuencia (300 kHz y 400 kHz).

Cuando se usan valores de baja frecuencia, para una potencia de láser dada, la energía de cada pulso aumenta y se pueden alcanzar valores de fluencia más altos. Las imágenes FESEM de la Figura 11 muestran la evolución de las estructuras formadas en la superficie debido al proceso de ablación a medida que los valores de fluencia disminuyen. Estos experimentos se realizaron bajo la influencia de la radiación Ultravioleta con una frecuencia de 400 kHz. A partir de las morfologías de la superficie en la figura 11, observamos que las estructuras que se forman tienen una contribución importante de procesos de ablación, mucho más importantes en la muestra I. Otro aspecto que se observa es que cuando aumenta la fluencia, el efecto es más uniforme en toda la superficie (véase la muestra I). Cuando la fluencia disminuye, se observa que, debido a la distribución de energía del haz, se muestra claramente la distribución de energía en una línea barrida por el láser. En este experimento, la distancia entre líneas era 15 micras y el tamaño del haz es de 17 micras.

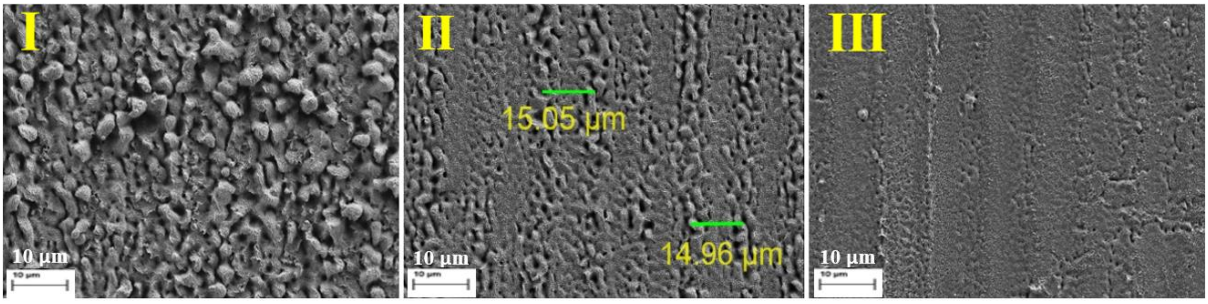

Figura 11: Imágenes FESEM de tres muestras tratadas con radiación UV a 400 kHz con velocidad de escaneo aproximadamente a 100 mm/s. Cada una de las muestras tiene diferentes niveles de potencia y valores de fluencia: ***(I) 1.58W ,1.74 J/cm², (II) 1.12 W, 1.23 J/cm², and (III) 0.8 W, 0.88 J/cm².***

Para poder conseguir valores de fluencia más altos, se han llevado a cabo nuevos experimentos con una frecuencia más baja (300 kHz). La Figura 12 muestra los resultados obtenidos después de los tratamientos de láser. Podemos observar claramente que el tamaño de las estructuras ablacionadas en la superficie aumenta cuando aumenta el valor de la fluencia. De acuerdo con la Tabla 5 del Anexo III, la muestra IV tiene la energía de pulso más alta en comparación con las otras muestras y, también exhibe el mayor tamaño de las estructuras ablacionadas.

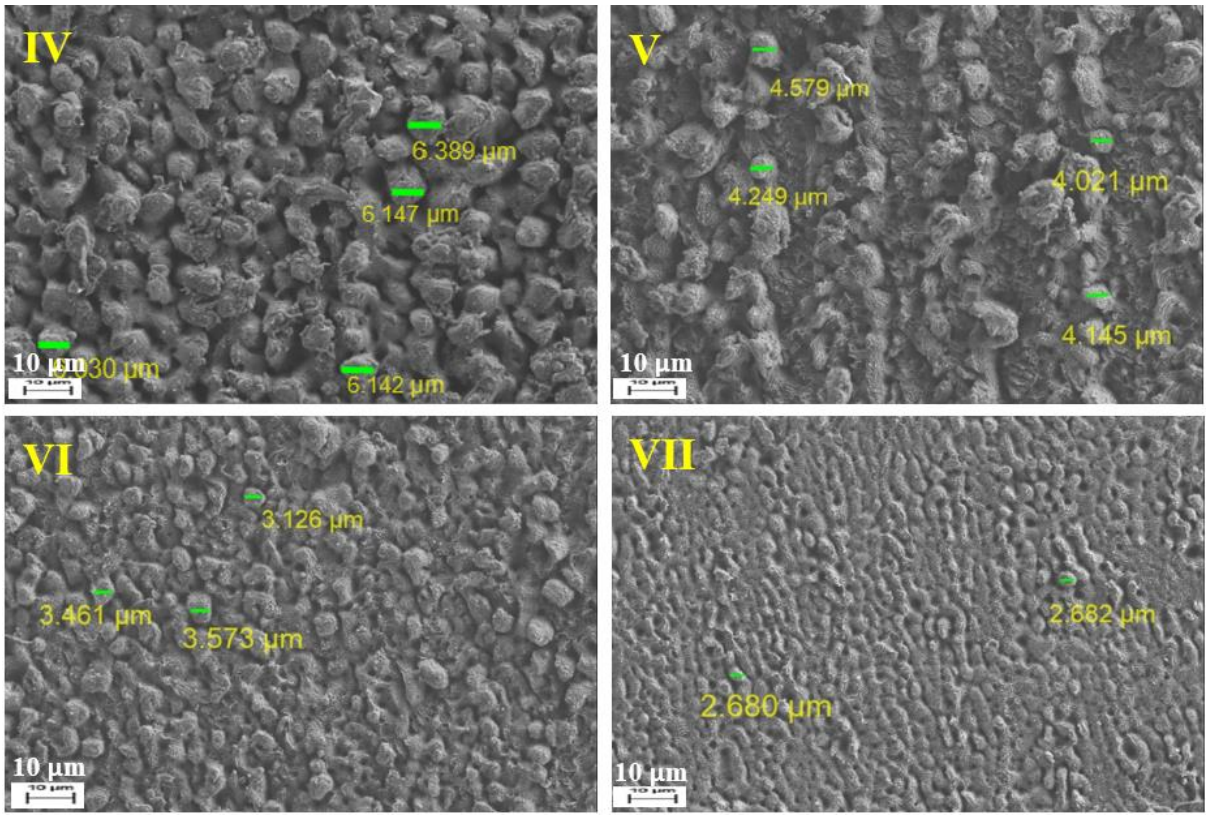

Figura 12: Las imágenes de muestras tratadas con radiación UV a 300 kHz y 100 mm/s muestran la evolución de las estructuras ablacionadas a medida que aumenta el valor de la fluencia. El valor de potencia y fluencia de cada muestra son: ***(IV) 2.4 W, 3.52 J/cm², (V) 1.4 W, 2.06 J/cm2, (VI) 1 W, 1.47 J/cm² and (VII) 0.6 W, 0.88 J/cm².***

Además de la fusión, estos parámetros del láser producen un importante proceso de ablación. La figura 13 muestra las mismas muestras que se presentaron en la Figura 12 con mayores aumentos. La profundidad y el tamaño de las estructuras ablacionadas son cada vez más grandes al aumentar la fluencia. También se observa que se generan nanoestructuras en la

superficie de las microestructuras con características similares a las obtenidas con bajos valores de fluencia.

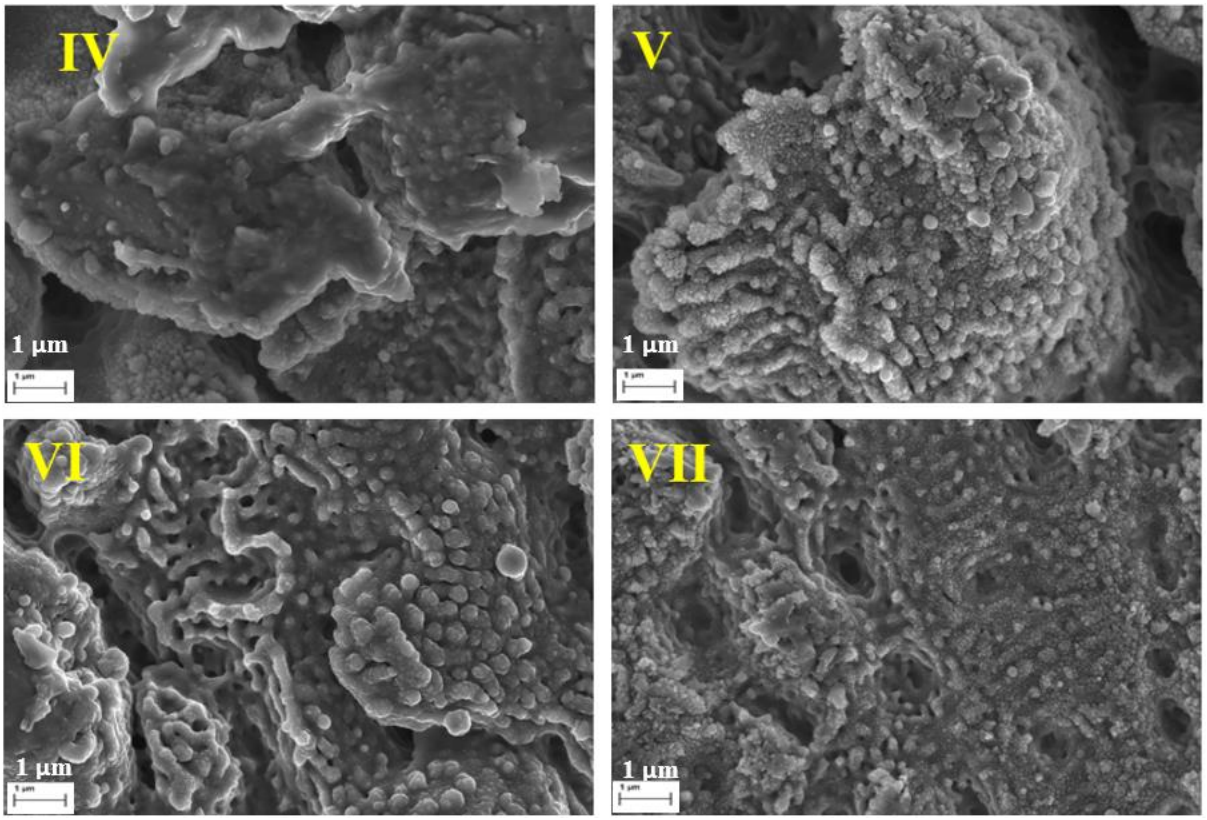

Figura 13: Las imágenes detalladas de los resultados en la Fig. 12 muestran un aspecto claro de las estructuras ablacionadas que se formaron en la superficie de la muestra.

Por otro lado, cuando el valor de la fluencia es menor, se generan procesos de fusión y se forman nanoestructuras con diferentes grados de ordenamiento. En la figura 14, se compara la nanoestructura obtenida usando un valor de fluencia de 0.44 J/cm^2 o un valor de 0.88 J/cm^2.

En la muestra 1, procesada con una fluencia igual a 0.44 J/cm^2 (circulo A), la distancia entre nano-puntos es cercana a la longitud de onda de la radiación láser (355 nm) y en ambas muestras (1 y 2), la periodicidad de las ondas formadas (círculos B y D) también muestran una periodicidad similar. Por lo tanto, podemos concluir que las ondas se forman, y pueden inducir un cierto orden en la generación de nano-puntos y de acuerdo con la teoría, las ondas que se forman son probablemente LSFL-I. Si se desea una estructura más uniforme, la superposición entre las líneas de escaneo del láser debería ser mayor para reducir las diferencias en los valores de fluencia local entre las diferentes regiones de la superficie. Esto se confirmará más adelante.

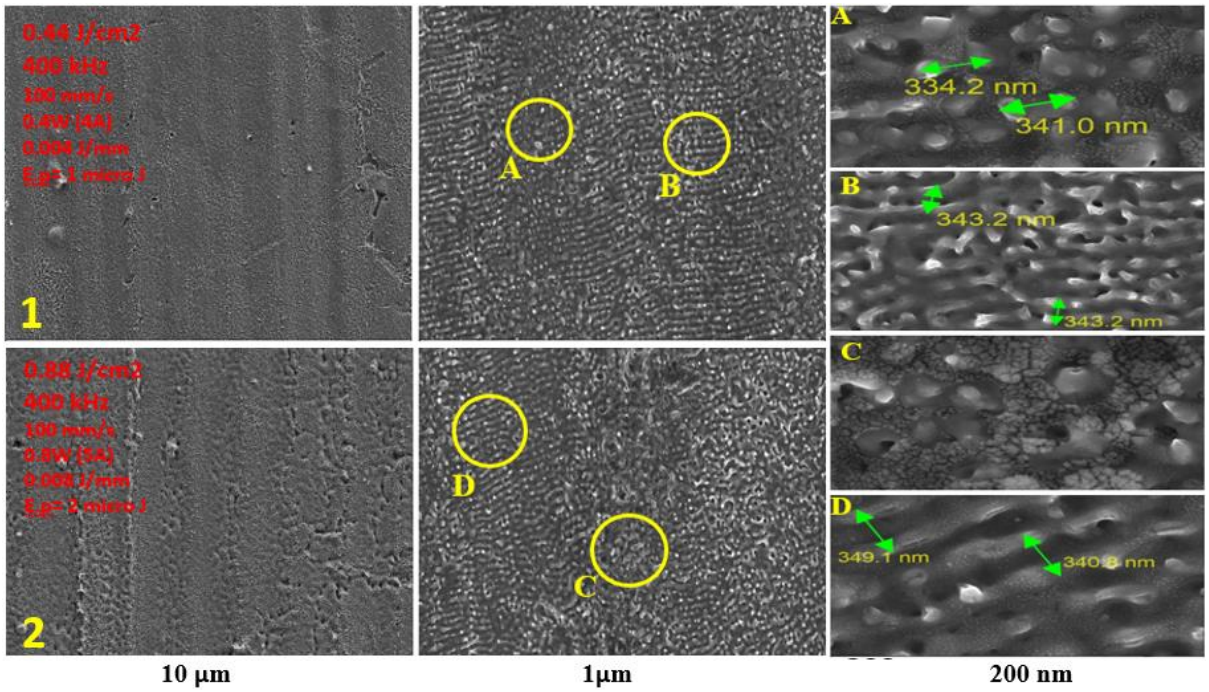

Figura 14: Imágenes FESEM de dos muestras después de ser tratadas con irradiación UV. Ambas muestras se usan para comparar la formación de ondulaciones a bajas tasas de repetición del láser. El aumento del círculo A, B, C y D se puede observar en la tercera columna de esta figura donde las estructuras en el círculo B y D exhiben la formación de ondas y A y C muestran la formación de nano-puntos con fondo amorfo.

La secuencia de estas estructuras formadas a medida que aumenta la fluencia del láser es: con los valores de fluencia más bajos, las nanoestructuras principales son nano-puntos, que se asocian al comienzo de la generación de ondas, como puede deducirse del orden que se ha detectado en algunas condiciones. La segunda estructura es la formación de ondulaciones bien definidas y finalmente las estructuras ablacionadas que son similares a las estructuras de picos que se obtuvieron con los láseres de fs [7].

B. La influencia de los valores de fluencia a alta frecuencia (800 kHz).

Teniendo en cuenta los parámetros de láser disponibles, los experimentos a alta frecuencia (800 kHz) proporcionan información adicional sobre el régimen de bajos valores de fluencia. El valor máximo de fluencia que se puede producir a 800 kHz es solo 0,78 J/cm^2. La Figura 15 muestra el aspecto de la superficie cuando se ha utilizado una fluencia de 0,16 J /cm^2. La estructura de las ondas no está claramente definida, solo se observa una pequeña cantidad de ondas y algunos nano-puntos.

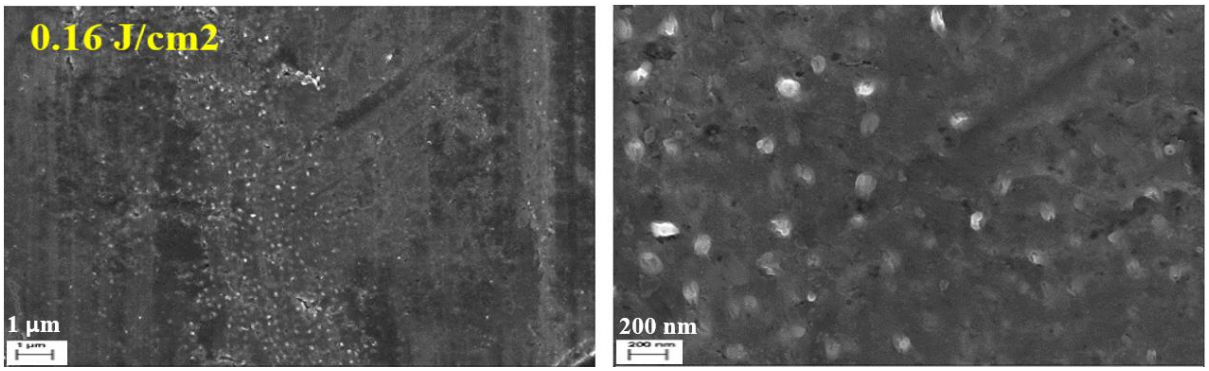

Figura 15: Una muestra tratada con el láser UV a 800 kHz y velocidad de escaneo de 100 mm/s y una fluencia de 0,16 J/cm².

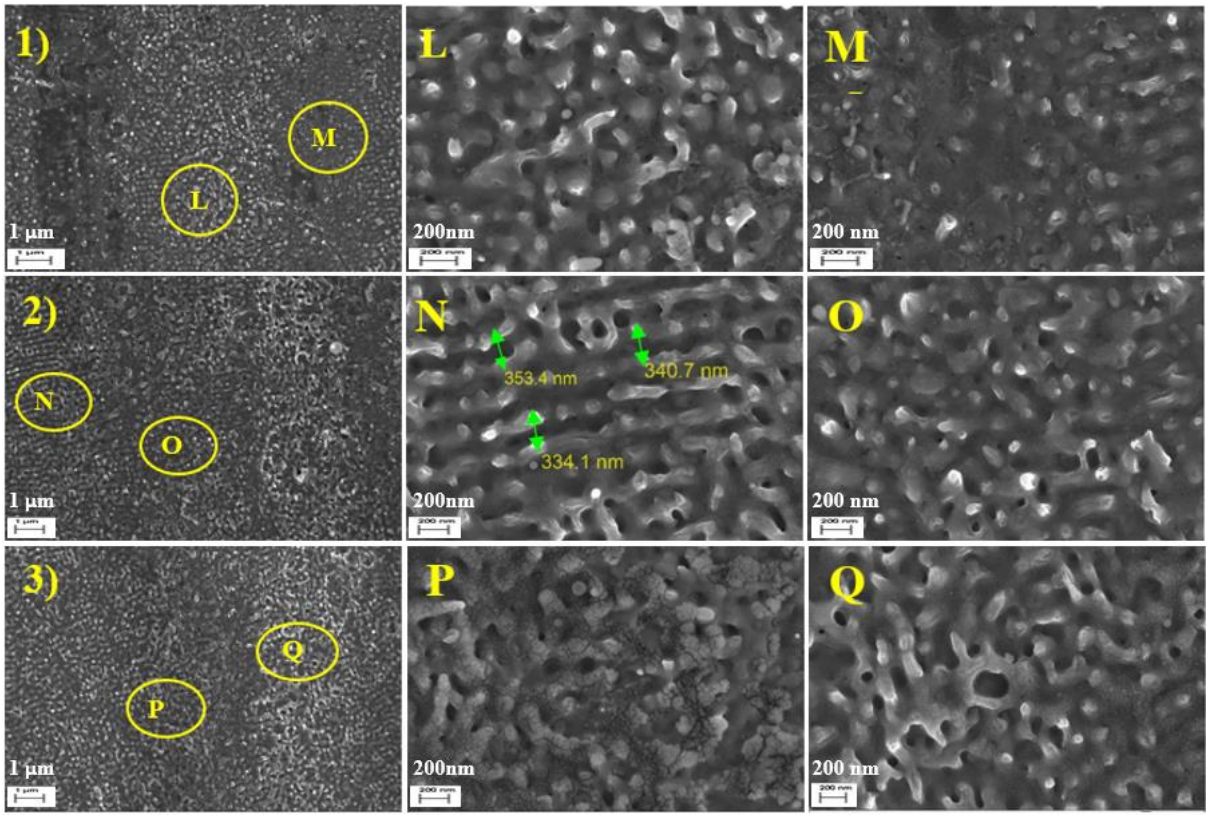

Figura 16: Tres muestras de los experimentos que se llevaron a cabo mediante el uso de la irradiación UV a altas tasas de repetición, 800 kHz. Se utilizan diferentes niveles de potencia y valores de fluencia: muestra ***(1) 0.5 W,0.27 J/cm², (2) 0.75 W, 0.41 J/cm² and (3) 1.42 W, 0.78 J/cm².***

La figura 16 muestra claramente la evolución de la nanoestructura cuando el valor de fluencia aumenta de 0,27 J/cm² a 0,78 J/cm². En este caso, la distancia entre las líneas de escaneo del láser es de 15 micras y el gradiente de energía en el haz láser también se refleja en distribución de nanoestructuras que se han creado en la superficie del metal. La Figura 16 muestra el aspecto de tres muestras procesadas con 0.27 J/cm², 0.41 J/cm² y 0.78 J/cm². En la segunda columna, se presentan detalles de las áreas más afectadas (centro del haz láser) y en la tercera columna se incluyen las regiones que se han visto menos afectadas por el láser (borde del haz láser). De acuerdo con la segunda columna, observamos que cuando los valores de fluencia aumentan, la disposición de las nanoestructuras comienza a formar ondulaciones antes de que las estructuras amorfas caóticas se formen con el valor de fluencia más alta (ver muestra

3). Se observa que las nanoestructuras generadas son ondas LSFL-1 ya que la periodicidad de las ondas formadas es cercana a la longitud de onda del láser UV.
Como se puede observar en estos experimentos, los gradientes de energía perpendiculares a la dirección de escaneo del láser producen una estructura no homogénea. Para tener una distribución de nanoestructuras más uniforme en toda el área, hemos realizado experimentos adicionales al reducir la distancia entre líneas de escaneo del láser hasta 5 micras. Con esta geometría, el valor de fluencia real aumenta, pero es más uniforme en toda la superficie.

Estos experimentos realizados con una distancia entre líneas de escaneo de 5 micras, han permitido la formación de nanoestructuras más uniformes en la superficie de la muestra. En la Figura 17 se muestran los resultados obtenidos con una fluencia de pulso de 0.27 J/cm^2 y 0.41 J/cm^2 y con una velocidad de escaneo de 750 mm/s. En la primera muestra, se forman estructuras uniformes de nano-puntos y ondas, mientras que, en la segunda muestra, la energía se ha incrementado excesivamente y el orden se ha perdido, lo que genera en nanoestructuras más irregulares en toda la superficie. Las imágenes de la derecha son la imagen de detalle de cada muestra.

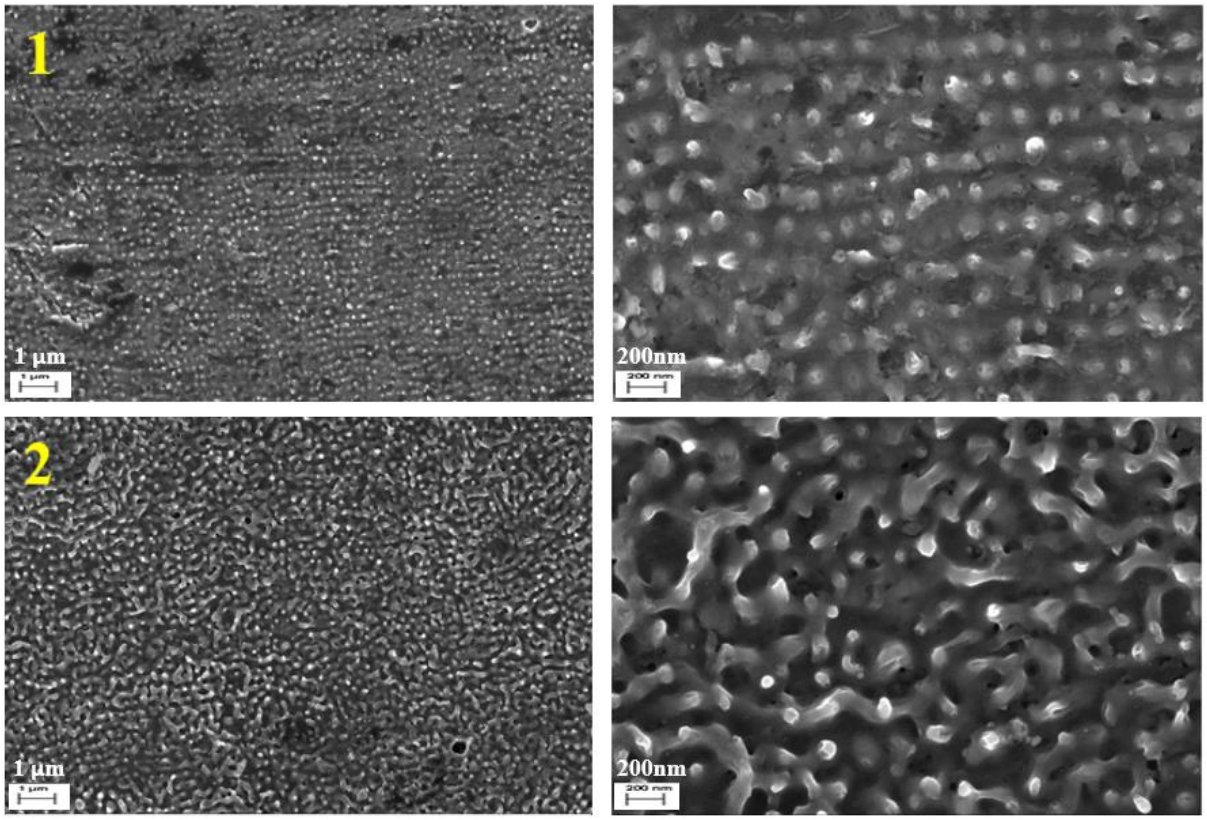

Figura 17: Dos muestras de Al 6061 tratadas con el láser UV a una frecuencia de 800 kHz y velocidad de barrido de 750 mm/s. Los nano-puntos se forman en la muestra 1 mientras que las estructuras irregulares se forman en la muestra 2. El valor de fluencia y la potencia para cada muestra son: ***(1) 0.27 J/cm², 0.5W and (2) 0.41 J/cm², 0.75 W.***

A2.3 La influencia de la energía de incubación.

En la sección anterior, hemos analizado cómo el valor de fluencia puede influir en la micro- y nanoestructura inducida en la superficie. Es importante tener en cuenta que, debido a la alta frecuencia de los láseres usados, siempre hay una superposición en la dirección del movimiento del láser. Por ejemplo, cuando se usa una frecuencia de 800 kHz, la distancia entre dos puntos de láser es de 0,125 micras para una velocidad de láser de 100 mm/s, y de 2,5 micras si esta velocidad aumenta hasta 2000 mm/s. Estas distancias aumentan hasta 0,33 (100 mm/s) y 6,7 micras (2000 mm/s) si la frecuencia se reduce hasta 300 kHz. La magnitud que hemos llamado energía de incubación se puede considerar como una medida de este efecto.

Para evaluar qué magnitud es más importante (fluencia del haz láser o la energía de incubación), se han diseñado varios experimentos en los que se seleccionan los parámetros del láser para mantener una de las magnitudes mientras que la otra se modifica. Para modificar la energía de incubación mientras se mantienen los valores de fluencia, modificamos la velocidad de escaneo y manteniendo la frecuencia fija.

En el primer conjunto de muestras, el valor de fluencia se ha mantenido constante a 1,42 J/cm^2 con una frecuencia de 300 kHz, la velocidad del láser y su potencia se combinaron para explorar un régimen de valores de incubación más bajo, de 0,010 J/mm a 0,002 J/ mm. Las microestructuras de las muestras se presentan en la Figura 18. Debido al alto valor de la fluencia, se forman estructuras ablacionadas en estas muestras. Se muestra claramente que todas las muestras (A, B y C) exhiben las mismas estructuras en su superficie. Sin embargo, es difícil a notar cualquier cambio en las muestras a medida que disminuye la energía de incubación. Estos resultados parecen indicar que el valor de la fluencia juega el papel más importante en la generación de microestructuras.

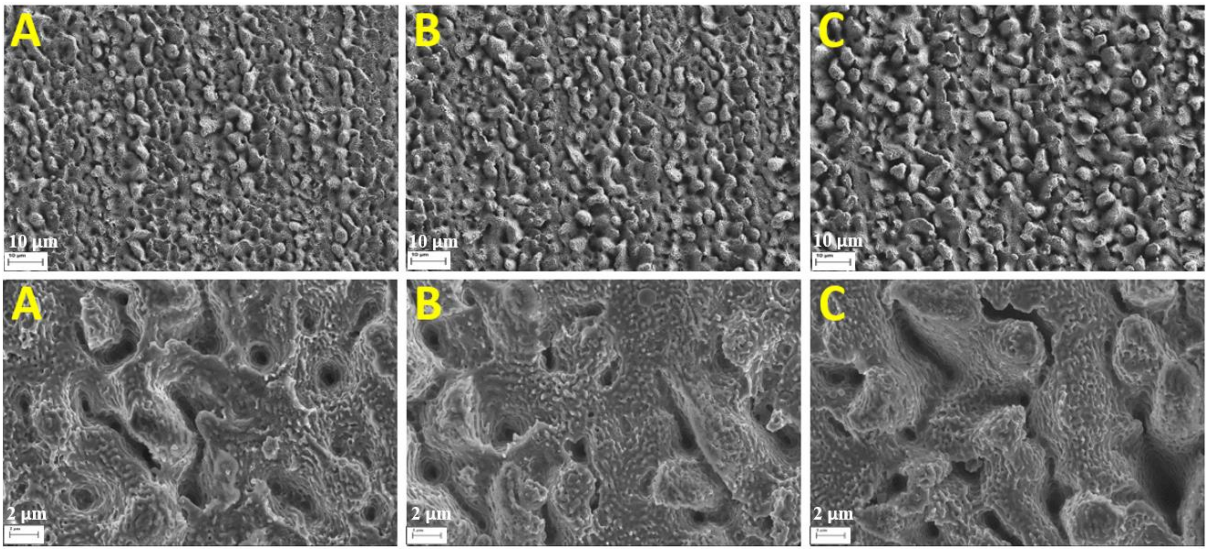

Figura 18: Imágenes FESEM tomadas con dos aumentos, las imágenes superiores a 1000 X e inferiores a 5000 X. Los experimentos se llevaron a cabo bajo la irradiación UV a la misma frecuencia y fluencia (300 kHz y 1,42 J /cm^2). Cada una de las muestras tiene diferente energía de incubación; ***(A) 0.010 J/mm, (B) 0.003 J/mm, and (C) 0.002 J/mm.***

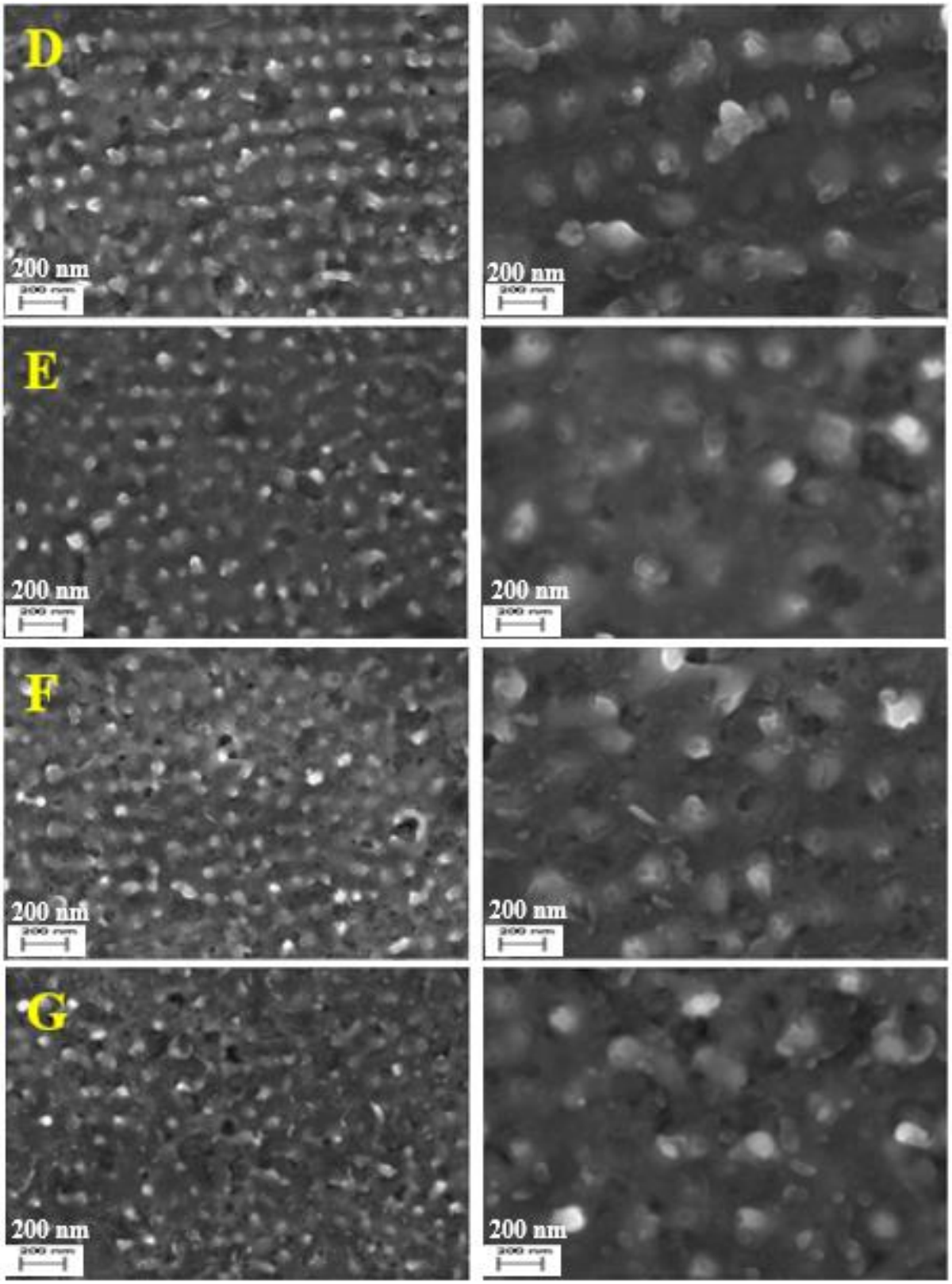

Figura 19: Morfologías superficiales de muestras tratadas con un valor de fluencia igual a 0.27 J /cm² a una frecuencia de 800 kHz. La energía de incubación de cada muestra es: ***(D)0.00067 J/mm, (E)0.00033 J/mm, (F)0.00025, and (G)0.00020 J/mm.***

Esta conclusión también se ha confirmado con un conjunto adicional de experimentos realizados a alta frecuencia, 800 kHz, con un valor determinado de fluencia, 0,27 J/cm^2. Como hemos observado en la sección anterior, con este nivel de fluencia, se forman nanoestructuras en la superficie debido al proceso de fusión. Las fotografías presentadas en la Figura 19 muestran las microestructuras obtenidas utilizando cuatro conjuntos de velocidades de láser (750 mm/s, 1500 mm/s, 2000 mm/s y 2500 mm/s) con los mismos valores de potencia y fluencia del láser. En estos experimentos, la distancia entre las líneas de escaneo es de 5 micras. Se puede observar que los nano-puntos se forman uniformemente en toda la superficie. La velocidad de escaneo utilizada para estas cuatro muestras es diferente y, en consecuencia, la energía de incubación se ha incrementado en más de tres veces.

A partir de los resultados de estos experimentos, podemos concluir que el cambio en la energía de incubación tiene menos efecto que la fluencia en la generación de micro- y nanoestructuras en ambos procesos: ablación y fusión.

A2.4 La influencia del ángulo entre la dirección de escaneo del láser y su dirección de polarización.

Para cualquier experimento llevado a cabo mediante el uso de láser, la polarización es uno de los parámetros más importantes que deben considerarse cuidadosamente. No tenemos ninguna información sobre la polarización del láser que se ha utilizado en este trabajo. Pero como hemos mencionado previamente, en las nanoestructuras inducidas por la radiación de láser, las ondulaciones tienden a ordenarse en la dirección perpendicular a la polarización del láser. Para estudiar este efecto, se realizaron varios experimentos en los que se modificó la dirección de polarización. La Figura 20 muestra las microestructuras observadas en la superficie usando el láser UV a 300 kHz con una velocidad de escaneo de 100 mm/s y un valor de fluencia igual a 1.47 J/cm^2. A este alto valor de fluencia, el proceso de ablación es relevante y, aparte de las nanoestructuras, también se crean microestructuras de picos. En este caso, se usa la configuración del escaneo de haz y la distancia entre cada línea de escaneo es de 15 micras. La Figura 20 muestra las imágenes de FESEM de las muestras tratadas en diferentes direcciones de escaneo: 0 °, 90 °, 180 ° y 270 °. El ángulo se midió tomando como referencia la línea horizontal en el papel. Se puede observar que las microestructuras que se forman en las muestras están orientadas verticalmente e independientemente con la dirección de escaneo. Estos resultados indican que el láser tiene una polarización lineal y teniendo en cuenta el orden que se obtiene en las nanoestructuras se puede deducir que la dirección de polarización es muy cercana a los 90º.

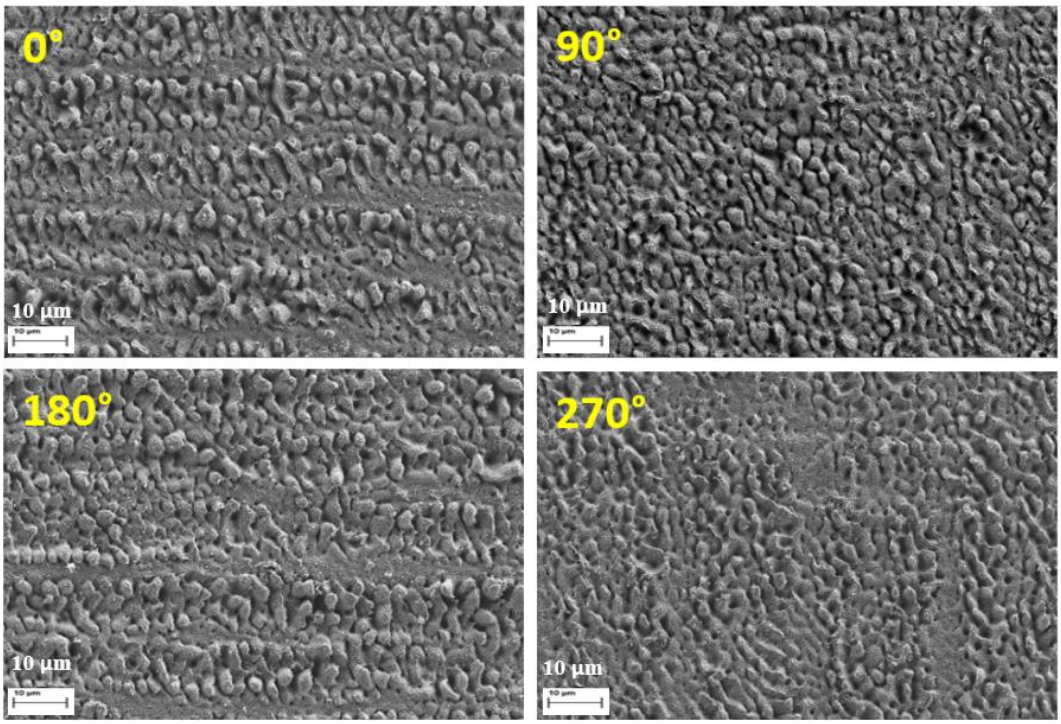

Figura 20: Imágenes FESEM de cuatro muestras que fueron tratadas bajo la influencia de la radiación UV (300 kHz, 100 mm/s) tomadas con un aumento de 1000 X. Las muestras fueron tratadas a diferentes direcciones de escaneo de 0 °, 90 °, 180 ° y 270 ° respectivamente.

Los resultados anteriores también parecen indicar que la interacción del láser con la superficie metálica es más fuerte cuando el haz láser realiza el escaneo en la dirección de la polarización y además de todo esto, también hemos identificado que la interacción es más fuerte en los defectos de la superficie de la muestra. Para separar ambas contribuciones, se realizaron nuevos conjuntos de experimentos con un conjunto de parámetros de láser completamente diferente y utilizando la configuración de escaneo en línea. En esta configuración, el láser se dibuja una línea y la muestra se mueve en la dirección perpendicular (ver Figura 21). En la primera configuración, el movimiento del láser tiene lugar en la configuración 0º, con el láser moviéndose en la dirección perpendicular con respecto a su dirección de polarización. Además, este movimiento del láser es paralelo a la dirección de laminación mecánica de la muestra. En la segunda configuración, el movimiento del láser se ha realizado en la configuración de 90º (paralelo a la dirección de polarización) pero la muestra también ha girado a 90º para mantener la orientación con respecto a la laminación mecánica y evitar las diferencias asociadas con los defectos de laminación mecánica. Las micrografías presentadas en la Figura 22 muestran el aspecto de las muestras después de ser irradiadas a 800 kHz y una fluencia de 0.413 J/cm^2. Las diferencias entre las muestras están asociadas a la velocidad del láser (100 mm/s, 300 mm/s y 750 mm/s) (ver Tabla 12 en el Anexo III). La velocidad de la mesa de desplazamiento que mueve la muestra también se ha adaptado para mantener la superposición entre líneas durante el procesado.

Se observa que en las muestras que se han procesado a 90º (paralelas a la dirección de polarización) el tratamiento ha sido más fuerte que en las que se procesaron a 0º (perpendicular a la dirección de polarización). Estos resultados confirman los resultados iniciales que se obtuvieron en los experimentos realizados con la configuración de barrido de haz, en los que la dirección de escaneo se modificó sin mover la muestra. Como conclusión

de todos estos resultados, para analizar la influencia de los diferentes parámetros de procesamiento del láser, se recomienda encarecidamente usar una configuración de 90º, con el láser moviéndose en paralelo a la dirección de la polarización del láser.

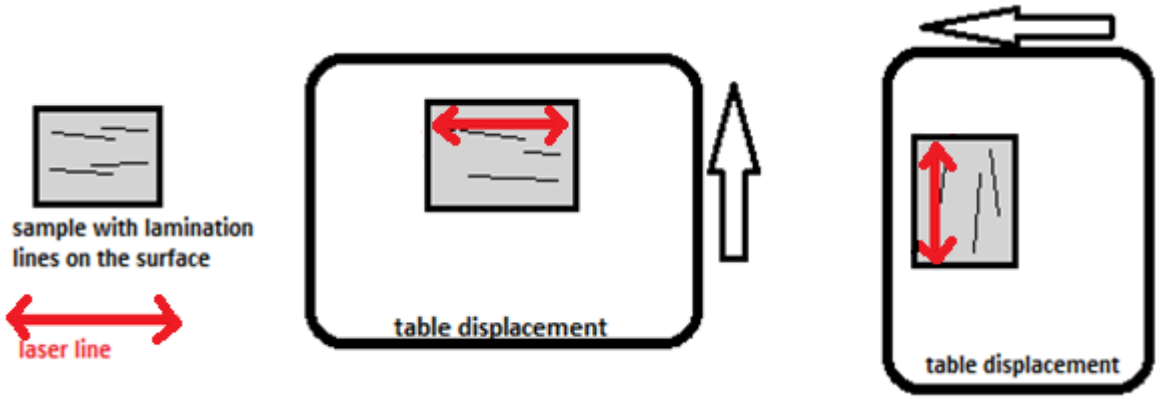

Figura 21: La primera imagen muestra que la línea roja de escaneo de láser está en la configuración de 0 °, mientras que la segunda imagen muestra que la línea roja de escaneo láser tiene una configuración de 90 °.

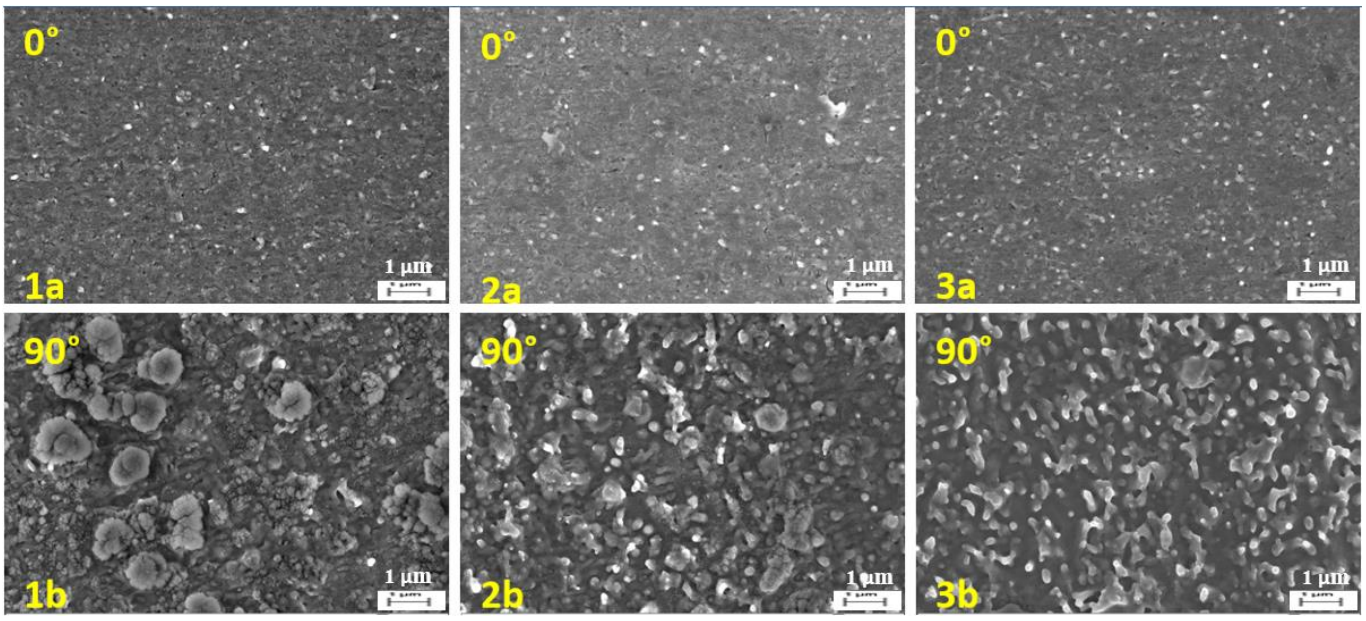

Figura 22: Morfologías de la superficie de las muestras tratadas a diferentes ángulos de escaneo y diferentes velocidades. Imágenes en la primera fila: muestra ***(1a) 0° ,100 mm/s, (2a) 0°,300 mm/s, and (3a) 0°, 750 mm/s.*** *Imágenes en la segunda fila:* ***(1b) 90° ,100 mm/s, (2b) 90°,300 mm/s, and (3b) 90°, 750 mm/s.***

A2.5 La influencia de la atmósfera durante el tratamiento con láser.

La atmósfera que se usa durante el tratamiento con láser también puede modificar estas nanoestructuras. En este trabajo, hemos comprobado qué ocurre si estos experimentos se realizan en atmósfera de Argón. Se llevaron a cabo utilizando el láser UV con una frecuencia de 800 kHz y con la configuración de escaneo de línea. Las líneas de escaneo estaban separadas por una distancia de 5 µm y la velocidad de desplazamiento de la mesa de desplazamiento utilizada depende de la velocidad de escaneo del láser. Los experimentos en Argón se llevaron a cabo utilizando una cámara con un cristal de cuarzo adjunto en su tapa,

la presión interna de la cámara se ajustó a 1,4 atm en atmosfera de Argón. Los valores reales de fluencia que actúan sobre la superficie de la muestra en estas condiciones son más bajos que en el aire porque un porcentaje de la energía de laser se absorbe en la ventana de cuarzo. Para observar la interacción del láser en Al6061 en diferentes condiciones, hemos diseñado varios experimentos en los que los resultados obtenidos para cada condición se comparan de acuerdo con la energía de incubación y el valor de fluencia, respectivamente. Los valores de fluencia se modifican cambiando la potencia de salida, mientras que los valores de energía de incubación se modifican utilizando diferentes velocidades de escaneo.

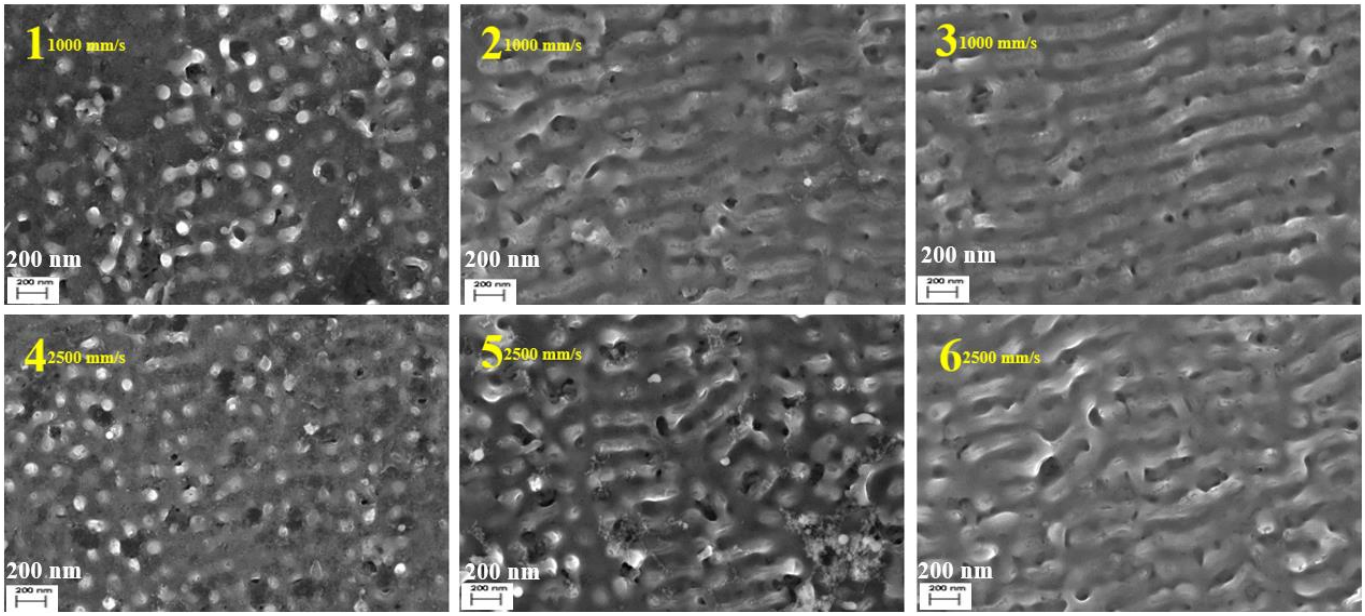

Figura 23: Imágenes FESEM de 6 muestras tratadas con láser en el Argón con frecuencia de 800 kHz. Se aplican diferentes velocidades y potencias por cada muestra: Muestra ***(1) 1000 mm/s, 0.75 W, (2) 1000 mm/s, 1.05 W, (3) 1000 mm/s, 1.4 W, (4) 2500 mm/s, 0.75 W, (5) 2500 mm/s, 1.05 W and (6) 2500 mm/s, 1.4 W.***

En la figura 23 se muestran los resultados obtenidos en muestras procesadas en Ar con unos valores de fluencia nominal entre 0.41 J/cm^2 y 0.77 J/cm^2. La primera fila corresponde a las muestras que se han procesado con la velocidad más baja, 1000 mm/s y la segunda fila con 2500 mm/s. Al igual que las muestras procesadas en aire, las condiciones de procesado conducen a la formación de nanoestructuras en la superficie, pero la principal diferencia es que, en el caso de las muestras tratadas en atmosfera de Ar, se ha alcanzado un nivel de orden superior.

También se ha comprobado que la periodicidad de la nanoestructura también es muy similar a la longitud de onda del láser. Y finalmente, otro hecho curioso es que las superficies de las muestras tratadas con Ar presentan algunos colores que se modifican cuando cambia el ángulo de iluminación. La Figura 25 muestra el ejemplo de colores que se han obtenido con cuatro ángulos de iluminación diferentes. Se propone que el alto grado de ordenamiento de la nanoestructura es capaz de crear una red de difracción que proporciona algunos colores a la muestra dependiendo del ángulo de iluminación.

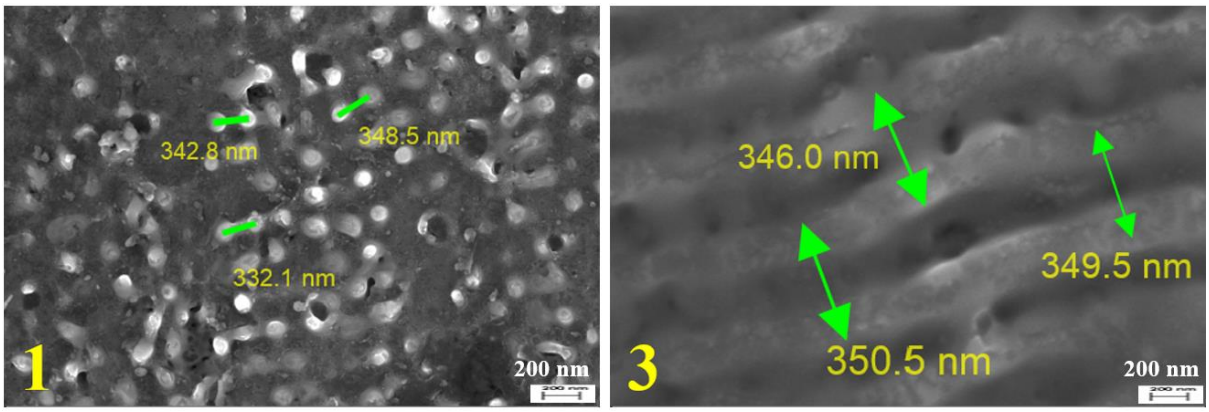

Figura 24: Imágenes FESEM de la muestra 1 y 3 en la Figura 23 en atmósferas de Argón a una distancia más cercana. Los nano-puntos y ondas muestran una distancia y periodicidad cerca de la longitud de onda del espectro ultravioleta, 355 nm.

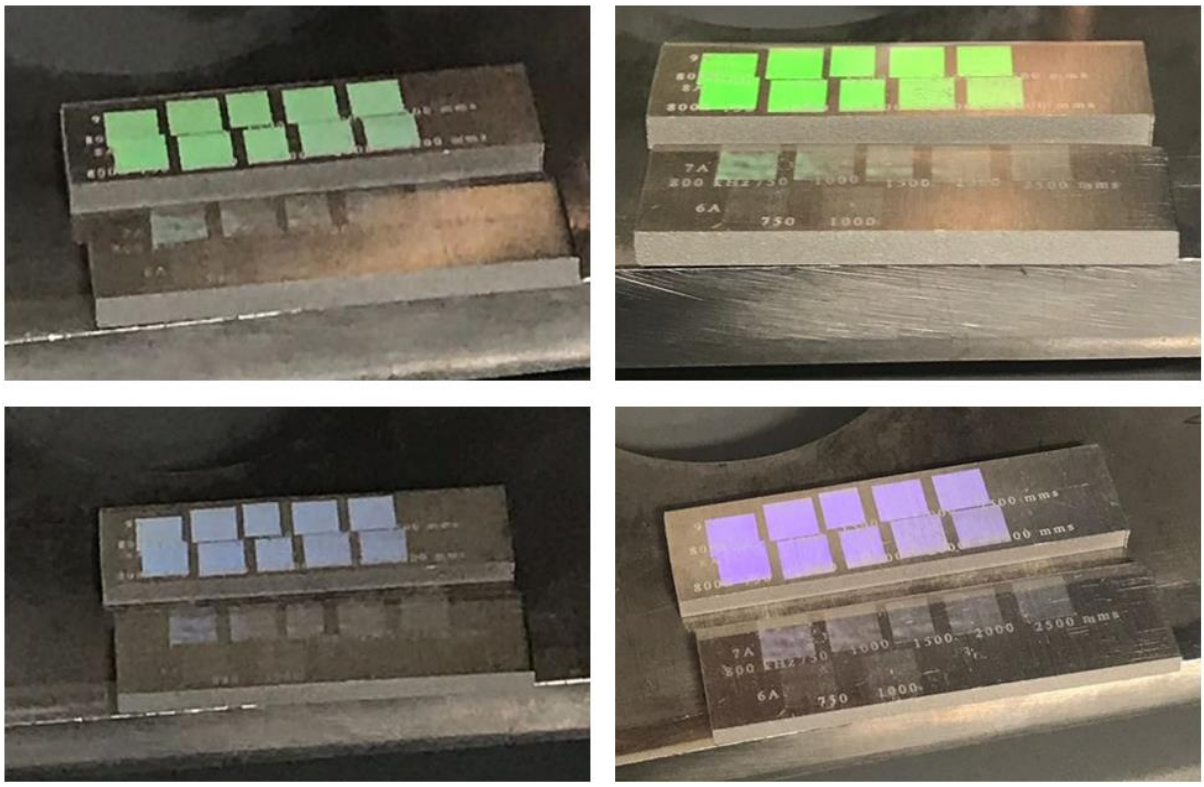

Figura 25: Las imágenes muestran cuatro posiciones diferentes de la muestra después de haber sido irradiadas con láser UV en atmósfera de Argón, donde ilumina colores como el verde, el azul y el violeta.

A3. CONCLUSIONES

En este estudio, se ha investigado experimentalmente la interacción de láseres de pulsos cortos (sub-nano) en Aluminio 6061 mediante el uso de radiación ultravioleta y radiación infrarroja. El objetivo principal es analizar la generación de nano y microestructuras en las estas superficies metálicas.

Los resultados obtenidos de todos los experimentos que se realizaron con el láser infrarrojo muestran que la interacción que se produce en el Al6061 es principalmente térmica. El único cambio que se observa en este estudio cuando modificamos los parámetros del láser es que la cantidad de material que funde aumenta a medida que aumenta el valor de la fluencia. Con una cantidad suficiente de fluencia, la fusión tiene lugar cubriendo toda la superficie.

En el caso de los experimentos que se llevaron a cabo utilizando el láser ultravioleta, se observa que se generan estructuras de fusión o de ablación dependiendo de las condiciones láser y es posible alcanzar alto grados de orden. Se ha observado que el valor de fluencia es el parámetro principal que determina las modificaciones inducidas en la superficie. Para un nivel suficiente de fluencia, se comienzan a formar micro y nanoestructuras en la muestra. Sin embargo, si el valor de fluencia es demasiado bajo, solo se obtiene una capa muy delgada de material fundido.

Se pueden obtener altos valores de fluencia utilizando baja frecuencia ya que la energía por pulso es mayor, mientras que los valores bajos de fluencia se pueden obtener al trabajar con alta frecuencia. Se encuentra que, con valores altos de fluencia, es más probable que ocurra el proceso de ablación. Mientras que, para los valores intermedios de fluencia se comienzan a formar en la superficie de la muestra nanoestructuras como ondulaciones y nano-puntos. La distancia entre los nano-puntos y la periodicidad de las ondas que se forman está cerca de la longitud de onda de la irradiación láser, lo que indica que las ondas generadas se pueden clasificar como una estructura LSFL-I. Además, se ha establecido que, controlando la superposición entre las líneas de exploración para homogeneizar la distribución de energía en la dirección perpendicular del movimiento del láser, es posible obtener algunas estructuras homogéneas en un amplio rango de áreas en la superficie. Esto se ha demostrado experimentalmente reduciendo la distancia de las líneas de escaneo hasta 5 micras.

También hemos estudiado la influencia de la energía de incubación en la superficie de Aluminio. El efecto de la energía de incubación se asocia con la distancia entre dos puntos de láser en función del escaneo de velocidad y la frecuencia utilizada. Los resultados de este estudio muestran que la energía de incubación tiene mucho menos efecto que la fluencia en la generación de micro y nanoestructuras en el proceso de ablación y fusión.

Otro aspecto importante a considerar en el tratamiento láser es la dirección de polarización del láser. Los resultados obtenidos indican que la interacción es más fuerte cuando el láser se mueve en paralelo a la dirección de polarización.

La influencia de la atmósfera durante los tratamientos con láser también juega un papel importante en la interacción del láser y el material. En atmósfera de Argón, las

nanoestructuras formadas están más orientadas y bien ordenadas, creando una red de difracción que proporciona colores a la muestra. Podemos observar diferentes colores en la muestra dependiendo del ángulo de iluminación.

En consecuencia, el uso de láseres UV emitiendo pulsos de varios centenares de picosegundos abre nuevas oportunidades en el desarrollo de nanoestructuras en metales superficiales y ello permite abrir nuevas líneas de investigación que pueden cubrir el análisis de su uso en diferentes aplicaciones: hidrofobicidad, hielofobicidad, decoración, aplicaciones antibacterianas, etc. Además, también se requieren esfuerzos de investigación para escalar estos tratamientos a muestras grandes con el fin de definir cómo transferir los parámetros de los tratamientos láser que se han permitido optimizar los resultados en muestras pequeñas a muestras de grandes dimensiones.

Los resultados de este proyecto se han presentado en el Congreso Nacional de Materiales que se ha celebrado del 4 al 6 de julio de 2018 en Salamanca. Fue una presentación oral titulada; Nanostructures in Al surfaces induced by interaction with UV ps-lasers, siendo los autores Z. Binti-Haron, J.A. Rojo, L.A. Angurel, G.F. de la Fuente, R. Navarro.